CONTENTS

Variable-temperature NMR studies of 2-(pyridin-2-yl)-1H-benzo[d]imidazole

Anchi Yeh[1]*, Chi-Yu Shih[1], Lieh-Li Lin[1], Shung-Jim Yang[2] and Cheng-Tung Chang[3]

[1]Department of Chemical Engineering, Chengshiu University, Kaohsiung, Taiwan, R.O.C.[2]Department of Chemical Engineering, Vanung University, Chung-Li, Taiwan, R.O.C.[3]Department of Products, Taiwan Textile Research Institute, Taipei, Taiwan, R.O.C

Received November 20, 2009

Abstract Method of variable-temperature of ^{1}H-NMR as well as^{13}C-NMR can be used to determine the location of coalescence temperature on the NMR spectrum. To solve the Gutowsky-Holm equation, the activation rotation-energy can be computed. Hence, for the synthesized compound of 2-(pyridin-2-yl)-1H-benzo[d]imidazole, we observed the coalescence temperature of H_9 and H_{10} located at 283K on ^{1}H-NMR spectrum but the calculated activation rotation-energy was 12.69kcal/mole. Meanwhile, the coalescence temperature of H_8 and H_{11} was at 303K on ^{1}H-NMR spectrum but the activation rotation-energy was 15.20kcal/mole. Additionally, the coalescence temperature of C_9 and C_{10} on ^{13}C-NMR spectrum was also at 303K as well as the calculated activation rotation-energy was14.4kcal/mole. [Life Science Journal. 2009; 6(4): 1– 4] (ISSN: 1097 – 8135)

Kay words: NMR spectrum, Gutowsky-Holm equation

1. Introduction

Natural anti-cancer compounds, for instance, berberine, cryptolepine and camptothecin are basically poly-ring structured. Neidle et al. (2003) reported the mechanism of the anti-cancer for some of poly-ring compounds may have the stability if combining with DNA, such as Imidazole ring. Compounds with bisbenzimidazole group can be bonded to DNA's minor groove [1-5]. The temperature and the rotation energy of the molecules can be observed through Variable-temperature NMR [6]. For molecule planar structure, when it does not free to rotate at the temperature below the bearing range of DNA, the structure can be easier bonding to DNA. This report demonstrates the temperature and energy of 2-(pyridin-2-yl)-1H-benzo[d]imidazole in rotation via using variable temperature of ^{1}H-NMR and ^{13}C-NMR.

*Correspondence: acyeh@csu.ecu.tw, Dr. Yeh, Anchi

2. Material and Methods

Picolinic acid (20 mmol, 3.4634 g), 2,3-diaminonaphthalene (20 mmol, 3.1640 g), and polyphosphoric acid (PPA, 20ml) were added to an empty flask. The mixture was heated at 200^{o}C for 4 hours. After cooling to room temperature, de-ionized water (500ml) shall be added with stirring. The solid was collected by suction filtration and purified by column chromatography with ethyl acetate/hexane (1:1). Colorless crystal of 2-(pyridin-2-yl)-1H-benzo[d]imidazole was obtained in 80% yield. All NMR works were done by using 500 MHz and DMF-d[7].

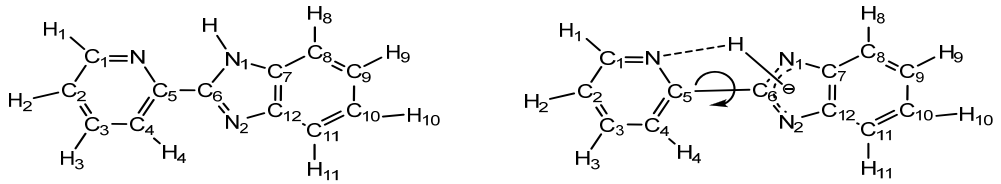

A B

Figure 1. (A) Structure of 2-(pyridin-2-yl)-1H-benzo[d]imidazole, (B) Rotation of 2-(pyridin-2-yl)-1H-benzo[d]imidazole

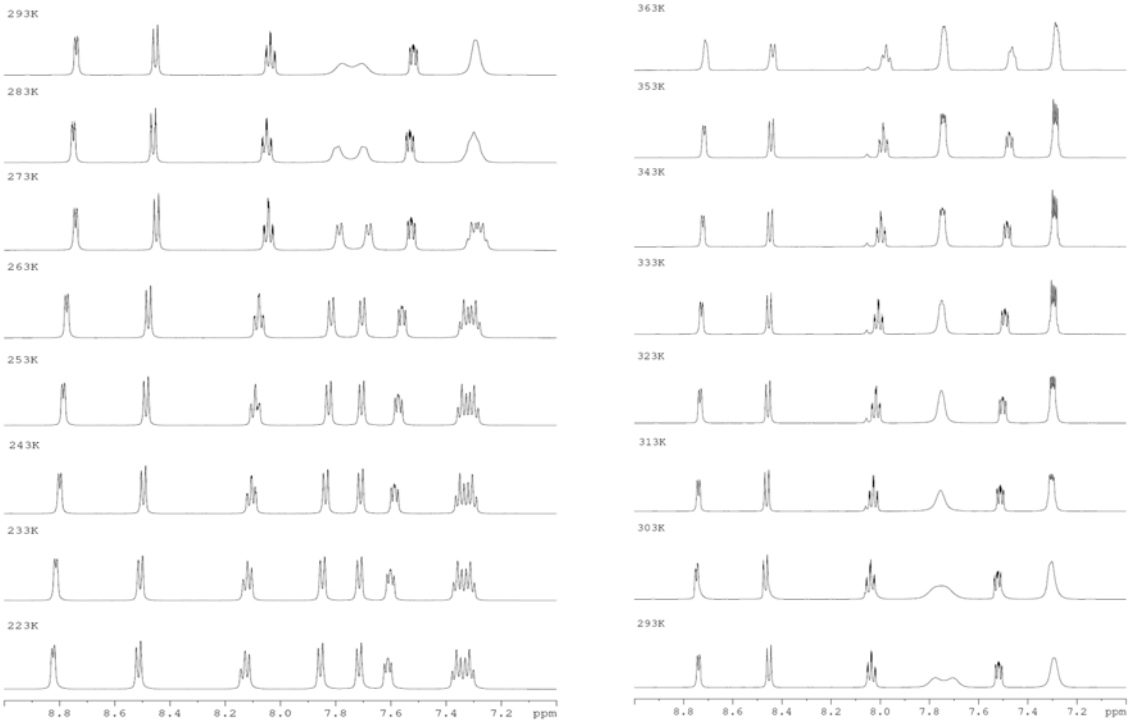

Figure 2. Variable-temperature ^{1}H-NMR of BIP. (Left) low temperature, (Right) high

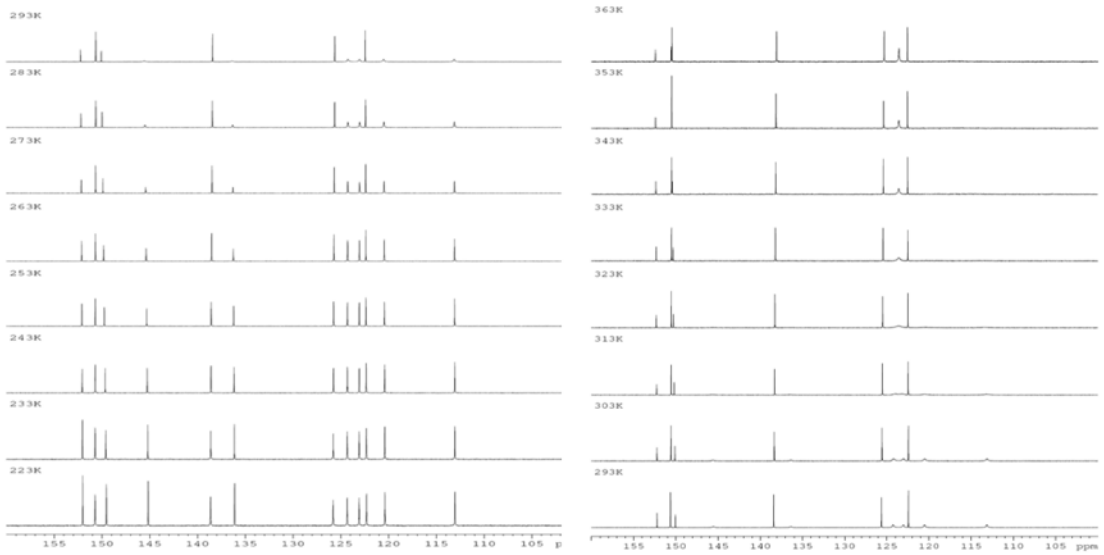

Figure 3. Variable-temperature ^{13}C-NMR of BIP. (Left) low temperature, (Right) high temperature

3. Results and Discussion

3-1 ^{1}H-NMR spectrum analysis

The C_5-C_6 bond is a single bond of 2-(pyridin-2-yl)-1H-benzo[d]imidazole. At the low temperature, single bond would not free rotate but compose stable comformational molecule（Figure 1）. In Figure 2 (in left), it depicts that the characteristic of variable-temperature of ^{1}H-NMR at low temperature. When the temperature below 263K, 2-(pyridin-2-yl)-1H-benzo[d]imidazole was a stable comformational molecule. The spectra of ^{1}H-NMR is listed as follows:

8.82ppm (H_1,d), 8.51ppm (H_4,d), 8.11ppm (H_3,dd), 7.86 ppm (H_{11},d), 7.71ppm (H_8,d), 7.60ppm, (H_2,dd), 7.38 ppm, (H_{10},dd), 7.31ppm (H_9,dd).

In Benzylimidazole, H_{11} and H_{10} were located at down field but H_8 and H_9 at up field for N_1 is an electron-donating amine group and N_2 is electron-withdrawing imine group. So H_8 and H_9 have relative high electron density compares to H_{11} and H_{10} which located at down field.

As the temperature rises to 283K, the single bond of C_5-C_6 starts to rotate slowly. The activation rotation-energy is strong enough to make the chemical-shift of H_9 and H_{10} being overlapped and leads to a phenomenon of broad (Figure 2). According to Gutowsky-Holm equation ($\Delta G = 0.00457 T_C \left(9.97 + \log\left(\frac{T_C}{\Delta\delta} \right) \right)$, coalescence temperature (*Tc*) [7] is the combination temperature of 2 peaks where $\Delta\delta$ is the difference between the two peaks as the chemical-shift. The coalescence temperature of H_9 and H_{10} is located at 283K. It activation rotation-energy is 12.69 kcal/mole. However, at this temperature, H_8 and H_{11} can not be distinguished.

As the temperature rises to 303K, the speed of rotation starts to increase. It makes the chemical-shift of H_8 and H_{11} being overlapped. (As Figure 2 (Right) is high variable temperature of ^{1}H-NMR). Here the activation energy of rotation is 15.2kcal/mole. So 303K should be the coalescence temperature of H_8 and H_{11}. $H_{9\text{-}10}$ and $H_{8\text{-}11}$ intensity would be enhanced as the temperature goes up. The H of pyridine group may not even be affected into change on benzylimidazole group at 353K. When the temperature goes up to 363K, the broad are appeared of pyridine group. The observation results should be affected on the fast rotation of Benzylimidazole group. Because of the limited NMR machine, we are only to be able to work up to 363K.

3-2 ^{13}C-NMR spectrum analysis

A stable conformational molecule has been formed at low temperature. Figure 3 (Left) shows the 13C-NMR spectrum at low variable temperature. Temperature control is from 223K to 293K. When the temperature is 223K, the spectrum of 13C-NMR is as follows:
151.9ppm(C_5), 150.5ppm(C_1),149.2ppm(C_6), 144.9ppm(C_{12}), 138.3ppm(C_3),135.8ppm(C_7), 125.5ppm(C_4), 124.0 ppm(C_{10}), 122.8 ppm(C_9), 122.0ppm(C_2),120.1 ppm(C_{11}), 112.8ppm(C_8).

As in Figure 3 (Left), C_{11} and C_{10} are in down field but C_8 and C_9 are in up filed. As the temperature rises from 223K to 293K, the intensity of C (C_8, C_{11}, C_9, C_{10}, C_7, C_{12}, C_6) is reducing in benzylimidazole group. However, the reducing rate of C_6 is relatively less than other locations of C. The effect from rotation to the C_6 is thus smaller because it is the pivot point of rotation. From the spectrum of high variable temperature of ^{13}C-NMR (As figure 3 Right), we could know the coalescence temperature is located at 313K of benzylimidazole group. By solving Gutowsky- Holm equation, rotation of C_9 and C_{10} in benzylimdazole group is about 14.4kcal/mole. Moreover, the intensity peaks of C_8, C_{11}, C_7, C_{12} start getting broad at 293K, and the peak

disappeared at 313K. Even when the temperature goes up to 363K, the peaks of C_8, C_{11}, C_7, C_{12} are all invisible. The chemical-shift of C_8, C_{11}, C_7, C_{12} aparts too far to be combined into a new peak at 363K. In contrary, the chemical-shift of C_9, C_{10} is less apart from each other. Therefore, a new peak has been combined at 313K and its intensity is increased by raising temperature. The chemical-shift of C_6 would be moved to downfield when the density of peak was affected by raising temperature. The chemical-shift of C_6 is the same as C_1 at 353K, but being more downfield at 363K. The N of pyridine and H of imidazole ring would be made strong interaction with each other which may cause part of N carrying with positive charges. However, the electron density of C_6 increases for the part of N_1- C_6-N_2 carrying with negative charge and causing chemical-shift of C6 at up field. But the rotation rate goes up as the temperature rising and some parts of negative charges fell over slowly on N_1 and N_2. C_6 carrying with negative charge can turn into quaternary-C from tertiary-C. Meanwhile, the chemical-shift of C_6 would have moved toward downfield.

4. Conclusions

The 2-(pyridin-2-yl)-1H-benzo[d]imidazole was synthesized and we found the lowest coalescence temperature under 283K and activation rotation-energy was 12.69kcal/mole. The investigation turns out that the compounds 2-(pyridin-2-yl)- 1H-benzo[d] imidazole potentially at 283K can be easy bonded with DNA.

References

1. Bailly, C.; Chessari, G.; Carrasco, C.; Joubert, A.; Mann, J.; Wilson, W. D.; Neidle, S. Sequence-specific minor groove binding by bis-benzimidazoles: water molecules in ligand recognition. Nucleic Acids Res. 2003, 31, 1514-24.
2. Le Sann, C.; Baron, A.; Mann, J.; van den Berg, H.; Gunaratnam, M.; Neidle, S. New mustard-linked 2-aryl-bis-benzimidazoles with anti-proliferative activity. Org. Biomol. Chem. 2006, 4, 1305-12.
3. Seaton, A.; Higgins, C.; Mann, J.; Baron, A.; Bailly, C.; Neidle, S.; van den Berg, H. Mechanistic and anti-proliferative studies of two novel, biologically active bis-benzimidazoles. Eur. J. Cancer. 2003, 39, 2548-55.
4. Joubert, A.; Sun, X. W.; Johansson, E.; Bailly, C.;
5. Mann, J.; Neidle, S. Sequence-selective targeting of long stretches of the DNA minor groove by a novel dimeric bis-benzimidazole. Biochemistry. 2003, 42, 5984-92.
6. Peng, X.; Wu, Y.; Fan, J.; Tian, M.; Han, K. Colorimetric and ratiometric fluorescence sensing of fluoride: tuning selectivity in proton transfer. J. Org. Chem. 2005, 70, 10524-31.
7. Samuel H. Cellman, Gregory P. Dado, Cui-Bai Liang, and Bruce R. Adam, *J. Am. Chem. soc*. 1991, *113*, 1164-1173
8. Lukehart, C. M. Fundamental Transition Metal Organomentallic Chemistry; Wadsworth Inc, Belment, California, 1985. P196.

Reliability of Wireless Body Area Networks used for Ambulatory Monitoring and Health Care

Ali Peiravi

Department of Electrical Engineering, School of Engineering, Ferdowsi University of Mashhad

Mashhad, IRAN

Received November 30 2009

Abstract: Ambulatory monitoring and health care using wireless sensor networks is an active area of applied research. The general network topology used for wireless body area networks is the star topology with the sensor nodes sending their data to a central processing node for data fusion. Reliability of these networks is very important since they deal with human life. Reported applications have had performance and reliability problems. In this paper, several reported applications of wireless body area networks are reviewed and the reliability of a sample WBAN is computed. [Life Science Journal 2009;6(4):5-14]. (ISSN: 1097-8135).

Keywords: Reliability, wireless body area network, ambulatory monitoring, MEMS sensors

Introduction

Measurement of human position, balance, posture, orientation and body status is not only of interest to the medical scientists but also of importance in the entertainment field for computer generated especial effects. The complexities of motion analysis and the various parameters involved in the estimation or measurement of body position and orientation usually require the use of a complex set of wireless sensor nodes in the form of a wireless body area network and including accelerometers, gyroscopes, magnetometers, etc. plus the application of data fusion. In some applications, estimation may require the inclusion of some form of a Kalman filter or a particle filter.

Data fusion may be defined as the use of techniques to combine data from multiple sources and gather that information in order to achieve inferences that are more efficient and potentially more accurate than if they were achieved by means of a single source. There are various fusion processes that are usually described as low, intermediate or high level that depend on the processing stage at which data fusion takes place (Mandic et al. 2005).

In low level data fusion several sources of raw data are combined to produce new raw data that is expected to be more useful than the inputs. In intermediate level data fusion that may also be called feature level fusion, various features are combined into a feature map that may then be used by further processing. High level data fusion usually refers to a situation where decisions coming from several experts are fused together. These include voting methods, statistical methods, fuzzy logic, etc.

Another potential application of data fusion is in capturing motion. Such areas as interactive game and learning, animation, film special effects, health-care and navigation may be named. Human motion

Corresponding to: ali_peiravi@yahoo.com,
Dr. Ali Peiravi

capture techniques using multiple high resolution cameras in especial studios are highly costly and complex. With the recent developments in MEMS technology, micro inertial sensors-on-hip (MMocap), low cost real-time human motion capture systems have become possible.

Earlier works

An early application of ambulatory measurements was reported by Tanka et al. (1994) for long term monitoring of posture. They argued that human postures such as standing, sitting, lying, walking, etc. may be estimated from the angles corresponding to gravitational direction in three portions of the body, namely the chest, the thigh and the legs which may be measured using tri-axial accelerometers as shown in Fig. 1.

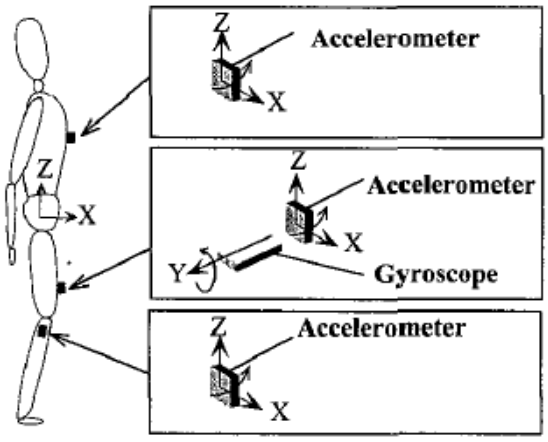

Figure 1. Accelerometers and gyroscope for measuring body posture and walking speed adopted from Motoi et al. (2003).

The angles in question may be obtained from the low frequency signals of these accelerometers. Later on, Motoi et al. (2003) suggested the addition of a gyroscope on the thigh for measuring walking speed whereby the angular change in the saggital plane is obtained by integrating the gyroscope's signal during walking. They concluded that fairly good results with a reasonable degree of accuracy may be obtained for walking speeds of less than 0.6m/s.

What has caused major progress in this area in recent years is mainly due to the developments in wireless sensor networks, nanoelectronics, MEMS technology and advances in data fusion. Solaiman et al. (1999) presented a monosensor/multiple source data fusion system for the detection of the esophagus in ultrasound images where the authors describe an approach in which various features extracted from the image are first combined using fuzzy processing and fuzzy reasoning methods. Models of the underlying physical image formation process were also used for feature extraction.

Sensors

Recent technological advances in sensors, low-power integrated circuits, and wireless communications have enabled the design of low-cost, miniature, lightweight, intelligent physiological sensor platforms that can be seamlessly integrated into a wireless body area network.

Accelerometry may be used as sensors for monitoring human movements. They have been used to monitor a range of different movements, including gait, sit-to-stand transfers, postural sway, falls, and various forms of physical activity. The accelerations generated during human movement vary across the body and depend on the activity being performed. Their magnitude usually increases from the head to the ankle with the largest value in the vertical direction. Running produces the greatest magnitude of acceleration in the vertical direction of 8.1–12.0 g at the ankle, up to 5.0 g at the low back and up to 4.0g at the head. Accelerations up to 8.1g at the angle are produced during walking down stairs. Other

activities such as trampoline jumping, walking up stairs, level walking and cycling produce acceleration up to 7.0g at the ankle during trampolining, 7.4 g walking up stairs and 2.9–3.7 g during level walking. The upper body accelerations in the vertical direction have been found to range from -0.3 to 0.8g during walking, whereas horizontal accelerations range from -0.3 to 0.4g at the low back and from −0.2 to 0.2g at the head.

Mathie et al. (2004) reviewed the use of accelerometer-based systems in each of these areas and present an integrated approach in which a single, waist-mounted accelerometry system is used to monitor a range of different parameters of human movement in an unsupervised setting.

Nyan et al. (2004) presented a comparison of experimental results for sensors mounted on different locations on the human body and different sensitivity in the usage of MEMS accelerometers based on the eigenvector-based signal identification algorithm for multi-dimensional signal identification related to ambulatory daily activities. They used ADXL105 single axis accelerometers and a Kistler 8392B capacitive silicon micromachined 3-D accelerometer. The outputs of the accelerometers were sampled at 256HZ and then filtered using a 50Hz cutoff low pass digital filter. Their main goal was to extract features from the signals in order to identify daily human activities.

Information management for critical care monitoring is a very difficult task and medical staff are often overwhelmed by the amount of data provided by the increased number of specific monitoring devices and instrumentation, and the lack of an effective automated system. Arrhythmia detection produces a large amount of undesirable alarms. Hern´andez et al. (1999) presented a multisensor/multisource data fusion scheme to improve atrial (AA) and ventricular activity (VA) detection in critical care environments. They integrated complementary data from hemodynamic processes or from the esophageal ECG (EECG) with the usual electrocardiogram (ECG) signals. They proposed a general structure based on a distributed detection scheme applicable to both VA and AA detection. VA detection makes use of the ECG and pressure signal, while AA detection is based on combining ECG and EECG.

Wireless body area networks (WBANs) promise ambulatory health monitoring for extended periods of time and near real-time updates of patients' medical records through the Internet or intranet. Jovanov et al. (2006) presented a WBAN as shown in Figure 2 utilizing a common off-the-shelf wireless sensor platform with a ZigBee-compliant radio interface and an ultra low-power microcontroller. The standard platform interfaces to custom sensor boards that are equipped with accelerometers for motion monitoring and a bioamplifier for electrocardiogram or electromyogram monitoring. They used TinyOS operating system to develop the software modules for on-board processing, communication, and network synchronization.

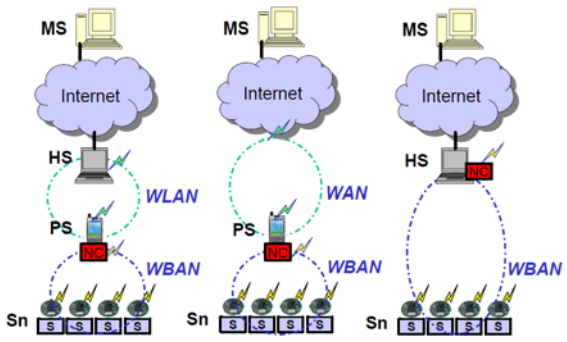

Figure 2. The Wireless Body Area Network (WBAN) for ambulatory monitoring adopted from Jovanov et al. (2006)

Dong et al. (2007) presented a physical activity monitoring system in body sensor networks using data fusion for providing real time body status

information and identifying body activities. The data collected from several accelerometer sensors placed on different parts of the body were fused to identify and track physical activity. They used Kalman filter, hidden Markov model, and biaxial accelerometers. When the accelerometers are placed on the thigh, the flexion angle of the thigh would be the angle between the accelerometer and the direction of gravity as shown by θ in Fig. 3. Thus the swing velocity or the angular velocity would be $v = \frac{d\theta}{dt}$

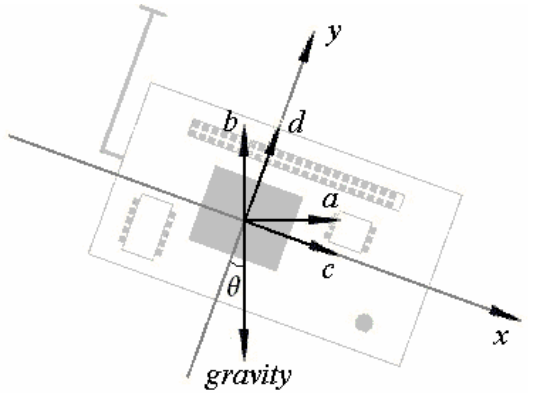

Figure 3. The variables involved in the accelerometer adopted from Dong et al. (2007)

They applied this system to monitoring and identifying daily activities in laboratory and comparatively intensive activities in a gym room with the performance evaluation done based on video. They used data fusion at a higher level by setting up an activity description table where the parameters involved in deciding what activity each body part is involved in are tabulated. For example, for the thigh, they have included flexion angle, dynamic energy, periodicity of 0.5-2 Hz and cycling hidden markov model state are listed. Comparative results indicate that body status of daily activities can be estimated with good accuracy in real time, and can be measured with a high degree of accuracy with a short system latency using a Kalman filter, discrete fourier transform and hidden markov model.

Iso-Ketola et al. (2008) proposed a wearable measurement system called HipGuard for patients recovering from a hip replacement operation. HipGuard, should be used at home during the recovery period of 8 to 12 weeks after surgery. It measures the posture and monitors the load put on the operated leg using seven wireless posture sensor nodes for measuring the orientation of the hip and the legs, and a wireless load sensor node for measuring the load put on the operated leg. An audio signal or a haptic vibration is used to inform the patient in case the position of the operated hip or the load put on the operated hip approaches previously set limits.

Small size and low power consumption are the main requirements in these systems. The orientation measurements are done in the posture sensor nodes using accelerometers, magnetic sensors and gyroscopes as shown in Figure 4.

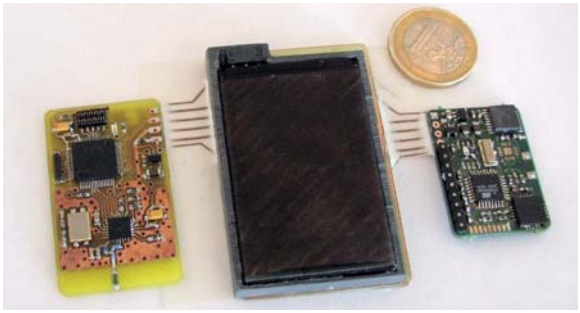

Figure 4. The electronic circuits used in the posture sensor node adopted from Iso-Ketola et al. (2008)

The load sensor nodes are capacitive with a self restoring collapsible insulator material placed in the insole of the patient's shoe on the operated side. Since it is difficult to measure the whole force that is directed to the foot, measurements from two selected areas under the heel and the ball of the foot are fused together to obtain an estimate. The only drawback of this system is that the sensors are not integrated with the patient's body and have a degree of error and the measurements do not yield the exact position of the

hip bone and the thigh bone since the movement of the muscles and joints between the skin and the skeleton produce some inaccuracy. A sampling rate of 40Hz is used in the wireless sensor network to obtain data from the posture sensor nodes to calculate the posture of the hip with each sensor node calculating its horizontal and vertical angle. Thus, there is no need to transmit the individual values of the three axes of the accelerometers and the two axes of the magnetometer to the control unit.

Zhiqiang et al. (2009) presented a motion estimation algorithm by hierarchical fusion of sensor data and constraints of human dynamic model for human upper limb motion capture. In this study, a particle filter is used to fuse 3D accelerometer and 3D microgyroscope sensor data to estimate upper limb motion recursively. Orientations of upper limb segments are presented in quaternion, which is computationally effective and able to avoid singularity problem. Since drift is an important problem in motion estimation with inertial sensors, the geometrical constraints in elbow joint are modeled and fused to the particle filter process to compensate drift and improve the estimation accuracy.

Magnetometer signals from sensors are usually affected by the presence of ferromagnetic materials or other magnetic fields since these magnetic materials disturb the local earth magnetic field and thus affect the orientation estimation. This usually poses a problem in ambulatory applications. Roetenberg et al. (2005) presented the design of a complementary Kalman filter to estimate orientation of human body segments by fusing gyroscope, accelerometer, and magnetometer signals from miniature sensors. The gyroscope bias error, orientation error, and magnetic disturbance error are all estimated in the Kalman filter. They tested the Kalman filter under both quasi-static and dynamic conditions with ferromagnetic materials close to the sensor module. The quasi-static experiments implied static positions and rotations around the three axes. In the dynamic experiments, three-dimensional rotations were performed near a metal tool case. The comparison of orientation estimated by the filter with that obtained with an optical reference system called Vicon showed accurate and drift-free orientation estimates. The average static error reported was 1.4° (standard deviation 0.4) in the magnetically disturbed experiments. The dynamic error reported was 2.6° root means square.

Dejnabadi et al. (2006) proposed a new method of estimating lower limbs orientations using a combination of accelerometers and gyroscopes. Their model was based on estimating the accelerations of ankle and knee joints by placing virtual sensors at the centers of rotation. In their technique, human locomotion and biomechanical constraints were taken into consideration. They used data fusion and fused the data of gyroscopes and accelerometers to obtain stable and drift-free estimates of segment orientation. Their method was validated by measuring lower limb motions of eight subjects, walking at three different speeds, and comparing the results with a reference motion measurement system. The results they presented were very close to those of the reference system presenting very small errors (Shank: rms=1.0, Thigh: rms=1.6°) and excellent correlation coefficients (Shank: r=0.999, Thigh: r=0.998). Their ambulatory system is portable, easily mountable, and can be used for long term monitoring.

Roetenberg et al. (2007) presented the design and testing of a portable magnetic system combined with miniature inertial sensors for ambulatory 6 degrees of freedom human motion tracking. In their study, the magnetic system consisted of three orthogonal coils as the source fixed to the body and 3-D magnetic sensors that were fixed to the remote body segments in order to measure the fields generated by the source.

Performance and Reliability of WBAN

In recent years, interests in the application of Wireless Body Area Network (WBAN) have grown considerably. A WBAN can be used to develop a patient monitoring system which offers flexibility and mobility to patients. However, there are serious performance and reliability issues in WBANs that must be addressed. The network topology that is generally used in wireless sensor networks for such

ambulatory studies is of the star configuration as shown in Fig. 5. This is because nodes usually are sensor nodes and do not need to communicate with each other. Therefore, the star topology is used and each sensor node communicates with the central node using a hub. This raises reliability questions as the hub or the central node may fail leading to total system failure. Even the communication links may perform poorly or fail . Since data fusion is used in almost all applications, even the failure of any of the sensors or the communication links would result in system failure.

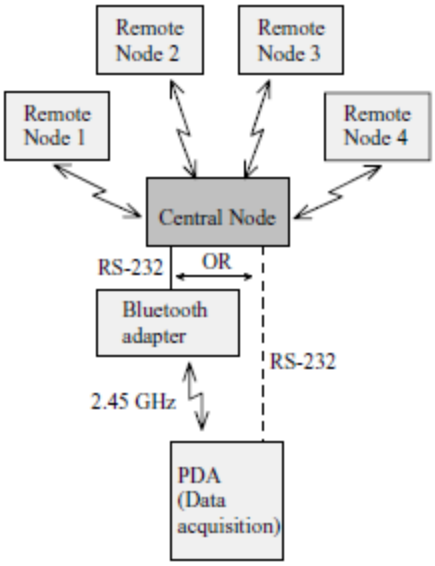

Figure 5. The general network topology used in WBAN adopted from Ylisaukko-oja et al. (2004)

Ylisaukko-oja et al. (2004) presented the implementation and practical use of an unobtrusive five-point acceleration sensing wireless body area network (WBAN) with mobile device data logging capabilities shown in Figure 5. They used TDMA based MAC protocol and RS232 for serial communications with external devices. They reported good communications performance in laboratory conditions but weaker field test performance. Their tests indicated significant losses in communication. Under laboratory conditions, they lost the remote slots from 0.31% to 3.09% in various parts of the test while in the field tests, they lost central data up to 3.84% and lost remote slots from 13.66% to 52.51%. This indicates a high degree of reliability problems especially in communications.

Various other approaches have been proposed for performance evaluation of WBAN systems. For example, Hamel et al. (2008) investigated the performance issues in wearable wireless body area sensor networks by considering various wireless technologies and platforms. They developed a Zigbee-based WBAN system with custom sensor platforms and evaluated its performance both in the laboratory and at home. They concluded that the use of a typical setup with four wireless sensor nodes with eight sensor inputs per node sampled at 100 Hz offers the most reliable radio communication performance and reliability.

Use of a WBAN allows the flexibility of setting up a remote monitoring system via either the internet or an intranet. The main advantage of WBAN is the automatic real-time collection of signals that are needed in medical treatment and healthcare. One may even go further and extend the range of services provided to remote locations using either the internet or satellite communications. Li et al. (2008) presented an experimental system comprised of a wireless body area network (WBAN) and satellite communication links to enable remote medical treatment and healthcare services. They implemented the WBAN using ultra-wideband technology and adopted multi-hop mechanism to achieve a reliable connection. By introducing satellite communication links as shown in Figure 6 it is possible to use WBAN's to perform remote health monitoring and provide remote instructions for emergency medical care in case of emergencies in isolated areas. Multi-hop mechanism of WBAN is

shown to work well and the relative delay of WBAN data delivery via satellite links is strongly dependent on the satellite link capacity.

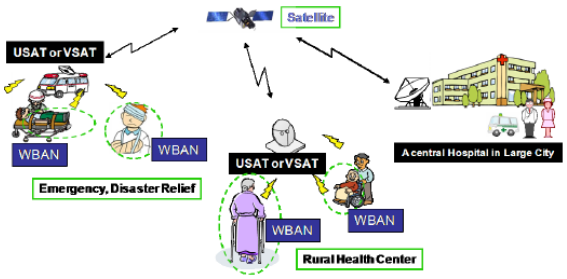

Figure 6. WBAN used in connection with satellite communications to provide remote health care monitoring and advice adopted from Li et al. (2008).

Performance of the data fusion in such applications may also be studied. For example, Similä et al. (2006) evaluated the performance of a wireless acceleration sensor network such as shown in Fig 5 in balance estimation. The test has been carried out in eight patients and seven healthy controls. The patients group had larger values in lateral amplitudes of the sensor displacement and smaller values in vertical displacement amplitudes of the sensor. The step time variations for the patients were larger than those for the controls. They used fuzzy logic and clustering classifiers and obtained promising results suggesting that a person with balance deficits can be recognized with this system. They used the SOM toolbox for clustering and the leave-one-out method to obtain membership functions for their fuzzy logic analysis.

Khan et al. (2008) studied the performance of an IEEE802.15.4/Zigbee MAC based WBAN operating in different patient monitoring environments using an OPNET based simulation model. Their results indicated that patient monitoring using WBAN over the internet could be performed from remote locations with a reasonable delay if the WBAN is not directly connected to the main hospital network via a service node, and that the multihop network should be used instead of a fixed network to optimize the transmission time.

Reliability of such networks is highly important since they deal with humans and lives may be endangered in case of failures. The estimates of failure rate and mean time to failure for the components that are typically used in WBAN systems for ambulatory monitoring are listed in Table 1 plus an indication of the source of data.

Table 1 – Estimation of failure rate and mean time to failure for common components used in WBAN

Component	$\lambda(FPMH$	MTTF (Hours)	Data Source
Accelerometer	20.3327	49181	NPRD-95
Gyroscope	45.7778	21844	NPRD-95
Magnetometer	20	50000	Honeywell
PDA (Data Acquisition Unit	200	5000	Newland PT980 Series RS232/USB
Bluetooth Adapter	1	1000000	Sena Parani Bluetooth adapter

The reliability of the common star type topology of WBAN systems may be computed based on the fact that the sensor nodes are usually all needed in the data fusion, and that all the components must work for the WBAN system to work. Therefore, the reliability of a system composed of n components would easily be estimated by computing the overall failure rate of the system as shown in (1):

$$\lambda_{WBAN} = \sum_{i=1}^{n} \lambda_i \quad (1)$$

Then the reliability of the WBAN system would be as shown in (2) assuming that the system is in its useful life period and obeying the exponential lifetime probability distribution.

$$R_{WBAN} = e^{-\lambda_{WBAN} t} \quad (2)$$

Then we can easily compute the system reliability. For example, the total failure rate for the WBAN system shown in Fig 5 adopted from Ylisaukko-oja et al. (2004) will be as indicated in Table 2 assuming that three of the sensor nodes consist of accelerometers and one is a gyroscope.

Table 2 - Estimation of the total failure rate of the WBAN shown in Fig 5.

Component	No. of components	$\lambda(FPMH)$	Total Failure Rate
Accelerometer	3	20.3327	60.9981
Gyroscope	1	45.7778	45.7778
PDA (Data Acquisition Unit	1	200	200
Bluetooth Adapter	1	1	1
Central Node	1	1	1
Total Estimated Failure Rate		$\lambda_{WBAN} = \sum_{i=1}^{n} \lambda_i =$ 308.7759	

Single failures in such systems lead to total system malfunctioning or failure. Going from star topology to a higher degree of connectivity by adopting a loop network would not solve this reliability issue with single node failure since still all the nodes have to communicate with the central processing node via a hub the failure of which would lead to total system failure. Therefore, other approaches should be pursued.

In addition to single mode failures, there is a possibility of multiple mode failures and multiple failures that makes it even harder to address the reliability concerns. Wang et al. (2010) have addressed the reliability modeling of wireless body area networks with the aim of increasing the reliability in the presence of multi-type failures, while saving energy. They classified the nodes into types with regard to their capabilities on relaying and sensing and modeled their behavior in the presence of failures such as energy exhaustion and/or malicious attacks using a semi-markov process.

Conclusion

Although a lot of progress has been reported in the application of WBAN, a lot more work should be done in improving the performance and reliability of wireless body area networks used for health monitoring and care. Topology, protocols, mix of sensors and their redundancy plus more advanced means of data or decision fusion and feature extraction are needed to make better and more reliable ambulatory monitoring and health care systems.

References

1. Dejnabadi, H.; Jolles, B.M.; Casanova, E.; Fua, P.; Aminian, K., "Estimation and visualization of sagittal kinematics of lower limbs orientation using body-fixed sensors," Biomedical Engineering, IEEE Transactions on , Vol.53, No.7, pp.1385-1393, July 2006.
2. Dong, L., Wu, J., Chen, X., "Real-time physical activity monitoring by data fusion in body sensor networks," FUSION 2007 - 10th International Conference on Information Fusion, 9-12 July 2007, pp.1-7.s
3. Hamel, M., Fontaine, R., Boissy, P., "In-home telerehabilitation for geriatric patients", IEEE Engineering in Medicine and Biology Magazine, July/August 2008, pp. 29-37.
4. Hernandez, A.I.; Carrault, G.; Mora, F.; Thoraval, L.; Passariello, G.; Schleich, J. M., "Multisensor fusion for atrial and ventricular activity detection in coronary care monitoring," IEEE Transactions on Biomedical Engineering, Vol. 46, No. 10, pp.1188-1190, Oct. 1990.
5. Iso-Ketola, P.; Karinsalo, T.; Vanhala, J., "HipGuard: A wearable measurement system for patients recovering from a hip operation", Proceedings of the 2nd International Conference on Pervasive Computing Technologies for

Healthcare 2008, PervasiveHealth 2008, pp.196-199.

6. Jovanov, E.; Milenkovic, A.; Otto, C.; De Groen, P.; Johnson, B.; Warren, S.; Taibi, G., "A WBAN system for ambulatory monitoring of physical activity and health status: applications and challenges," 27th Annual International Conference of the Engineering in Medicine and Biology Society, 2005. IEEE-EMBS 2005. pp.3810-3813, 17-18 Jan. 2006.
7. Khan, Jamil Y.; Yuce, Mehmet R.; Karami, Farbood, "Performance evaluation of a Wireless Body Area sensor network for remote patient monitoring," 30th Annual International Conference of the IEEE Engineering in Medicine and Biology Society, 2008, EMBS 2008., pp.1266-1269, 20-25 Aug. 2008.
8. Li, Huan-Bang; Takahashi, T.; Toyoda, M.; Katayama, N.; Mori, Y.; Kohno, R., "An experimental system enabling WBAN data delivery via satellite communication links," IEEE International Symposium on Wireless Communication Systems - ISWCS '08, pp.354-358, 21-24 Oct. 2008.
9. Mandic, Danilo P. et al. "Data fusion for modern engineering applications: an overview," Artificial Neural Networks: Formal Models and Their Applications - ICANN 2005, 15th International Conference, Warsaw, Poland, September 11-15, 2005, Proceedings, Part II 2005.
10. Mathie, M. J. ; Coster, A. C.; Lovell, N. H.; Celler, B. G., "Accelerometry: providing an integrated, practical method for long-term, ambulatory monitoring of human movement" Physiological measurement, Vol. 25, No. 2, April 2004, pp.R1-R20.
11. Motoi, K.; Tanaka, S.; Nogawa, M.; Yamakoshi, K., "Evaluation of a new sensor system for ambulatory monitoring of human posture and walking speed using accelerometers and gyroscope," SICE 2003 Annual Conference , Vol.2, pp. 1232-1235, 4-6 Aug. 2003, Fukui, Japan.
12. Nyan, Myo Naing; Tay, Francis Eng Hock; Koh, Teck Hong; Sitoh, Yih Yiow; Tan, Kwong Luck "Location and sensitivity comparison of MEMS accelerometers in signal identification for ambulatory monitoring," Proceedings of the 54th Electronic Components and Technology Conference, , 1-4 June 2004, Vol.1, pp. 956-960.
13. Roetenberg, D.; Luinge, H. J.; Baten, C. T. M.; Veltink, P. H., "Compensation of magnetic disturbances improves inertial and magnetic sensing of human body segment orientation," IEEE Transactions on Neural Systems and Rehabilitation Engineering, Vol.13, No.3, pp.395-405, Sept. 2005.
14. Roetenberg, D.; Slycke, P.J.; Veltink, P.H., "Ambulatory Position and Orientation Tracking Fusing Magnetic and Inertial Sensing," Biomedical Engineering, IEEE Transactions on , vol.54, no.5, pp.883-890, May 2007.
15. Roetenberg, D.; Baton, Chris, T. M.; Veltink, P.H., "Estimating body segment orientation by applying inertial and magnetic sensing near ferromagnetic materials," IEEE Trans. on Neural Systems and Rehabilitation Engineering, Vol. 15, No. 3, Sept.2007, pp. 469-471.
16. Similä, H.; Kaartinen, J.; Lindholm, M.; Saarinen, A.; Mahjneh, I., "Human balance etimation using a Wireless 3D acceleration sensor network,"Proceedings of the 28th EMBS

Annual International Conference, New York, USA, August 30-Sept 3, 2006, pp.1493-1496.

17. Solaiman, B.; Debon, R.; Pipelier, F.; Cauvin, J. -M.; Roux, C., "Information fusion: Application to data and model fusion for ultrasound image segmentation," IEEE Transactions on Biomedical Engineering, Vol. 46, No. 10, Oct. 1999, pp.1171-1175.
18. Tanaka1, S.; Yamakoshi, K.;Rolfe, P., "New portable instrument for long-term ambulatory monitoring of posture change using miniature electro-magnetic inclinometers," Medical and Biological Engineering and Computing, Vol. 32, No. 3, May 1994, pp.357-360.
19. Wang, S., IEEE, Park, J. T., "Modeling and analysis of multi-type failures in wireless body area networks with semi-markov model," to appear in IEEE Communications Letters, 2010.
20. Ylisaukko-oja, A.; Vildjiounaite, E.; Mantyjarvi, J., "Five-point acceleration sensing wireless body area network - design and practical experiences," Eighth International Symposium on Wearable Computers, 2004. ISWC 2004, Vol.1, pp. 184-185, 31 Oct.-3 Nov. 2004.
21. Zhiqiang, Z.; Zhipei, H.; Jiankang, W., "Hierarchical information fusion for human upper limb motion capture," 12th International Conference on Information Fusion, FUSION 2009, pp.1704-1711.

.

Human Cranium Dynamic Analysis

Bo Wun Huang[1], Huang Kuang Kung[1], Kuan-Yu Chang[2], Po Kai Hsu[1], Jung-Ge Tseng[1*]

1 Graduate Institute of Mechatronics Engineering, Cheng Shiu University, Kaohsiung 833, Taiwan, R.O.C. 2 Mackay Memorial Hospital Taitung Branch, Taitung, Taiwan, ROC

Received November 20, 2009

Abstract: More and more brain related illnesses such as brain tumor, cerebral hemorrhage, nasopharyngeal carcinoma, cerebral artery/vein deformity, Parkinson's disease, epilepsy, etc., can be treated through skull surgery. However, the current automation technology of craniotomy is not matured and depends on physician's personal experience and technique. It is necessary to improve the operational security and success rate by fully understand the characteristic of cranium. This research investigates the dynamic property of cranium by experimental and theoretical analysis through skull model made in polystyrene. Reverse engineering analysis is adopted to build up geometric 3D skull CAD (Computer Aided Design) model. FEA (Finite element analysis) is conducted by transferring this 3D skull CAD model into ANSYS (FEA package) acceptable model. Experimental vibration measurement is obtained for the polystyrene skull model and the first few measured natural frequencies are obtained. Measured damping feature of the cranium model is discussed as well and together with other dynamic characteristics to provide complete information about the skull for medical doctor reference. [Life Science Journal. 2009; 6(4): 15– 22] (ISSN: 1097 – 8135)

Keywords Cranium vibration; dynamic characteristic; natural frequency; reverse engineering; brain related illness.

1. Introduction

Cranium is the hardest part and protects the most important part, brain – the commanding center, of human beings. Cranial neurosurgery need to treat patients suffering from brain lesions, traumatic brain injury (TBI), stroke, brain neuroglia tumor, cerebral hemorrhage, nasopharyngeal carcinoma, cerebral artery/vein deformity, etc., via craniotomy process. This treatment paradigm is costly, carries the risks associated with infection, additional surgery, and may cause cosmetic deformities. Owing to fast development of microsurgery, robotics are largely used in skull base surgery [1], minimally invasive surgery (a local anaesthetic, smaller cut, shorter operation time) becomes trend of brain surgery which allow doctors to remove the tumor, stop cerebral hemorrhage, and also surgically implant deep brain stimulators for the treatment of Parkinson's disease, epilepsy and cerebellar tremor. The procedure is also widely used in neuroscience for extracellular recording, brain imaging, and for neurological manipulations such as electrical stimulation and chemical titration. There exist high risks for the patient when proceeding brain surgery no matter how advanced the technology is [2]. The craniotomy is still one of the most complicate and difficult surgery. It is suggested to reduce the risk as much as possible by fully understanding the dynamic characteristic of human cranium for selecting the best surgery method, position, and cutting parameter of the skull.

Khalil et al.[3] conduct an experimental investigation to identify the resonance frequencies of two kinds of freely vibrating human dry skulls and extrapolate their results to living skulls taking into account of known and estimated differences in mechanical properties. Hakansson et al. [4] investigate of the free damped natural frequencies of human skull in vivo and damping coefficient is reported. Charalambopoulos et al. [5] deal with the free vibrations of the 3D viscoelastic human skull. Brantberg et al. [6] investigate the mechanisms for skull tap induced vestibular evoked myogenic potentials (VEMP) and found that skull tapping causes both skull vibration and head acceleration.

Yue et al. [7] analyze the strain of the thin-walled shell by the stress-strain calculation of a human skull with changing ICP (Intracranial pressure). Many patients exhibit excessive localized wear and tear of the

*Correspondence: james.tseng@csu.edu.tw
Dr. Bo Wun Huang

temporomandibular joint, due to the forces that develop in the human joint during function exceed tissue tolerance. Hashimoto and Clark [8] conduct experimental measurement of vibration transmission between the cranium and mandible in healthy humans during variations of jaw position. Kerr and Adams [9] find out cranial base and jaw relationship. Several papers [10~12] discuss endodontic evaluation, facial types, facial relationships, respectively. [10~12]

Lin and Tsai [13] address a method to construct 3D finite element model by using PA (Posterior to Anterior) view and lateral view of cephalographs to compensate the deficient traditional cephalometry analysis. Su and Chang analyze the stresses in post-restored teeth by finite element method and the variables evaluated were loading modes, shapes, diameters, materials of the posts. Similar approach has been down by others. [14~16]

The purpose of this research is to find basic dynamic characteristic of human cranium such as natural frequencies, damping ratios, mode shapes, etc. and to increase the success rate during skull surgery. Reverse engineering is performed to obtain computer 3D diagram of the polystyrene skull model. This computer 3D model is then fed into ANSYS FEM (Finite Element Method) software [17] to carry out dynamic analysis. First few fundamental natural frequencies were measured by vibration test and compared with FEM results.

2. Reverse engineering (RE) nite element analysis

As computer-aided design (CAD) has become more popular, reverse engineering (RE) has become a viable method to create a 3D virtual model of an existing physical part for use in 3D CAD, CAM, CAE or other software.[18] The reverse-engineering process involves measuring an object, reconstructing it as a 3D model, manufacturing the mold and product. The physical object can be measured using 3D scanning technologies like CMMs (Coordinate Measuring Machine), laser scanners, structured light digitizers or computed tomography. The measured data alone, usually represented as a point cloud, lacks topological information and is therefore often processed and modeled into a more usable format such as a triangular-faced mesh, a set of NURBS surfaces or a CAD model. Reverse engineering is also used by businesses to bring existing physical geometry into digital product development environments, to make a digital 3D record of their own products or to assess competitors' products. It is used to analyze, for instance, how a product works, what it does, and what components it consists of, estimate costs, and identify potential patent infringement, etc.

A low error, fast measuring speed, non-contact laser scanner, the ATOS optical measuring machine manufactured by GOM, Germany (shown in Figure 1), is adopted to measure the complex 3D profile of polystyrene skull model (shown in Figure 2).

Figure 1. ATOS non-contact laser scanning system

Figure 2. Polystyrene skull model

The ATOS system is composed by an optical grating projector and two industrial CCD cameras. It digitizes three dimensional work pieces by projecting a grid onto the part and using two cameras, in two different positions, at two different angles with respect to the work piece to triangulate the location of the intersection points on the grid. The point locations triangulated by the

ATOS system may then be stored as a point cloud (over half million points) and may also be transformed into facet bodies, such as STL polygon meshes, by software components supplied by GOM or third party. The resulting STL diagram from ATOS system which reconstructs the complex 3D cranium model in electronic file is shown in Fig. 3.

Figure 3. 3D Computer cranium model reconstructed by ATOS system

3. Finite element analysis

3.1. Fundamental theory

The equation of motion of the skull can be derived via finite element method by apply Lagrange equation as follows:

$$\frac{d}{dt}\left(\frac{\partial L}{\partial \dot{\vec{Q}}}\right)-\left(\frac{\partial L}{\partial \vec{Q}}\right)+\left(\frac{\partial R}{\partial \dot{\vec{Q}}}\right)=\{0\} \qquad (1)$$

where, L=T-V is Lagrange function, T and V are kinetic and potential energy of the skull model, respectively. R is dissipation function. $\vec{Q}$ and $\dot{\vec{Q}}$ represent displacement and velocity of the skull model. The discretized equation of motion of the skull structure is:

$$[M]\,\ddot{\vec{Q}}(t)+[C]\,\dot{\vec{Q}}(t)+[K]\,\vec{Q}(t)=\vec{P}(t) \qquad (2)$$

where, $\ddot{\vec{Q}}$ is the acceleration vector of the node of skull model. For an undamped, no external force linear system, the equation of motion becomes:

$$[M]\,\ddot{\vec{Q}}(t)+[K]\,\vec{Q}(t)=0. \qquad (3)$$

The displacement of this linear undamped linear system is in the complex plane and can be assumed as follows:

$$\vec{Q}=\{\phi\}e^{i\omega t} \qquad (4)$$

where, $\{\phi\}$ and ω are the mode shapes and the natural frequencies of the skull structure, respectively. Substitute equation (4) into equation (3), one can get:

$$(-\omega^2[M]+[K])\{\phi\}=0. \qquad (5)$$

Solve for the eigenvalue and eigenvector in equation (5) can get natural frequencies ω and displacement vectors (mode shapes) $\{\phi\}$ of the skull structure.

3.2. FE model establishment and analysis

The reconstructed 3D Computer cranium model by ATOS system is imported into ANSYS FE software to build up the FE model. Standard procedure is followed to select elements, cut off elements, set up material properties (shown in Table 1) and boundary conditions, etc. Around 120,000 elements are built and the full scale 3D skull FE model is shown in Figure 4.

Table 1. Material property of Polystyrene

Material property	value
Young's modulus	1.14 GPa
Density	1,380 Kg/m^3
Poisson's ratio	0.3

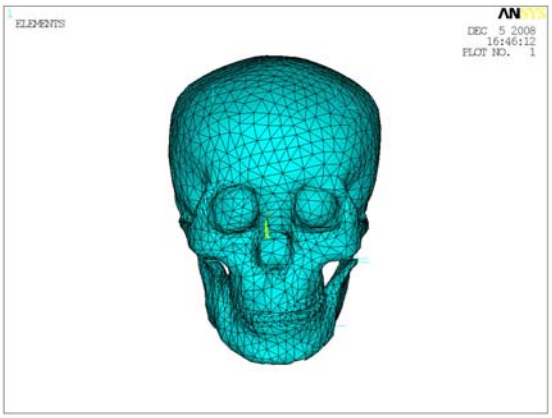

Figure 4. 3D FE model with around 120,000 elements

Before go into detail of analysis, the element numbers convergence test has been done and 100,000

elements are sufficient and used for carry out the full scale vibration analysis for the 3D skull system. First four modes of the skull system are observed from the ANSYS results and their degenerated natural frequencies are around 1500 Hz (shown in Table 2) with different mode shapes as shown in Figure 5 ~ Figure 8.

Table 2. First four theoretical frequencies of skull model

Frequencies / Mode	Hz
First mode	1,500
Second mode	1,500
Third mode	1,501
Fourth mode	1,501

Note that the fourth mode shape shown in Fig. 8 has vibration amplitude on the back of the skull so it can not be seen clearly at front view.

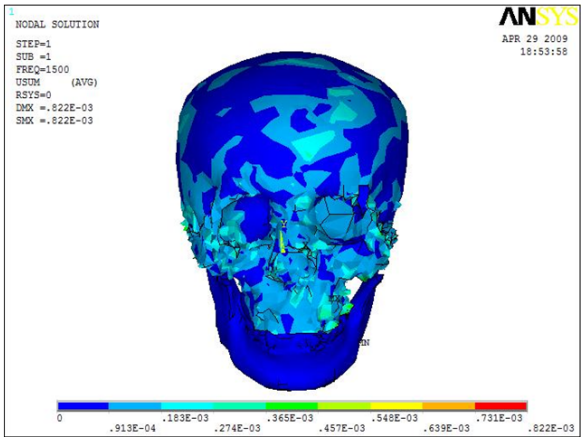

Figure 5. First mode of 3D skull model

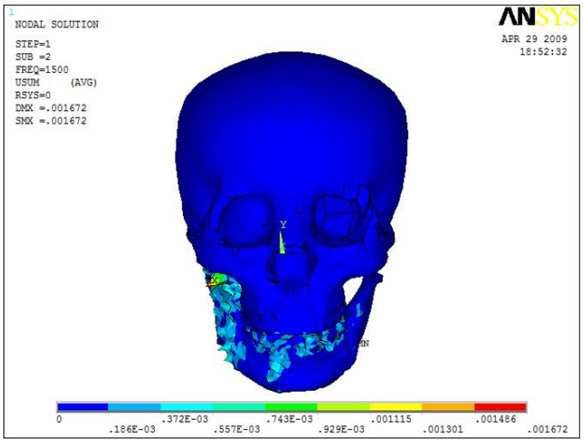

Figure 6. Second mode of 3D skull model

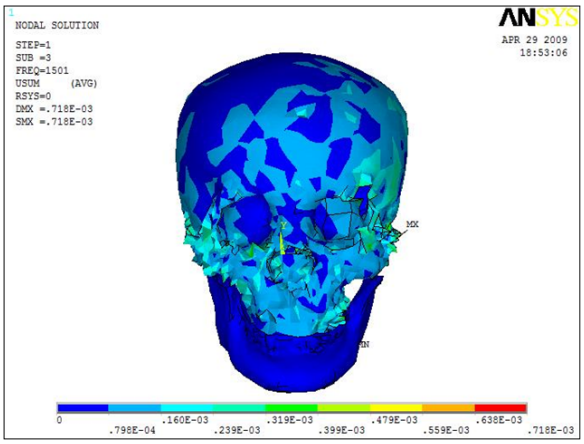

Figure 7. Third mode of 3D skull model

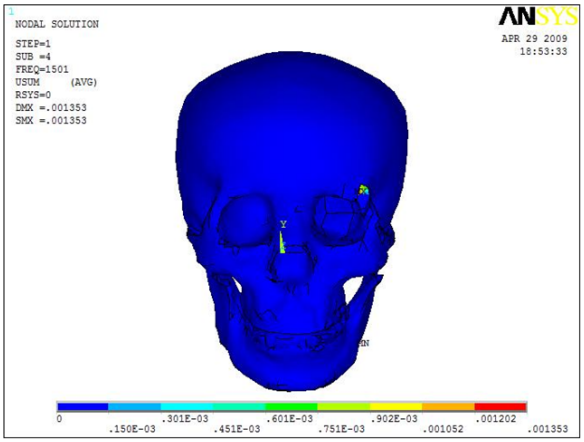

Figure 8. Fourth mode of 3D skull model

4. Experimental analysis

The experimental set up is shown in Fig. 9 to measure the vibration frequency, time response, and damping ratio, etc. for the Polystyrene skull model. The skull model is fixed at the center near cerebellum position. An impact hammer and an accelerometer are connected to channel 1 and 2, respectively, of HP 35670A spectrum analyzer. The impact hammer hits on different positions: top, front, back, right, and left of the Polystyrene skull model in sequence during the measurement and the micro accelerometer is fixed on the top of the skull. Combine the hammer's input signal with the micro accelerometer's output response signal of the Polystyrene skull model, the natural frequencies and time responses are obtained by HP analyzer. The frequency

spectrums when the impact hammer is hitting on top, right, and back of the Polystyrene skull model are shown in Fig. 10~12. The measured fundamental frequencies are 1,410 Hz, 1,790 Hz, 1,888 Hz, 1,984 Hz, 2,320 Hz, 3,792 Hz, etc., as shown in Table 3.

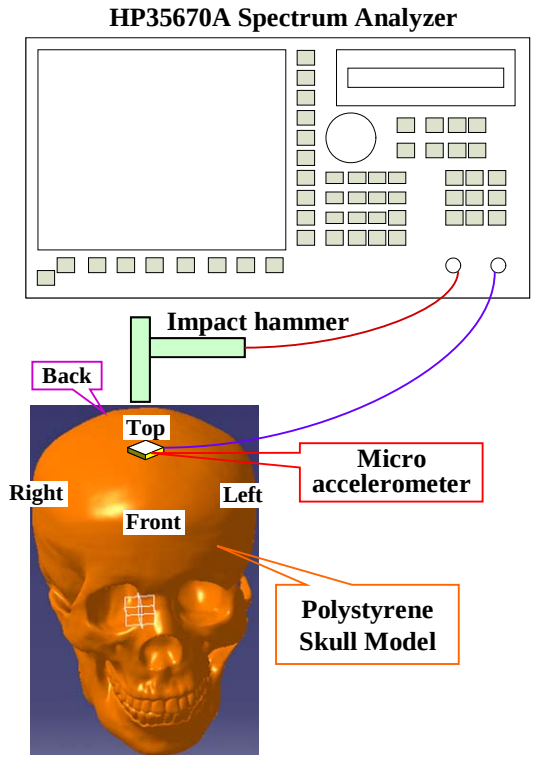

Figure 9. Experimental set up of the Polystyrene skull model

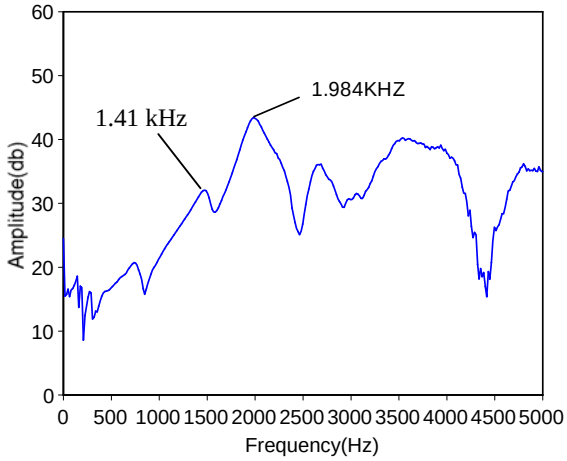

Figure 10. Frequency spectrum when hits on the top of the skull model

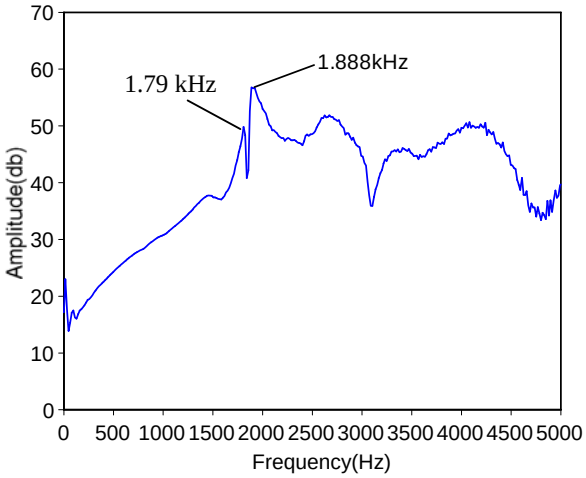

Figure 11. Frequency spectrum when hits on the right of the skull model

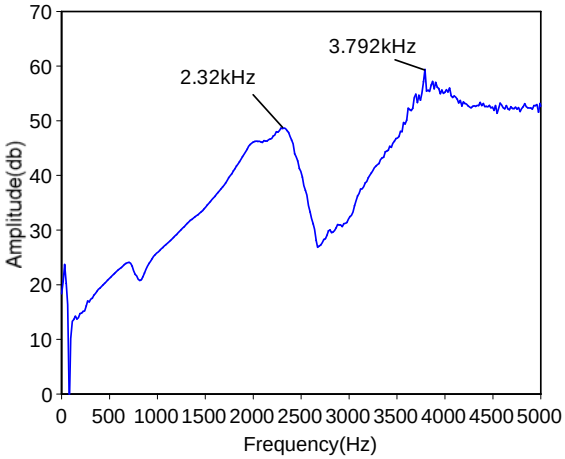

Figure 12. Frequency spectrum when hits on the back of the skull model

Table 3. First six measured frequencies of skull model

Mode \ Frequencies	Hz
First mode	1,410
Second mode	1,790
Third mode	1,888
Fourth mode	1,984
Fifth mode	2,320
sixth mode	3,792

These spectrum figures (Figures 10~12) indicate when hit on different positions, some frequencies will show up and some don't due to complicated distribution

of the nodal lines or circles on the 3D skull model. In other words, when the input excitation or output response points are on or very near to a nodal line or circle, the specific mode will be suppressed and can not shown as a peak value in the frequency spectrum. Therefore the purpose of hitting different positions of the skull is to find as much modes as possible for a complete experimental result.

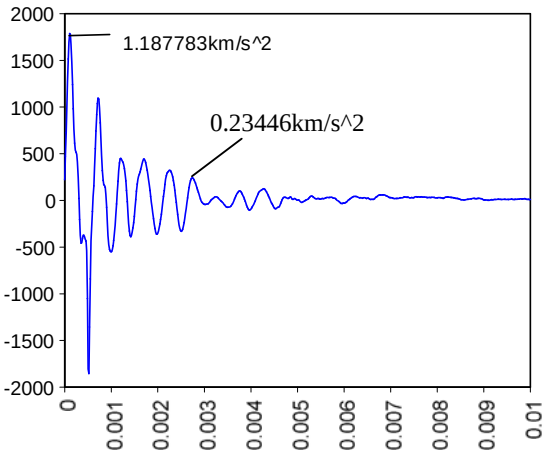

Figure 13. Time response when hits on the top of the skull model

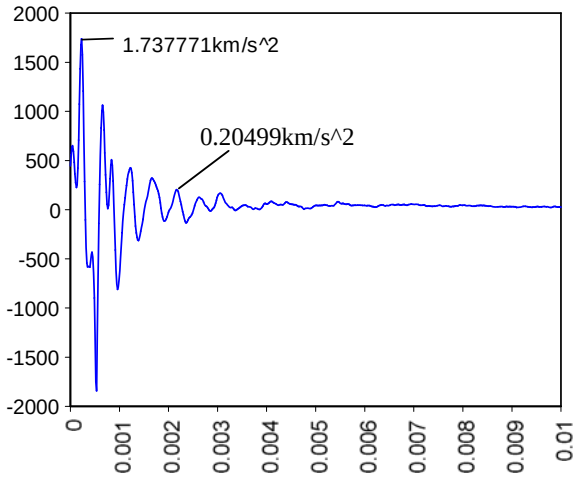

Figure 14. Time response when hits on the back of the skull model

Measured time responses are obtained for the impact hammer hits on different positions: top, front, back, right, and left of the polystyrene skull model in sequence while accelerometer fixed on the top of the skull model. The time responses when impact hammer hits on the top and back are shown in Fig. 13 and Fig. 14.

5. Discussion

The FEM analyzed and measured fundamental frequency of the skull is compared in Table 4. It can be seen that the FEM analyzed and measured first frequency are 1500 Hz and 1410 Hz, respectively. The errors between them are about 6.4% and falls into practical acceptable range between theoretical predict and experimental results.

Table 4. Comparison between FEM analyzed and measured fundamental frequency of skull model

Mode / Frequency	First mode
FEM analyzed (Hz)	1500
Measured (Hz)	1410
Error (%)	6.4%

Damping ratio (ζ) of the polystyrene skull model can be obtained by employing the following equation:

$$\zeta = \frac{\delta}{\sqrt{(2\pi)^2 + \delta^2}} \tag{6}$$

where $\delta = \frac{1}{m}\ln\left\{\frac{X_1}{X_{m+1}}\right\}$. X_1 is the first peak and X_{m+1} is the $(m+1)^{th}$ peak in time response diagram, m is an integer and represents the number of cycle times.

By substituting X_1=1.188, X_{m+1}=0.2345, m=5, etc., from Fig. 13, into equation (6), the measured damping ratios ζ_1 = 0.051. Similarly, by substituting X_1=1.738, X_{m+1}=0.205, m=5, etc., from Fig. 14, into equation (6), the measured damping ratios ζ_2 = 0.055. All six time responses obtain from different hitting position by the impact hammer are calculated in the same manner and the average damping ratio of the skull is ζ_{avg} = 0.053.

6. Summary

This research investigates the dynamic characteristic of a polystyrene skull model. The aim for this research field is to understand the vibration phenomena of the polystyrene first and then use this model to analyze the normal modes and related

parameters of real human cranium in the future. Therefore, the result of this research is quite useful for physician's reference.

Several aspects are discovered during this research and listed as follows:

1. Reverse engineering is a very useful and effective way to rebuild a 3D complex geometry and allow the researchers to continue proceeding with the real analysis work.
2. FE analysis is performed according to the large amount of geometric data point obtained from ATOS system. The error between the first natural frequency of the polystyrene skull model obtained from both FEM solution and measurement is about 6.4%. The promising result shows that the approach model proposed by this paper is on the right track and can be further expanding of its usage.
3. Measurements of different positions in the experiment is a necessary procedure to find out complete natural frequencies in the spectrum.

Acknowledgements

This work was coworked with Dr. Wang in xx hospital and finished in Vibration and Noise Laboratory Cheng Shiu University. The author would like to thank the National Science Council, Taiwan, Republic of China, for financially supporting this research through Grant NSC95-2212-E-230-006.

References

1. B. Plinkert, P.K. Plinkert, Robotics in skull base surgery, International Congress Series, 2001, 1230: 138–142.
2. Melville J. Da Cruz, Paul Fagan, MD, Marcus Atlas, and Celene McNeill, Drill induced hearing lost in the nonoperative ear, Otolaryngology- Head and Neck Surgery, 1997, 117:555-558.
3. T. B. Khalil, D. C. Viano, D. L. Smith, Experimental analysis of the vibrational characteristics of the human skull, Journal of Sound and Vibration, 1979, 63 (3): 351-376.
4. B. Håkansson, A. Brandt and P. Carlsson, Resonance frequencies of the human skull in vivo, Journal of Acoustic Society of America, 1994, 95 (3):1474–1481.
5. A. Charalambopoulos, D. I. Fotiadis, C. V. Massalas, Free vibrations of the viscoelastic human skull, International Journal of Engineering Science, 1998, 36 (5/6): 565-576.
6. Krister Brantberg, Lennart Löfqvist, Magnus Westin, Arne Tribukait, Skull tap induced vestibular evoked myogenic potentials: An ipsilateral vibration response and a bilateral head acceleration response? Clinical Neurophysiology, 2008, 119:2363–2369.
7. Xianfang Yue, Li Wang, Feng Zhou, Amendment on the strain measurement of thin-walled human skull shell as intracranial pressure changes, Journal of University of Science and Technology BeiJing, 2008, 15 (2):202-208.
8. Kazuyoshi Hashimoto, Glenn T. Clark, The effect of altering jaw position on the transmission of vibration between the skull and teeth in humans, Archives of Oral Biology, 2001, 46:1031–1038.
9. W. J. S. Kerr and C.P. Adams, Cranial base and jaw relationship", American Journal of Physical Anthropology, 1998, 77:213-220.
10. Kuo-Chih Su, Chih Han Chang, Biomechanical evaluation endodontic posts-finite element analysis, 2006. Master Thesis, National Cheng Kung University, Tainan, Taiwan, R.O.C.
11. V. A. Sassouni, A classification of skeletal facial types, American Journal of Orthodontics and Dentofacial Orthopedics, 1969, 55: 109-123.
12. W. B.Downs, Variations in facial relationships: their significance in treatment and prognosis, American Journal of Orthodontics and Dentofacial Orthopedics, 1948, 34: 812.
13. Chi Shiun Lin, Chin Chong Tsai, The morphological research on the construction of mandible finite element model using 2D cephalomatric images, Master Thesis, Tunghai University, 2004.
14. B. H. Grayson, N. Weintraub, F. L. Bookstein, and J. G. McCarty, A Comparative Cephalometric Study of the Cranial Base in the Craniofacial Anomalies: Part I: Tensor Analysis. Cleft Palate Craniofacial Journal, 1985, 22: 75-86.

15. A. F. Ayoub, Strirrups Dr., The practicability of finite-element analysis for assessing changes in human craniofacial morphology from cephalograph, Archives of Oral Biology, 1993, 38: 679-683.

16. G. D. Singh, J. A. Jr. McNamara and S. Lozanoff, Thin-plate spline analysis of the cranial base in subjects with class III malocclusion, European Journal of Orthodontics, 1997, 19:341-353.

17. Huang Kuang Kung, Bo Wun Huang, Hung Shiung Chen, ANSYS and Computer Aided Engineering Analysis, 2004, Cheng Shiu University, Kaohsiung, Taiwan, R.O.C.

18. Chong-Ching Chang, Reverse engineering and the integration application, 1999, Gau Lih Book Co. Ltd., ISBN 957-584-664-8.

Finite element modeling of kirschner pin and bone thermal contact during drilling

Yuan-Kun Tu [1], You-Yao Hong [2], Yung-Chuan Chen [2]

1 Medical Vice-Superintendent, E-Da Hospital and I-Shou University, Kaohsiung Hsien, Taiwan 2 Department of Vehicle Engineering, National Pingtung University of Science and Technology, Pingtung, Taiwan 91201

Received November 10, 2009

Abstract The aim of this study is to develop an analysis method which can be applied to simulate the temperature rise during bone drilling. This study uses a dynamic elastic-plastic finite element model to simulate a process of a Kirschner pin drilling through the bone. The results indicate that lowering the initial temperature of Kirschner pin can decrease the temperature rise as well as the thermal affected zone. [Life Science Journal. 2009; 6(4):23 - 27] (ISSN: 1097 – 8135)

Keywords kirschner pin; temperature; bone, thermal contact; finite element analysis

1. Introduction

Kirschner wires or K pins are sharpened, smooth stainless steel pins used for temporary fixation during some operations. Several experiments indicate that the bone drilling may cause thermal necrosis. The pins are often driven into the bone through the skin using a power or hand drill. The heat generated during bone drilling is proportional to the drilling speed. Some of it may be conducted to the bone, which may cause serious damage if the temperature rises higher than 55 °C [1].

Khanna et al [2] indicated that K-wires had poor drilling qualities because they lacked sharp angled cutting facets and flutes. Eriksson and Albrektsson [3] showed that under certain conditions the temperature of bone during osseous drilling might exceed 70 °C . Hilly and Shuaib [1] studied the temperature effects on the drilling of human and bovine bone. The results indicated that a drilling speed of 800-1400 rpm was suggested when drilled with a diameter of 3.2mm drill-bit to provide the best cutting condition and to maintain the temperature at a manageable level. Mustafa et al [4] investigated the effect of force on the drilling speed and measured the energy consumed during the drilling process. The results suggested that drilling at high speed with a large force could reduce the bone temperature. Bachus et al [5] studied the drilling force on cortical temperatures. It demonstrated that by applying a larger force to the drill, both the maximum cortical temperature and its duration above 50 °C might be effectively reduced, decreasing the possibility of thermal necrosis in the cortical bone. Allan et al [6] reported that the temperature rise in bone drilling was related to the amount of drilling wear. In addition, it has been shown that the finite element method is a useful tool to simulation the drilling process [7-8]. Davidson and James [7] developed thermo-mechanical equations to predict the heat generation due to drilling. In simulations, a heat transfer model was coupled with the finite element model to predict the temperature rise during bone drilling.

Although various studies have addressed the influence of drilling in bones, these literatures contain only limited information regarding the temperature rise in K-pin-bone contact problems during drilling. In this study, various initial temperature of K-pin is investigated to explore the effect of parameters on the temperature rise.

*Corresponding Author: chuan@mail.npust.edu.tw
Professor Yung-Chuan Chen,

2. Finite element model

In this study, a three-dimensional elastic-plastic dynamic temperature-displacement finite element model is used to simulate the process of a K-pin drilling through the bone. Simulations are performed using a commercial finite element package ABAQUS and a dynamic failure criterion is applied to control the element removal. The K-pin and the bone contact geometry used in this study are shown in Figure 1.

The region of interest is the immediate surrounding of the drill hole where the temperature is highest. Hence the domain for the numerical simulation is chosen to be a circular disc. The diameter of the K-pin used in this study is taken as 2 mm. The tip radius R, as shown in Fig. 1, is employed to simulate the bluntness of the K-pin. The tip radius of the K-pin is 0.1mm. The point of the drill hole edge, i.e. x=2 and z=0 mm, is taken as the origin of the coordinate system. The corresponding finite element model is shown in Figure 2. The contact behavior between the K-pin and the bone is modeled using approximately 21859 contact elements in each simulation. The mesh is constructed using eight-node three-dimensional brick elements. The finite element model comprises a total of 41875 elements and 43892 nodes. To explore the effects of initial temperature of K-pin on the temperature distribution, four initial temperatures T_o, i.e. $0^\circ C$, $10^\circ C$, $25^\circ C$ and $37^\circ C$, are simulated. Two applied forces, 20N and 30N, are taken. The drilling speed is taken as 1200 rpm. The initial temperature of bone is assumed as $37^\circ C$. The mechanical properties used in the finite element analysis are summarized in Table 1.

Table 1. Mechanical properties of K-pin and bone used in finite element simulations

	K-pin [9,10]	Bone [10]
Density (Kg/m^3)	7840	2100
Young's modulus (GPa)	210	17
Yielding strength (MPa)	608	135
Tension strength (MPa)	1000	148
Specific Heat (J/kg℃)	490	1260
Poisson's ratio	0.3	0.35
Conductivity(Watt/m℃)	16	0.38

3. Results and Discussions

In this research, a dynamic elastic-plastic finite element model is employed to study how lowering Kirschner pins' temperature can affect the temperature rise in bone during drilling.

Figure 3 shows the variation of bone temperature along the radial direction of the bone for various initial temperature T_o with drilling time T_{sec} =1 sec. The results shown in this figure are taken from the bone

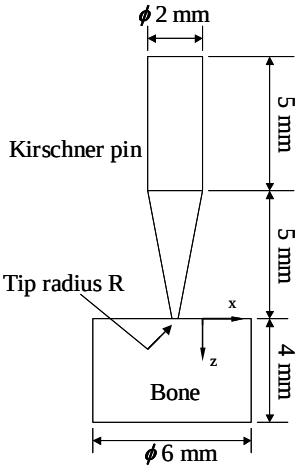

Figure 1. Geometry of Kirschner pin and bone

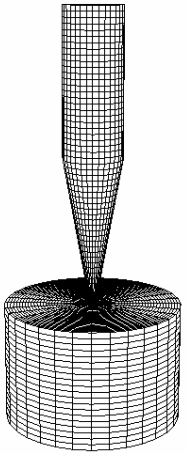

Figure 2. Finite element model of Kirschner pin and bone

surface, i.e. z= 0 mm. The applied force is F= 20 N. The results indicate that the bone temperature increases as the initial temperature of the k-pin increases. Hence, the bone temperature can be reduced as the K-pin has a lower initial temperature. In Figure 3, the peak bone

temperatures are 40.1 °C and 38.4 °C for the K-pin with an initial temperature of 37 °C and 0 °C, respectively. All the temperatures shown in Figure 3 are under 55 °C. Figure 4 plots the variation in the bone temperature for four different initial temperatures of K-pin with drilling time of 3 sec. Compared with Figure 3, it shows that as the drilling time increases, the bone temperature increases. It can be seen that the temperature distributions on the bone surface increase rapidly when the drilling time is 3 sec. Also, the peak temperature changes apparently as the initial temperature of the K-pin changes. This shows that lowering the initial K-pin temperature can reduce the temperature rise in bone during bone drilling. However, the bone temperatures at some regions are higher than 55 °C. In this study, the region that bone temperature exceeds 55 °C is defined as the thermal affected zone (TAZ). The TAZ can be used as an index to adjudge the damage zone of the bone. For example, as the solid line shown in Fig. 4, the TAZ is about 0.35 mm for the case of a K-pin with an initial temperature of 37 °C. However, the TAZ is 0 mm for a K-pin with an initial temperature of 0 °C. From Figure 4, a simulation result shows that the bone temperature will not exceed 55 °C if the initial K-pin temperature is 0 °C. In addition, the TAZs can be determined as 0.33 mm and

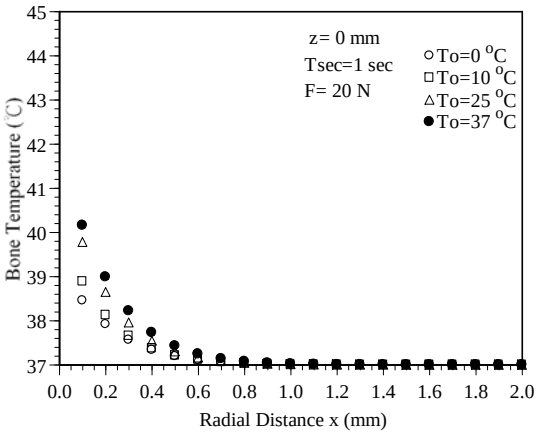

Figure 3. Variation of bone temperature along the radial direction as a function of initial temperature T_o with drilling time of 1 sec

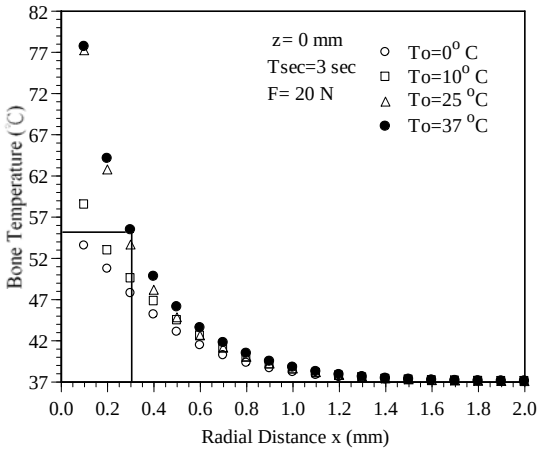

Figure 4. Variation of bone temperature along the radial direction as a function of initial temperature T_o with drilling time of 3 sec

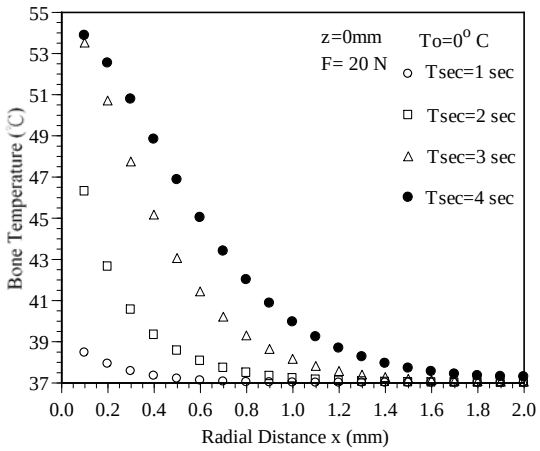

Figure 5. Variation of bone temperature along the radial direction as a function of drilling time

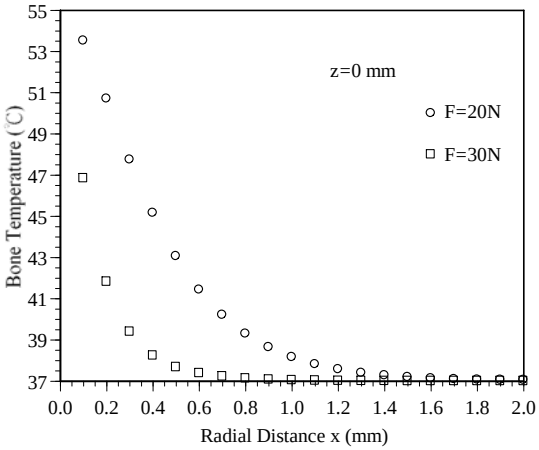

Figure 6. Variation of bone temperature along the radial direction as a function of applied force

be varied along the radial direction at the distance of 0.16 mm for a K-pin with initial temperatures of 25°C and 10°C , respectively. The results indicate that a K-pin with low initial temperature can reduce bone temperature rise during drilling. The results also indicate that the cortical bone is a poor conductor because the TAZ is not obvious. The effect of drilling time on the bone temperature distribution is shown in Fig. 5. The initial K-pin temperature is 0°C . It is obvious that the bone temperature increases with the drilling time. This can be attributed to that more friction heat is created as the drilling time increases. It is clear that all the temperatures on the bone surface are under 55°C . Figure 6 shows the variation of bone temperature along the radial direction for two applied forces. The drilling times shown in Fig. 6 are 3 seconds and 1.3 seconds for the applied forces of 20N and 30N, respectively.

In these two cases, the K-pins have the same drilling depth. It is observed that the bone temperature can be reduced effectively as the applied force is increased form 20 N to 30 N. The results shown above are taken from the bone surface. The temperature distributions in bone during drilling along longitudinal direction (the z-axis) are shown in Figs. 7 and 8. These two figures show the bone temperature distributions for various drilling time with applied forces of 20N and 30N, respectively. In these cases, the K-pin has an initial temperature of 0°C . Although, the drilling time shown in Figs. 7 and 8 are different, the drilling depths represented by the same symbols in these two figures are the same. It is clear that the bone temperature increases with the drilling time. The peak temperature can reach as high as 61°C when the drilling time is 4 seconds for the applied force of 20N, as shown in Fig. 7. Accordingly, a larger applied force is proposed to reduce the peak temperature in bone, as shown in Fig. 8. The peak temperature is reduced to 52°C as the applied force is increased to 30N. From the discussion above, the K-pin with a lower initial temperature or a larger applied force can reduce the bone temperature rise easily in surgical operation.

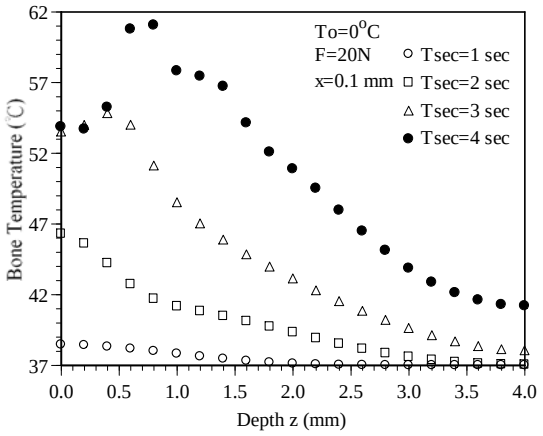

Figure. 7. Variation of bone temperature along the depth as a function of drilling time for the applied force of 20N

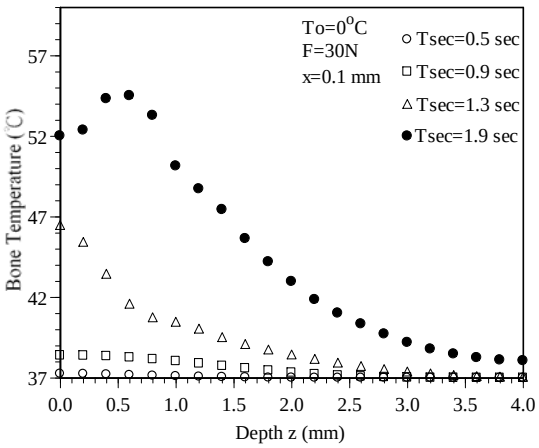

Figure 8. Variation of bone temperature along the depth as a function of drilling time for the applied force of 30N

4. Conclusion

This study has performed numerical investigations into the temperature rise distribution in bone during drilling. The numerical analysis has been conducted using an elastic-plastic dynamic temperature-displacement finite element model. The effect of initial temperature of K-pin and applied force on the temperature rise has been examined. Based upon the numerical results, the following conclusions can be drawn:

1. The proposed dynamic elastic-plastic finite element model can be used to simulate the temperature rise for a K-pin drilling through the bone.
2. A K-pin with a lower initial temperature can reduce the temperature rise in bone during drilling.
3. The size of the thermal affected zone can be reduced for a K-pin with a lower initial temperature.
4. A larger applied force can reduce temperature rise effectively.

References

1. Hillery MT, and Shuaib I. Temperature effects in the drilling of human and bovine bone. Journal of Materials Processing Technology, 1999, 92-93: 302-308.
2. Khanna A, Plessas SJ, Barrett P, and Bainbridge LC. The Thermal Effects of Kirschner Wire Fixation on Small Bones. Journal of Hand Surgery, 1999, 24: 355-357.
3. Eriksson A, Albrektsson T. Temperature threshold levels for heat-induced bone tissue injury: a vital-microscopic study in the rabbit. Journal of Prosthetic Dentistry 1983, 50: 101-107.
4. Abouzgia MB, James DF. Measurements of shaft speed while drilling through bone. Journal of Oral and Maxillofacial Surgery, 1995, 53:1308-1315.
5. Bachus KN, Rondina MT, Hutchinson DT. The effects of drilling force on cortical temperatures and their duration: An in vitro study. Journal of Medical Physics and Engineering 2000, 22: 685-691.
6. Allan W, Williams ED, Kerawala CJ. Effects of repeated drill use on temperature of bone during preparation for osteosynthesis self-tapping screws. Journal of Oral and Maxillofacial Surger , 2005, 43: 314-319.
7. Davidson SRH, James DF. Drilling in bone: modeling heat generation and temperature distribution. Journal of Biomechanical Engineering, 2003, 125: 305-314.
8. Guo YB, Dornfeld DA. Finite element modeling of burr formation process in drilling 304 stainless steel. Journal of Manufacturing Science and Engineering, 2000, 122: 612-619.
9. Borzacchiello A, Ambrosio L, Nicolai, L, Harper EJ, Tanner KE, Bonfield W. Comparison between the polymerization behavior of a new bone cement and a commercial one: modeling and in vitro analysis. Journal of Materials Science, 1998, 9: 835-838.
10. http://www.matwed.com

Natural Properties in a Micro Drill Cutting into Bones

Chang Kuan Yu[1], Chang Hong Chang[1], Yu Pu Ping[2], Yen Ke Tien[2] and Huang Bo Wun[2]

1. Mackay Memorial Hospital Taitung Branch, Taitung, Taiwan, ROC

2. Cheng Shiu University, Kaohsiung , Taiwan, ROC

Received March 10, 2009

Abstract: The natural frequency in a micro drill into bones was investigated in this article. During actual service, the spinning speed subjected to some small fluctuation in a drilling process can't keep perfect constant, so the micro drill may be broken in this process. Therefore, the natural properties of this micro drill must understand. For the sake of increasing demand for better quality and higher production rate, the dynamic properties in a drilling bone process must be to pay much attention. In this article, a pre-twisted beam is used to simulate the drill. The drilling force is measured by using drilling bone experiment. The effects of spinning speed and pre-twisted angle of the drill in dynamic properties are considered to study. [Life Science Journal. 2009; 6(4): 28 – 33] (ISSN: 1097 – 8135)

Keywords: Micro drilling, Bones, Natural properties.

1. Introduction

For surgical operation, microsurgery is popularly employed to remedy some sickness, because it is more safe and rapid fully recover from an illness. However, a little microsurgery is used to remedy the brain illness. For this, a micro drilling for cranial bones, microsurgery for cranial bones, is considered to study. Drilling is frequently employed for metal cutting operation. In the manufacturing, the drilling operation is conducted on an extensive variety of machine tool, which includes drilling machine, milling machine, machining center and so forth. A precisely drilled hole leads to a high quality product and its accuracy is based upon the drilling process [1, 2]. A point has to be particularly mentioned, the most of holes location errors, reaming and fracture of drill may occur at this process, when the drill is exactly drilling into a work piece. To improve the performance and capability of the drilling, it is necessary to understand the dynamic characteristics of process for drilling. Hence, due to drilling process, a time dependent instability problem of a drill is consider to present. In this present investigation, the dynamic instability caused by rotating speed and thrust force is also considered to study in this drilling process.

*Corresponding Author: huangbw@csu.edu.tw

Dr. Bo Wun Huang

In a real drilling process, keeping a spinning speed perfect constant is almost impossible because of the drilling speed subjected to some small fluctuation. Theoretically, at some specified rotation speed, this small speed fluctuation may lead the system to a dynamic unstable condition. Most of the studies about instability in a system focus on time independent problem [3-6]. Only a few studies on the time dependent instability in the drilling process have been conducted. Even if the instability lead to undesirable effects such as chatter and drill breakage etc., It is found that traditional analysis of drilling has focused on drill itself, such as [7-10]. Many papers [6, 8, 11, 12], reported the vibration in a pre-twisted beam, which was modeled as a drill. The effects of pre-twisted angle, spinning speed on vibration in a drill had been presented. Buckling load and natural frequency of a drill bit also had been investigated, as [13-15].

Previous researchers have studied mathematical models of complex drill bit to estimate natural frequency or cutting property. The effects of complex geometry or cutting chip on cutting and dynamic property of drill bit were paid attentions to research. Even a variation in geometry or symmetry error can make a very strong influence on cutting and dynamic property of a drill, such as [16-19]. Such models can provide competently useful information to design a drill bit. Some investigators turn their interest to the instability of a drill, as [12, 20, 21]. Results indicate that the effects of spinning

speed, pre-twisted angle and axial force may change the dynamic instability.

So far, a study dynamic property in the micro drilling with bones has not found by authors yet. The aim of this paper is to consider the dynamic property in micro drilling bones process to present.

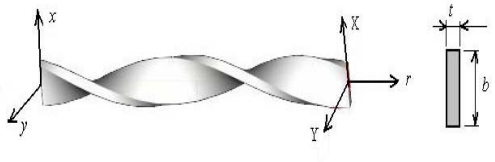

Figure 1. The schematic diagram of the body for drill

2 Theory and Formulations

The effect of complex cross-section of drill has been studied [22]. A little difference between the complex and rectangular cross-section on the dynamic characteristic of a drill has been found. For the sake of convenience, in this article, the simple pre-twisted beam with a rectangular cross-section is employed to simulate a drill. The drill, a cantilever pre-twisted beam, with a spinning speed Ω is illustrated in Fig. 1. The length of the drill is L. t and b are used to denote the thickness and breadth of the drill respectively. In this study, the deflection components $v(r,t)$ and $u(r,t)$ denote the two transverse flexible deflection of the drill.

The equation of motion of a spinning drill is displayed as

$$\frac{\partial^2}{\partial r^2}\left(EI_{yy}\frac{\partial^2 u}{\partial r^2}+EI_{xy}\frac{\partial^2 v}{\partial r^2}\right)-\frac{\partial}{\partial r}\left(\bar{I}_{yy}\frac{\partial^3 u}{\partial t^2\partial r}+\bar{I}_{xy}\frac{\partial^3 v}{\partial t^2\partial r}\right)$$

$$+\mu\frac{\partial^2 u}{\partial t^2}-2\mu\Omega\frac{\partial v}{\partial t}-\mu\Omega^2 u-\mu\dot{\Omega}v=0 \qquad (1a)$$

$$\frac{\partial^2}{\partial r^2}\left(EI_{xx}\frac{\partial^2 v}{\partial r^2}+EI_{xy}\frac{\partial^2 u}{\partial r^2}\right)-\frac{\partial}{\partial r}\left(\bar{I}_{xx}\frac{\partial^3 v}{\partial t^2\partial r}+\bar{I}_{xy}\frac{\partial^3 u}{\partial t^2\partial r}\right)$$

$$+\mu\frac{\partial^2 v}{\partial t^2}+2\mu\Omega\frac{\partial u}{\partial t}-\mu\Omega^2 v+\mu\dot{\Omega}u=0 \qquad (1b)$$

where a symbol prime $(')$ denotes a partial derivative with respect to r. In this equation, E and μ are the Young's modulus and mass per unit length respectively, and I_{xx}, I_{yy} and I_{xy} are the moments of area. Consider the drill to be pre-twisted with a uniform twist angle β, and then the area moments of inertia at the position r can be derived as

$$I_{xx}=I_{XX}\cos^2\left(\frac{r}{L}\beta\right)+I_{YY}\sin^2\left(\frac{r}{L}\beta\right) \qquad (2a)$$

$$I_{yy}=I_{XX}\sin^2\left(\frac{r}{L}\beta\right)+I_{YY}\cos^2\left(\frac{r}{L}\beta\right) \qquad (2b)$$

$$I_{xy}=\left(I_{YY}-I_{XX}\right)\sin\left(\frac{r}{L}\beta\right)\cos\left(\frac{r}{L}\beta\right) \qquad (2c)$$

where

$$I_{XX}=\frac{b\,t^3}{12} \qquad (3a)$$

$$I_{YY}=\frac{b^3 t}{12} \qquad (3b)$$

, and $\bar{I}_{xx}$, $\bar{I}_{xy}$, $\bar{I}_{yy}$ are the moments of mass.

Boundaries of the drill can be displayed as

$$u_s=v_s=u_s'=v_s'=0, \quad \text{at} \quad r=0 \qquad (4a)$$

$$u_s''=v_s''=u_s'''=v_s'''=0, \quad \text{at} \quad r=L \qquad (4b)$$

The purpose of this investigation is to present the dynamic property in a micro drilling with bones. In a mathematical sense, a thrust force can be employed to simulate this drilling process. Considering the axial cutting force, the equation of motion can be rewrite as

$$\frac{\partial^2}{\partial r^2}\left(EI_{yy}\frac{\partial^2 u}{\partial r^2}+EI_{xy}\frac{\partial^2 v}{\partial r^2}\right)-\frac{\partial}{\partial r}\left(\bar{I}_{yy}\frac{\partial^3 u}{\partial t^2\partial r}+\bar{I}_{xy}\frac{\partial^3 v}{\partial t^2\partial r}\right)$$

$$+P\frac{\partial^2 u}{\partial r^2}+\mu\frac{\partial^2 u}{\partial t^2}-2\mu\Omega\frac{\partial v}{\partial t}-\mu\Omega^2 u-\mu\dot{\Omega}v=0 \qquad (5a)$$

$$\frac{\partial^2}{\partial r^2}\left(EI_{xx}\frac{\partial^2 v}{\partial r^2}+EI_{xy}\frac{\partial^2 u}{\partial r^2}\right)-\frac{\partial}{\partial r}\left(\bar{I}_{xx}\frac{\partial^3 v}{\partial t^2\partial r}+\bar{I}_{xy}\frac{\partial^3 u}{\partial t^2\partial r}\right)$$

$$+P\frac{\partial^2 v}{\partial r^2}+\mu\frac{\partial^2 u}{\partial t^2}+2\mu\Omega\frac{\partial v}{\partial t}-\mu\Omega^2 u+\mu\dot{\Omega}u=0 \qquad (5b)$$

where P is the drilling bones load.

The solutions for the above eigenvalue problem are expressed as

$$u(r,t)=\sum_{i=1}^{m}p_i(t)\phi_i(r) \qquad (6a)$$

$$v(r,t)=\sum_{i=1}^{m}q_i(t)\phi_i(r) \qquad (6b)$$

where $\phi_i(r)$ are the comparison functions of equations (5a) and (5b), and $p_i(t), q_i(t)$ are the corresponding weighting coefficients, which are to be determined. Five exact solutions of a uniform cantilever

beam, $\phi_i(r)$ in transverse direction are used to discrete the equations of motion.

An application of the Galerkin's method, the equations of motion can be derived in matrix form as

$$[M]\begin{Bmatrix}\ddot{p}\\ \ddot{q}\end{Bmatrix}+2\Omega_0[G]\begin{Bmatrix}\dot{p}\\ \dot{q}\end{Bmatrix}+\left\{[K]_a+P[K]_b+\Omega_0^2[K]_c\right\}\begin{Bmatrix}p\\ q\end{Bmatrix}=0 \quad (7)$$

where

$$[M]=\begin{bmatrix}[M]^1+[M]^2 & [M]^4\\ [M]^4 & [M]^1+[M]^3\end{bmatrix} \quad (8a)$$

$$[G]=\begin{bmatrix}[0] & -[M]^1\\ [M]^1 & [0]\end{bmatrix} \quad (8b)$$

$$[K]_a=\begin{bmatrix}[K]^1 & [K]^4\\ [K]^4 & [K]^2\end{bmatrix} \quad (8c)$$

$$[K]_b=\begin{bmatrix}-[K]^3 & [0]\\ [0] & -[K]^3\end{bmatrix} \quad (8d)$$

$$[K]_c=\begin{bmatrix}-[M]^1 & [0]\\ [0] & -[M]^1\end{bmatrix} \quad (8e)$$

To emphasize, these matrices can be illustrated to go into details as follows,

$$M_{ij}^1=\int_0^1 \mu\phi_i(\bar{r})\phi_j(\bar{r})d\bar{r} \quad (9a)$$

$$M_{ij}^2=\frac{\bar{I}_{yy}}{L^2}\int_0^1\frac{d\phi_i(\bar{r})}{d\bar{r}}\frac{d\phi_j(\bar{r})}{d\bar{r}}\,d\bar{r} \quad (9b)$$

$$M_{ij}^3=\frac{\bar{I}_{xx}}{L^2}\int_0^1\frac{d\phi_i(\bar{r})}{d\bar{r}}\frac{d\phi_j(\bar{r})}{d\bar{r}}\,d\bar{r} \quad (9c)$$

$$M_{ij}^4=\frac{\bar{I}_{xy}}{L^2}\int_0^1\frac{d\phi_i(\bar{r})}{d\bar{r}}\frac{d\phi_j(\bar{r})}{d\bar{r}}\,d\bar{r} \quad (9d)$$

$$K_{ij}^1=\frac{EI_{yy}}{L^4}\int_0^1\frac{d^2\phi_i(\bar{r})}{d\bar{r}^2}\frac{d^2\phi_j(\bar{r})}{d\bar{r}^2}\,d\bar{r} \quad (9e)$$

$$K_{ij}^2=\frac{EI_{xx}}{L^4}\int_0^1\frac{d^2\phi_i(\bar{r})}{d\bar{r}^2}\frac{d^2\phi_j(\bar{r})}{d\bar{r}^2}\,d\bar{r} \quad (13f)$$

$$K_{ij}^3=\frac{1}{L^2}\int_0^1\frac{d\ \phi_i(\bar{r})}{d\bar{r}}\frac{d\ \phi_j(\bar{r})}{d\bar{r}}\,d\bar{r} \quad (13g)$$

$$K_{ij}^4=\frac{EI_{xy}}{L^4}\int_0^1\frac{d^2\phi_i(\bar{r})}{d\bar{r}^2}\frac{d^2\phi_j(\bar{r})}{d\bar{r}^2}\,d\bar{r} \quad (13h)$$

The eigenvalue problem equation can be rewritten as.

$$[A]\{\dot{V}\}+[B]\{V\}=0 \quad (14)$$

3 Results and Discussion

The dynamic properties in a micro drilling bones process were investigated in this study. *D=1.0mm*, *d=0.3mm*, $L=5.5mm$, , $t=0.24mm$, $b=0.5mm$ and $\beta=1800^0\,(5.712\,rad/mm)$. In this work, the sinbone bone replacement, Purzer produced, is employed to study instead of real bone.

Figure 2. Experiment setup in a micro drill with bones

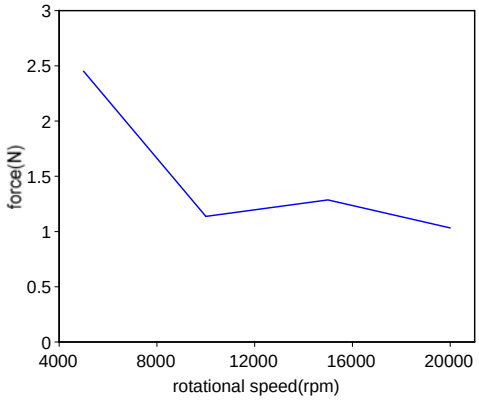

Figure 3. The variation in drilling force with different rotating speed.

Figure 2 shows the experiment setup in a micro drill

with bones. In this figure, the sinbone bone replacement drilled by a micro drill is found. The variation in drilling force with different rotating speed is illustrated in Fig. 3. The rotating speed from *4000 rpm* to *20000 rpm* is considered in this work. Experiment analysis shows that the drilling force may decreased as the rotating speed is increased. In this investigation, the rotating speed *15000 rpm* is employed to study the natural properties of a micro drill with a bone. As the rotating speed *15000 rpm* considered, the drilling force *1.286 N* can be obtained.

Figure 4 displays the natural frequency of a micro drill drilling into a bone. Only the lower mode is considered in this work. In this figure, the first order mode natural frequency *50315 Hz* and the second order mode natural frequency *53453 Hz* are found. The effect of rotating speed on natural frequency of a micro drill with a bone is studied. Figure 5 shows the natural frequency of a micro drill drilling a bone with different rotating speed. The first order mode natural frequencies may be depressed and second order mode natural frequencies may increase as the rotating speed is increased. Finally, the pretwisted angle effect is considered to study. The effect of pretwisted angle on natural frequency of a micro drill with a bone is displayed in Fig. 6. Numerical analysis shows that the first and second order mode natural frequencies will toward a higher frequency domain if the pretwisted angle is increased.

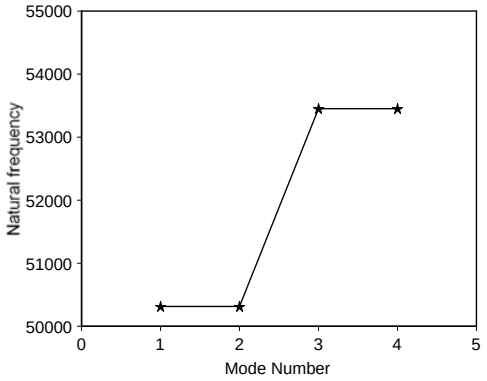

Figure 4. Natural frequencies of a micro drill drilling a bone.

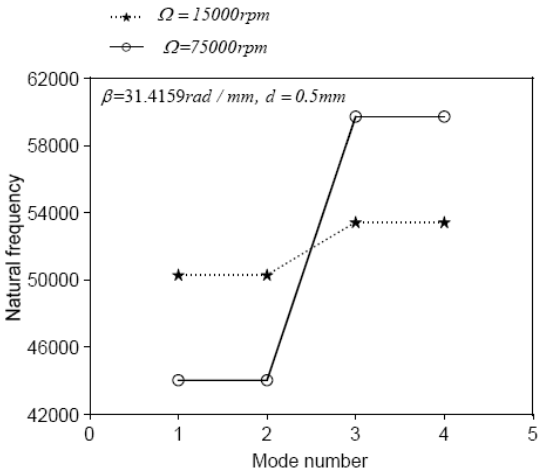

Figure 5. Natural frequencies in a micro drilling bone process with different rotating speed.

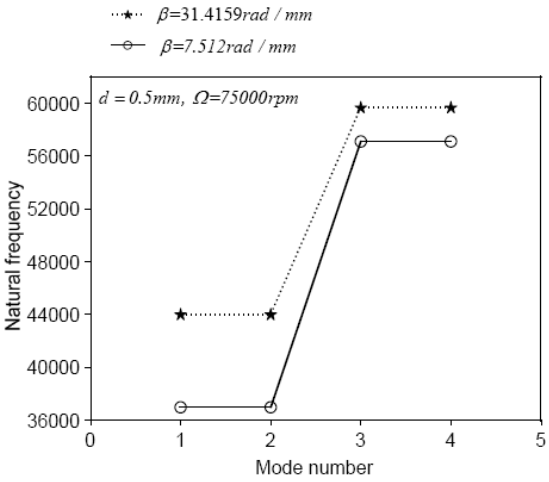

Figure 6. Natural frequencies in a micro drilling bone process with different pretwisted angle.

4 Conclusions

The dynamic property of a micro drill with a bone was investigated. The major conclusions drawn from the analysis and numerical results obtained in this study are summarized as follows:

(1) The analysis results indicate that a study of the dynamic drilling characteristics is necessary to improve drilling into a bone performance and capabilities, especially for high speed drilling.

(2) Experiment analysis shows the drilling force will be depressed as the rotating speed is increased if a micro drill drills into a bone.

(3) The effects of spinning speed and pre-twisted angle drastically change dynamic properties of a micro drill drilling a bone.

Acknowledgements

The financial support by the Ministry of Education, Republic of China..

References

1. Katz Z, Poustie A. On the hole quality and drill wandering relationship**.** International Journal of Advanced Manufacturing Technology, 2001, 17(4): 233-237

2. Gupta K, Ozdoganlar OB, Kapoor SG, DeVor RE. Modeling and prediction of hole profile in drilling. Part 1: modeling drill dynamics in the presence of drill alignment errors. ASME, Journal of Manufacturing Science and Engineering, 2003, 125(1): 6-13

3. Hsu CS. On a Restricted Class of Coupled Hill's Equations and Some Applications. ASME Journal of Applied Mechanics, 1961: 551-557.

4. Nayfey AH, Mook DT. Nonlinear Oscillation, 1979, New York: John Wiley

5. Young TH. Dynamic Response of A Pretwisted, Tapered Beam with Non-constant Rotating Speed. Journal of Sound and Vibration, 1991, 150(3): 435-446

6. Liao CL, Huang BW. Parametric Resonance of a spinning Pretwisted Beam with Time-Dependent Spinning Rate. Journal of Sound and Vibration, 1995, 180(1): 47-65

7. Rosard DD. Natural Frequency of Twisted Cantilever Beams. ASME Paper No. 52-A-15, 1952

8. Jarrett GW, Warner PC. The Vibration of Rotating Tapered Twisted Beam. ASME, Journal of Applied Mechanics, 1953: 381-389

9. Tekinalp O, Ulsoy AG.. Modeling and Finite Element Analysis of Drill Bit Vibration. ASME, Journal of Vibration, Acoustics, Stress, and Reliability in Design, 1989, 111: 148-155

10. Tekinalp O, Ulsoy AG. Effect of Geometric and Process Parameters in Drill Transverse Vibration. ASME, Journal of Engineering for Industry, 1990, 112: 189-194

11. Liao CL, Dang YH. Structural Characteristics of Spinning Pretwisted Orthotropic Beams. Computer & Structures, 1992, 45(4): 715-731

12. Liao CL, Huang BW. Parametric Instability of a Pretwisted Beam under Periodic Axial Force. International Journal of Mechanical Science. 1995, 37(4): 423-439

13. Magrab E, Gilsinn DE. Bucking loads and natural frequency of twist drills. Transactions of ASME, 1984, 106: 196-204

14. Ulsoy AG. A lumped parameter model for the transverse vibration of drill bit. Control of Manufacturing Processes and Robotic System, 1989: 15-25

15. Fuji H, Marui E, Ema S. Whirling Vibration in drilling part 3: Vibration analysis in Drilling Workpiece with a Pilot Hole. ASME, Journal of engineering for Industry, 1988, 110: 315-321

16. Rincon DM, Ulsoy AG. Complex Geometry, Rotary Inertia and Gyroscopic Moment Effects on Drill Vibrations. Journal of Sound and Vibration, 1995, 188(5) 701-715

17. Ren K, Ni J. Analyses of drill flute and cutting angles. International Journal of Advanced Manufacturing Technology, 1999, 15(8): 546-553

18. Spanos PD, Chevallier AM, Politis NP. Nonlinear stochastic drill-string vibrations. ASME, Journal of Vibration and Acoustics, 2002, 124(4): 512-518

19. Hsieh JF, Lin PD. Mathematical model of multiflute drill point. International Journal of Machine Tools and Manufacture, 2002, 42(10): 1181-1193

20. Iwastsubo T, Sugiyama Y, Ishihara K. Stability and Stationary Vibrations of Columns under Periodic Loads. Journal of Sound and Vibration, 1972, 23: 245-257.

21. Lee HP. Buckling and Dynamic Stability of Spinning Pre-twisted Beams under Compressive Axial Loads. International Journal of Mechanical Sciences, 1994, 36(11): 1011-1026

22. Huang BW. Vibration of a high speed drill. Proc. of National Science Council Research Projects. 2000, NSC 89-2212-E-230-006, Taiwan. (in Chinese)

The Efficacy of Community Based Intervention in Newborn Care Practices and Neonatal Illness Management in Morang District of Nepal

Sirjana Khanal[1], Weidong Zhang[1], Sudhir Khanal[2]

1. Department of Biostatistics & Epidemiology, College of Public Health, Zhengzhou University, Zhengzhou, China
2. Project Director of Morang Innovative Neonatal Intervention Program, JSI R & T, Nepal Family Health Program, Nepal. P.O. Box – 1600.

Received November 18, 2009

Abstract: Background: In developing countries like Nepal, most of the births take place in the home, where high-risk care practices are common. This study is focused to find the efficacy of a community based intervention in newborn care practices and neonatal illness management in Morang district of Nepal. **Methods**: In Morang district of Nepal, intervention (base line & follow on) and non intervention (control) area were randomly selected. A community based program was launched in intervention area. The program mobilized the female community health volunteer (FCHV) to provide antenatal service (ANC), essential newborn care (ENC) and identify, assess and basic management of sick newborn. The survey included 624, 620 and 613 eligible married women of reproductive age (MWRA) in baseline (BSL), follow on (FON) and non intervention (NI) group respectively. During the survey, data regarding ANC services, clean and safe delivery, implementing ENC practices and managing ill babies were collected. The data, thus collected were analyzed using SPSS for windows. **Results**: The population characteristics of all the three groups; BSL, FON and NI were similar. The number of women receiving ANC service increased from 85.4% to 89% after intervention. The practice of home delivery was low in FON (64.8%) than BSL (69.6%) and NI (70.1%). In case of home delivery, presence of skilled and trained attendant increased to 60.6% with introduction of intervention program. The total illness rate in BSL, FON and NI groups were 41.2%, 38.2% & 29.7% respectively. The most commonly observed danger sign was respiratory problem 38.1%, 41.8% and 30.2% respectively in three groups. A significant improvement was seen in ENC practices of early breastfeeding, cord care, warming baby and delay in bathing practices in FON group (p<0.005). The fatality rate in FON group was low (3.2%) than BSL (14.1%) and NI (15.6%). **Conclusion**: Neonatal illness can be diagnosed and managed earlier if proper training is given to grass root level health worker. The intervention in Morang district showed the reduced neonatal fatality rate and this program can be extended in other rural areas of Nepal. [Life Science Journal. 2009; 6(4): 34 - 40] (ISSN: 1097 – 8135)

Key words: Essential Newborn Care, Neonatal illness, Community Based Intervention

1. Introduction

Globally, each year around 10 million young children in low and middle income countries die and about 4 million children die within the first 28 days of life. Reduction of child mortality by two third between 1990 and 2015 is one of goal of MDG. During this period (1990-2006), children under 5 mortality rates in Nepal has been reduced from 117 to 82 and infant mortality rate from 82 to 48. [1] In the last 15 years, Nepal has observed a significant decline in the under 5 mortality. Nepal is one of those six countries who are on the track to achieve the MDG 4 for child health. [2].

Nepal's estimated neonatal mortality rate is 33/per 1000 lives birth. [1] Over 90% of births occur at home unattended by skilled health professionals. [3] Therefore there should be an effective intervention program to create awareness in rural areas regarding new born care practices at home to reduce neonatal morbidity and mortality. A large proportion of the babies who die could be saved with low tech and low cost interventions. MINI is one of such project which launched a community based program giving emphasis on ENC along with identification and management of the illness in babies in Morang district of Eastern Terai region of Nepal.

Corresponding Author:
Sirjana Khanal, Department of Biostatistics & Epidemiology, Zhengzhou University, China
khanalsirju@yahoo.com

The Project has been approved by Government of Nepal and is supported by Saving Newborn Lives Program (SNL-1) through Save the Children/US with support from the Bill & Melinda Gates Foundation, NFHP/USAID.

This study is a part of the MINI intervention program to describe the efficacy of the intervention for essential newborn care practices and management of neonatal illness.

2. Material and Methods

2.1 Location and population

Nepal is a developing country with a population of 23.2 million. [4] Morang is densely populated district of Eastern Terai region of Nepal with a population of 914,000 living in 65 VDCs and one municipality, smallest administrative units.

2.2 Study design

The intervention area included 21 VDCs and NI areas included 44 VDCs and were selected by randomization. However, 8 VDCs were excluded from intervention area because of political instability. MINI conducted a BSL survey in 2004 and then intervention program (mentioned below in 1.3) was launched. After 30 months of intervention, a FON survey was conducted. At the same time, FON survey was conducted in NI area as control group. During the study, the information was collected from all eligible MWRA giving birth in the last one year. The information collected was about mothers' age, her first pregnancy age,

literacy and no. of live child. Similarly, mothers were also interviewed about ANC service, delivery related practice, new born care practice and the problem seen in babies. A same proforma was developed to collect the information from all the three groups – BSL, FON and NI.

2.3 Intervention

A specific training was given to existing health workers to manage neonatal infections. FCHVs were specially trained to provide ANC counseling or health education to new mothers; weigh all newborns to identify those at higher-risk; use a simple clinical algorithm to assess sick newborns (based on an algorithm tested in other countries); manage local bacterial infections (ophthalmic, umbilical, skin); initiate treatment for PSBI with cotrim; facilitate treatment with injectable gentamicin by VHWs; follow up and record outcomes; and conduct simple birth and death recording.

2.4 Statistics

The data were analyzed using SPSS 16 for windows. The data were expressed in mean ± standard deviation or median and range. Chi square test was used for qualitative data and t- test was used for numerical variable. P value less than 0.05 was considered as significant.

3 Results

3.1 Population Characteristics

A total of 624, 620 and 613 of eligible mothers were interviewed in BSL, FON and NI group respectively. Population characteristics with maternal age, first pregnancy age, no of live child and mother's literacy are presented in table 1

3.2 Antenatal care service and delivery

ANC practice, home delivery and delivery attendant are presented in table 2.

Table 1. Population Characteristics

	INT_BSL		INT_FON		NON_INT		Pvalue
	No.of MWRA	%	No.of MWRA	%	No.of MWRA	%	
No. of House hold visited	5449		4411		4309		
Mothers	624		620		613		
Mothers' Age (years)							**0.929#**
15~	124	19.9	120	19.4	106	17.3	
21~	322	51.6	324	52.3	334	54.5	
27~	114	18.3	120	19.4	125	20.4	
33~	45	7.2	39	6.3	37	6.0	
39~	11	1.8	17	2.7	11	1.8	
45~	2	0.3	0	0.0	0	0.0	
Don't know*	6	1.0	0	0.0	0	0.0	
Mean ± Std. deviation	25 ± 5		25 ±5		25±5	0.0	
Mothers' Literacy							**0.090 ^**
Literate (can read easily)	227	36.4	287	46.3	245	40.0	
Semi Literate (read with difficulty)	68	10.9	58	9.4	66	10.8	
Iliterate (can't read)	329	52.7	275	44.4	302	49.3	
First Pregnancy age (years)							**0.067#**
<15	4	0.6	8	1.3	13	2.1	
15~	412	66.0	431	69.5	448	73.1	
21~	186	29.8	161	26.0	137	22.3	
27~	12	1.9	17	2.7	12	2.0	
33~	3	0.5	2	0.3	2	0.3	
39~	0	0.0	0	0.0	1	0.2	
45~	0	0.0	0	0.0	0	0.0	
Don't know*	7	1.1	1	0.2	0	0.0	
Mean ± std. deviation	19.6±3		19.4±3		19.2±3.1		
No of live child							**0.239 ^**
1~2	427	68.4	450	72.5	436	71.1	
3~4	167	26.8	139	22.5	157	25.6	
>4	30	4.8	31	5.0	20	3.3	

* Without considering missing value (don't know)

^ chi square test, # ANOVA test

Table 2. ANC and delivery

	INT_BSL		INT_FON		NON_INT		χ^2	P value
	NO. of MWRA	%	NO. of MWRA	%	NO. of MWRA	%		
ANC received	533	85.4	552	89.0	550	89.7	6.3	**0.043**
Median month	4		4		4			
First ANC visit at							25.1	**0.001**
1st Trimester	185	29.6	212	34.2	211	34.4		
2nd Trimester	275	44.1	305	49.2	305	49.8		
3rd Trimester	73	11.7	35	5.6	34	5.5		
Place of Delivery								
Home	434	69.6	402	64.8	430	70.1	19.7	**0.001**
Hospital	110	17.6	110	17.7	127	20.7		
Others	80	12.8	108	17.4	56	9.1		
Delivery assisted by							13.0	**0.001**
Skilled & trained Attendant	315	50.4	376	60.6	332	54.2		
Untrained Attendant	293	47.0	236	38.1	276	45.0		
No Attendant at all	16	2.6	8	1.3	5	0.8		

Table 3. ENC Practices

	INT_BSL		INT_FON		NON_INT		χ^2	P value
	No.of MWRA	%	No. of MWRA	%	No. of MWRA	%		
Cord care	177	28.4	375	60.5	261	42.6	130.8	0.001
Breastfeeding (within 1st hour of birth)	181	29	270	43.5	264	43	35.8	0.001
First colostrums fed	473	75.8	545	87.9	508	82.8	31.4	0.001
Baby wiped	367	58.8	394	63.5	328	53.5	12.8	0.002
Baby wrapped	433	69.3	446	71.9	381	62.1	14.5	0.001
Baby bathing (>24 hrs)	109	17.5	261	42	215	35	69.8	0.001
Weighing of baby (within 24 hrs)	178	28.5	313	50.4	209	34	68.9	0.001

In BSL, 533 (85.4%) women received ANC service and 552 (89%) and 550(89.7%) in FON and NI group. Most of the women seek first ANC service in 2nd trimester 44.1%, 49.2% and 49.8% respectively in BSL, FON and NI group. In BSL 434 (69.6%) women delivered the baby at home. Similarly in FON and NI group home delivery were 402 (64.8%) and 430 (70.1%) respectively. The skilled & trained attendant conducted 50.4%, 60.6% & 54.2% of the deliveries while untrained assisted in 47%, 38.1% and 45% cases respectively in the BSL, FON and NI group. In this study, birth attendant were grouped into skilled and trained attendant (doctor/Nurse/paramedics/Trained TBA) and untrained attendant (Family members, neighbours, relatives, untrained dais). There is a significant different in antenatal service and delivery practices among the groups. (ANC received $\chi^2 = 6.3$; $p<0.05$; home delivery $\chi^2 = 19.7$; $p<0.001$; delivery assistance by skilled $\chi^2 = 13.1$; $p<0.001$).

3.3 Essential Newborn Care Practices

There was a significant improvement in cord care among the groups ($\chi^2 = 130.8$, $p<0.001$). The practice of breastfeeding to babies within 1st hour of birth and feeding of colostrums was significant different among the groups ($\chi^2 = 35.8$, $p<0.001$ and $\chi^2 = 31.4$, $p<0.001$). Newborn was wiped immediately after birth. Babies were dried and wrapped in clothes. Both the practices were significantly improved after intervention ($\chi^2 = 12.8$; $p<0.005$ and $\chi^2 = 14.5$; $p<0.001$). The practice of delay to bath the babies were reported more after intervention. ($\chi^2 = 69.8$; $p<0.001$). The significant improvement in taking weight of babies after birth was seen ($\chi^2 = 68.9$; $p<0.001$) The newborn care practices are in table 3.

3.4 Status of Ill Babies

FCHVs had assessed ill babies in their villages using a standard algorithm. The danger signs of the newborn identified are listed in Table 4.

Table 4 Danger Signs Identified

	INT_BSL		INT_FON		NON_INT			
	No.of MWRA	%	No. of MWRA	%	No.of MWRA	%	χ^2	P value
Unable to suck milk	46	18	51	21.5	30	16.5	1.9	0.382
Difficulty in breathing	98	38.1	101	42.6	55	30.2	6.0	**0.050**
Lethargic	8	3	9	3.8	4	2.2	0.8	0.646
Redness around cord	5	2	18	7.6	5	2.7	11.1	**0.004**
Fever	164	64	157	66.2	123	67.6	0.7	0.697
Cold body	0	0	0	0.0	4	2.2	10.9	**0.004**
Watery + bloody stools	20	8	14	5.9	14	7.7	0.78	0.674
Yellow in eyes, skin	24	9	13	5.5	11	6.0	3.19	0.202
Failed to pass urine	3	1	3	1.3	4	2.2	0.89	0.641
Skin problem	9	4	32	13.5	15	8.2	16.2	**0.001**
Red eyes with discharge	14	5	11	4.6	8	4.4	0.29	0.861
Others	127	49	37	15.6	39	21.4	75.8	**0.001**
Total ill babies	257	41.2	237	38.2	182	29.7	18.9	0.001

Table 5 Effect Of Treatment In Neonatal Illness

	INT_BSL		**INT_FON**		**NON_INT**			
	NO. of MWRA	**%**	**NO. of MWRA**	**%**	**NO. of MWRA**	**%**	χ^2	P value
PSBI cases	99	38.5	157	66.2	64	35.2	52.8	0.001
Babies receiving cotrim	-	-	78	32.9	33	18.1	11.5	0.001
Babies receiving gentamicin	0	0	73	30.8	21	11.5	21.9	0.001
Death	14	5.4	5	2.1	10	5.5	215.6	0.001
Case Fatality Rate of PSBI		14.1		3.2		15.6		

In BSL, 257 babies were ill within 60 days of their life with illness rate of 41.2%. In FON, 237 were ill and illness rate was 38.2%. In NI group, 182 were ill with illness rate of 29.7%. The most commonly observed danger sign was respiratory problem 38.1%, 41.8% and 30.2% respectively. Other illness includes the danger sign like unable to feed, bluish palm and sole, excess cry or no cry, no urine, convulsion, abnormal movement and other unclassified illness. Two or more danger signs were seen in 66.2% of babies in FON group. They were considered as possible severe bacterial infection. The symptoms of difficulty in breathing, redness around cord, skin problem were significantly different among the groups (p<0.005) where as non specific symptoms or danger sign had significantly decreased (p<0.001).

3.5 Outcome

A total of 14, 5 and 10 babies died in BSL, FON and NI groups respectively. Case fatality rate of PSBI was 14.1%, 3.2% and 15.6% in BSL, FON and NI group, respectively. The treatment and its outcome are in table 5.
The PSBI cases of 99(38.5%), 157 (66.2%) and 64 (35.2%) were seen in BSL, FON and NI groups. There is a significant difference in PSBI cases among the group ($\chi 2$ = 52.8; p<0.001). There was no any information about the treatment of ill babies in BSL. In FON group ill babies were treated by FCHV and VHW with cotrim and gentamicin. Cotrim was given to 78 (32.9%) ill babies and 73 (30.8%) of babies received gentamicin in FON group. In NI, babies treated with cotrim and gentamicin were 33 (18.1%) and 21 (11.5%) respectively. These were also found to be significantly different. ($\chi 2$ = 11.5; p<0.001and $\chi 2$ = 21.9; p<0.001). Total death of ill babies were 14 (5.4% of total ill babies), 5 (2.1%) and 10 (5.5%) in BSL, FON and NI group. The total case fatality rate of PSBI are high in BSL (14.1%) and NI group (15.6%) compared to FON (3.2%).

4. Discussions

The infants who are born at home are almost all exposed to substantial infectious challenge during their neonatal period. The study shows illness is associated with the care taking practices. [5] In our study, we had taken three groups – BSL, FON and NI, to find the efficacy of intervention in the essential new born care practices and management of neonatal illness in Morang district of Nepal. ANC receiving practice has been increased from BSL to FON but no difference in NI group. In NI group, MWRA received ANC from the regular government health services but intervention was not done. In all the three groups, it has been seen that pregnant women went for first antenatal service mostly in 2nd trimester only. However, the new mothers should be encouraged for first ANC within first trimester. The previous findings show that home delivery is a common practice in rural part of Nepal. [1, 6] After intervention, in the FON group, home delivery was low

(64.8%). David O et al had reported 90% of home delivery in rural part of Nepal [3] In rural part of India also, home delivery is quite common. [7] Though the delivery attendant by untrained has been decreased, the skilled and trained health workers need to increase their coverage more during home delivery. In the study by David O et al, there were 11% of women who gave birth alone [3], we found a much lower rate of 1.3%.

Cord cutting practices have been identified as risk factors for neonatal infection. [8-12] During the delivery, in FON group, 60.5% of women had proper care of cord. This shows the increment in the use of clean and safe instruments. A.H. Baqui et al suggested a low coverage of clean cord care among home deliveries in South Asia. [3, 13, 14] The application of the material on the cord especially oil is a risk factor for the infection. [15-17] There is no any additional benefit of topical substances on the cord. [18,19] So MINI's recommendation of keeping cord dry as per World Health Organisation guidelines of ENC were followed widely in FON group. However, ointment/dettol/powder was commonly used in FON group and oil in NI group. Other case control studies suggested that the use of antiseptics may reduce the risk of neonatal sepsis. [20-22] In our study in FON group, the practice of applying substances on the cord has been decreased than that of BSL and NI group.

Breastfeeding is one of the most important contributors to neonatal health, growth and development. Several studies have demonstrated effective reduction of mortality rate in neonate with early and exclusive breastfeeding. [23-29] However, there are few studies that have evaluated the breastfeeding in neonatal outcome. Huffman et all concluded that early & exclusive breastfeeding played an important role in reducing neonatal mortality. [30] The benefits are enhanced if breastfeeding starts within one hour after birth. Many neonatal health problems can be avoided or reduced by such a pattern of breastfeeding. However many women are not aware of the benefits of early breastfeeding. Our study shows that 29%, 43.5% & 43% of babies were breastfed within 1 hour of birth in BSL, FON and NI group respectively which is very lower compare to previous studies of 63%.[31] Though early breastfeeding was lower, all most all the women practiced breastfeeding (including breastfeeding within 1 hour and after 1 hour). Though the constant effort by the health workers to promote breastfeeding has resulted positive findings but it is not up to the mark. So health worker should promote for the early breastfeeding. In other studies [32,33], the first colostrum was commonly given to babies in our report. The breastfed babies have less risk to the infection. The practices of wiping, drying & wrapping babies were increased in FON group than BSL and NI group showing the positive effect of intervention.

As per WHO guidelines, bathing of neonate should be postpone [34], but there is a trend to bathe the babies soon after birth. After intervention, the practice of delay bathing (>24hrs.) increased. Birth weight is an important indicator of child survival but this is difficult in developing countries since most of the deliveries are conducted at home where adequate facilities to weigh a new born does not exist. [35] So in many rural part of Nepal, it is difficult to take the weight of babies immediately after birth mainly in home delivery. In our study, FCHV has weighed the baby using spring balance and identified the low weight baby during intervention. Early identification of low birth weight babies (<2500 gms) is vital in preventing neonatal deaths. Low birth weight is one of the risk factor for the illness of baby which is consistent with previous studies of community based new born care practices and might be improved through appropriate behaviors change intervention. [9, 13, 36] Our study also focused in identification and management of neonatal illness by FCHV and its outcome. The term "illness" includes all the danger sign identified by other studies. [36] The danger sign includes no suckling, lethargic, cold or warm body, respiratory problem (grunting or chest drawing), skin pustules, red eyes with discharge, redness around cord, yellow in skin and eyes and others (blue palm & sole, no urine, weak/excess cry, abnormal movement, convulsion etc) The presence of more than two of these danger sign was considered as PSBI. Breathing problem was most frequently reported in FON group (42.6%). The incidence of breathing problem (pneumonia or ARIs) in community level is not known. However, significant proportion of newborn diagnosed with sepsis or severe infections may have associated with pneumonia. [37] For the treatment of this severe problem in developing countries in health care facility, WHO recommended administration of antibiotics. Majority of neonatal death are in rural part/in home and families are reluctant to seek care outside the home for neonatal illness. [36] Therefore, grass root health worker should be trained for the treatment of neonatal illness. MINI project focused on this and trained FCHV for the treatment and management of neonatal illness. Before intervention, danger sign of neonatal illness was not known to the community health worker. After intervention, FCHV has identified these danger sign as per the approved algorithm due to which danger signs were more identified in FON group compared to BSL and control groups. After identification of illness FCHV initiated for treatment after obtaining consent from family. If any of the sign of PSBI seen, FCHV initiated treatment with cotrim and facilitate referral to higher level of health worker for injectable gentamicin. The babies receiving cotrim and gentamicin in FON group were 33% & 30.8% respectively. It seems that the illness rate in babies in FON is higher than BSL and NI; however, the total outcome or the fatality rate is low in FON compared to BSL and NI which reveals the effectiveness in intervention. The case fatality rate for PSBI was 14.1% in BSL which reduced to 3.2% in FON while in NI it is still high (15.6%). In India (Gadchiroli) the trained health workers could identify sick newborns in their home and were able to treat with antibiotics (cotrim & gentamicin) reducing neonatal mortality. [38] Our study also confirms the findings that if health workers are trained to identify the danger sign then the infection in neonate will be reduced. Infection being one of the major cause of neonatal death [39,40], lives of newborn can be saved by preventing it on the home setting too for which health workers and mothers should also be trained to identify the danger sign.

4. Conclusion & Recommendation

Our study suggested that neonatal infection and death are preventable through interventions. The intervention should focus on training to grass root level health worker. The proper and effective training may lead to change in knowledge, attitude and practice in community. The trained

health workers are need of rural areas in Nepal where hospitals are not easily accessible. The intervention should focus on antenatal counseling, safe and hygienic delivery, implement essential newborn care practices, identify the danger sign, assess them and treat with prescribed antibiotics. Apart from these, it is also recommended to provide training to all mothers to identify the danger sign so that early treatment can be started.

Acknowledgements

The Authors would like to thank the Project Director of Morang Innovative Neonatal Intervention Program for the kind cooperation. The Project is funded by the Bill & Melinda Gates Foundation, NFHP/USAID, Saving Newborn Lives Program (SNL) through Save the Children/US.

References

1. Nepal Demographic and Health Survey 2006, Population Division - Ministry of Health and Population, Government of Nepal, New ERA and Macro International Inc.
2. Bryce J, Terreri N, Victora CG et al. Countdown to 2015: tracking intervention coverage for child survival. Lancet 2006；368:1067-76.
3. David O, Kirti MT，Dej S et al。 Cross sectional community based study of care of newborn infants in Nepal. BMJ 2002； 325:1063
4. Fact Sheets of Nepal, Ministry of Health and Population, Government of Nepal.
5. Luke CM, Darmstadt GL, Joanne K et al. Risk Factors for Umbilical Cord Infection among Newborns of Southern Nepal. American Journal of Epidemiology 2007；165(2):203-11.
6. Pradhan A, Aryal R, Regmi G et al。Nepal family health survey 1996. Kathmandu and Calverton: Ministry of Health, Nepal; New ERA; Macro International, 1997.
7. Baqui AH, Williams EK, Darmstadt GL et al。 Newborn care in rural Uttar Pradesh. Indian J Pediatr 2007；74 (3):241-7.
8. Moss W, Darmstadt GL, Marsh DR et al. Research priorities for the reduction of perinatal and neonatal morbidity and mortality in developing country communities. J Perinatol. 2002；22(6):484-95.
9. Darmstadt GL, Bhutta ZA, Cousens S et al. Evidence-based, cost-effective interventions: how many newborn babies can we save? The Lancet 2005; 365 (9463): 977-88.
10. WHO. Care of the umbilical cord: A review of the evidence. Geneva: World Health Organization:1998.
11. Bhutta ZA, Darmstadt GL, Ransom E . Using evidence to save newborn lives. Policy brief. Washington, D.C: Population Reference Bureau, 2003
12. Costello A, Manandhar D. eds. Improving newborn infant health in developing countries. London: Imperial College Press. 2000; 289 – 308.
13. Manandhar DS, David O, Shrestha BP et al. Effect of a participatory intervention with women's groups on birth outcomes in Nepal. Cluster-randomised controlled trial. Lancet 2004; 364 (9438): 970-9.
14. Nandan D, Mishra S. Delivery Practices in West Uttar Pradesh. Indian J Public Health 1996; 40(1): 20-21. 24.
15. Bennett J, Azhar N, Rahim F et al. Further observations on ghee as a risk factor for neonatal tetanus. Int J Epidemiol 1995; 24 (3): 643-7.
16. Hectar T, John B, Kahn AJ et al. Ghee applications to the umbilical cord: a risk factor for neonatal tetanus. Lancet 1989; 4;1 (8636):486-8.
17. John B, Cindy Ma, Hectar T et al. Neonatal tetanus associated with topical umbilical ghee: covert role of cow dung. International Journal of Epidemiology 1999; 28: 1172-5.
18. Zupan J, Garner P, Omari AA. Topical umbilical cord care at birth. The Cochrane Database Systematic Reviews 2004；(3):CD001057
19. Bourke E. Cord care: too much or too little. Aust J Adv Nursing 1990; 7:19-22.
20. Abhay TB, Rani AB, Reddy HM et al., Reduced incidence of neonatal morbidities: Effect of home-based neonatal care in rural Gadchiroli, India. J Perinatol 2005; 25: S 51-61.
21. Kulathilaka T, Jayakuru W. Development of epidemiological services in Sri Lanka and future challenges. J commun Phys Sri Lanka 2001; Millennium suppl:21-8.
22. Vittoz JP, Labarère J, Castell M et al. Effect of a training program for maternity ward professionals on duration of breastfeeding. Birth 2004;31 : 302- 7.
23. Lopez A, Villalpando S, Fajardo A. Breast-feeding lowers the frequency and duration of acute respiratory infection and diarrhea in infants under six months of age. J Nutr. 1997;127:436–443
24. Zaman K, Baqui A, Yunus M et al. Acute respiratory infections in children: a community-based longitudinal study in rural Bangladesh. J Trop Pediatr. 1997;43:133–137
25. Leach A, McArdle T, Banya W et al. Neonatal mortality in a rural area of the Gambia. Ann Trop Paediatr. 1999;19:33–43
26. Raisler J, Alexander C, O'Compo P. Breastfeeding and infant illness: a dose-response relationship? Am J Public Health. 1999;89:25–30
27. Perera B, Ganesan S, Jayarasa J et al. The impact of breastfeeding practices on respiratory and diarrhoeal disease in infancy: a study from Sri Lanka. J Trop Pediatr. 1999;45:115–118
28. Cesar J, Victora C, Barros F et al. Impact of breastfeeding on admission for pneumonia during postnatal period in Brazil: nested case-control study. BMJ. 1999;318:1316–1320
29. Arifeen S, Black RE, Antelman G et al. Exclusive breastfeeding reduces acute respiratory infection and diarrhea deaths among infants in Dhaka slums. Pediatrics. 2001; 108(4). Available at: www.pediatrics.org/cgi/content/full/108/4/e67
30. Huffman S, Zehner E, Victora C. Can improvements in breast-feeding practices reduce neonatal mortality in developing countries? Midwifery 2001;17:80–92.
31. Upul S, Dulitha NF, Ishani R. Newborn care practices at home: effect of a hospital-base intervention in Sri

Lanka. Journal of Tropical Pediatrics 2006; 53 (2); 113-8.
32. Singh MB, Haldiya KR, Lakshminarayana J. Infant feeding and weaning practice in some semi-arid rural areas of Rajasthan. J Indian Med Assoc 1997; 95:576-8.
33. Srivastava SP, Sharma VK, Kumar V. Breast feeding pattern in neonates. Indian Pediatr 1994;31:1079-82.
34. Promoting Effective Perinatal Care, Essential Newborn Care and Breastfeeding, Training modules, WHO Regional Office for Europe, 2002.
35. Fazlui H, AMZ Hussain. Detection of Low Birth-Weight New Born Babies by Anthropometric Measurements in Bangladesh. Indian J Pediatr 1991; 58 : 223-231.
36. Abhay TB, Rani AB, Baitule S et al. Effect of home-based neonatal care and management of sepsis on neonatal mortality: field trial in rural India. Lancet 1999; 354: 1955–61.
37. Bhutta ZA, Darmstadt GL, Babara JS. Et al. Outcomes in Developing Countries: A Review of the Evidence Community-Based Interventions for Improving Perinatal and Neonatal Health. Pediatrics 2005;115;519-617
38. Abhay TB, Rani AB, Barbara JS et al. Is Home-Based Diagnosis and Treatment of Neonatal Sepsis Feasible and Effective? Seven Years of Intervention in the Gadchiroli Field Trial (1996 to 2003). Journal of Perinatology; 2005；25:S62–S71.
39. Save the children. State of the World's Newborn. Save the Children, Washington DC; 2001
40. Barbara JS. Neonatal infections: a global perspective in: Remington JS, Klein JO, editors. Infectious Diseases of the Fetus and Newborn Infant. 6th ed. Philadelphia: WB Saunders Company (in press).

Corresponding Author:
Sirjana Khanal, Department of Biostatistics & Epidemiology, College of Public Health, Zhengzhou University, 100 Kexue Avenue, Zhengzhou, Henan 450001, China.
Telephone # +86 371 65257125
Email: khanalsirju@yahoo.com

Other Authors' Information:
Weidong Zhang, Professor & Director, Department of Biostatistics & Epidemiology, College of Public Health, Zhengzhou University, 100 Kexue Avenue, Zhengzhou, Henan 450001, China.
Email1: imooni@zzu.edu.cn
Email2: imooni@163.com

Sudhir Khanal, Project Director of Morang Innovative Neonatal Intervention Program, JSI R & T, Nepal Family Health Program, Nepal. P.O. Box – 1600.
Email: sudhirkhanal@hotmail.com

Study of Biological Effect of MC3T3-E1 *in vitro* by A Novel 2.4GHz Radiofrequency Electromagnetic Field Exposure System

Shen Cherng[1,*], Hsien-Chiao Teng[2]

[1] *Department of Computer Science and Information Engineering, Chengshiu University, Kaohsiung, Niaosong, Taiwan, ROC;* [2] *Department of Electrical Engineering, ROC Military Academy, Kaohsiung, Fanshagn, Taiwan, ROC;* [3]

Received February 2, 2009

Abstract — A 2.4GHz mobile-phone/blue-tooth radiofrequency electromagnetic field (RF-EMF) exposure system for cellular experiment MC3T3-E1 *in vitro* was designed to study the biological effects and demonstrated in this report. Experimental results have illustrated the observation of signal at 14Hz through algorithm analysis of the measured near field magnetic fluctuation and the modulation of gap junction intercellular communication (GJIC) within mouse osteoblast cells (MC3T3-E1) under RF-EMF power density at 0.3mWatt/cm^2. [Life Science Journal. 2009; 6(4): 41 – 49] (ISSN: 1097 – 8135).

Keywords: GJIC, Near Field, RF-EMF

1. Introduction

Mobile telephones, television and radio transmitters and radar produce RF fields. These fields can be used to transmit information over long distances as well as radio and television broadcasting all over the world. Microwaves are RF fields at high frequencies in the range of GHz range. At radio frequencies, electric and magnetic fields are closely interrelated and typically we measure their levels as power densities in watts per square centimeter (W/cm2). Bluetooth provides a way to connect and exchange information between devices such as mobile phones, telephones, laptops, personal computers, printers, Global Positioning System (GPS) receivers, digital cameras, and video game consoles through a secure, globally unlicensed Industrial, Scientific and Medical (ISM) 2.4 GHz short-range radio frequency bandwidth. The Bluetooth specifications are developed and licensed by the Bluetooth Special Interest Group (SIG). The Bluetooth SIG consists of companies in the areas of telecommunication, computing, networking, and consumer electronics [1,2].

*Corresponding Author: cherng@msu.edu

Shen Cherng, PhD

Bluetooth devices are divided into three power classes with a maximum output power of 100 mW (class 1), 2.5. mW (class 2), and 1 mW (class 3) and transmit distances ranging from 10 to 100 meters [3]. Both scientific and public concerns have been raised about the potential health impacts from regular use of microwave mobilphone [4]. Accordingly, even through numerous studies have reported no significant relationship between mobile phone use and health, a lot of scientists still have been dedicated research in the years on the possible and real effects of RF-EMF on biological system [6,7,8,9]. From our previously experiments cellular signal may be induced from the exposure of RF-EMF due to the outcome that we found a small power signal embedded in the ambient near field magnetic fluctuation [10]. Essentially, biological signal embedded in ambient fluctuation being found is not a surprising, such as cell membrane current is 10^{-15} ampere [11]. This signal is comparatively very much even less than the amount of sharp noise current from operation of the switch of electrical equipment when measuring the current [12]. As we know, ambient EMF fluctuation originates from a self-propagating wave in space, such as earth or through

active devices. Not only EMF has an electric and magnetic field components, which oscillate in phase perpendicular to each other and to the direction of energy propagation, but also can be classified into types according to the frequency of the waves; these types include radio waves, microwaves, terahertz radiation, infrared radiation, visible light, ultraviolet radiation, X-rays and gamma rays. Our previously experiments revealed that cells in vitro should be affected by electromagnetic field and the GJIC being modulated. Basically, GJIC is an indicator to express the cell's response affiliated with many pathological endpoints [13], such as cell aging, apoptosis, proliferation and differentiation, are associated with the modulation of GJIC. To measure GJIC modulation, scrape loading dye transfer of Lucifer yellow [13] was used in this report. The degree of modulation of GJIC can show the degree of cellular response to the EMF exposure. Therefore, in this report, we assured the impact of GJIC caused by RF-EMF by using a novel exposure system for the experiments. Previously, a proposed microstrip patch antenna providing a RF-EMF at 2.4GHz to the cultured rat liver epithelial cells with observable modulated GJIC was published in reference [14]. In this work, a more customized microstrip patch antenna providing a RF-EMF at 2.4GHz to the cultured mouse osteoblast cells with modulated GJIC was proposed for further discussion of the EMF impact to the cells *in vitro*. An inexpensive FR4 plate, a print circuit board (PCB) was used in convenience [15] for mounting the cell co-culture dish to the antenna. A customized designed check-shape radiator was constructed for measuring gain and justifying the transmitting power. The scanning probed near field magnetic fluctuation was recorded to correlate the GJIC modulation within the cells in GJIC assay by the exposure RF-EMF at 2.4GHz [16]. Usually, possible EMF sources that may cause the biological effects include the ambient field [17, 18], cells internally resonant signals, and the RF-EMF originated near field cross polarization fluctuation etc. are equally important to the health impact study of the EMF related biological effect concerns. In this work, we adjusted the size of the ground of the antenna to reduce the perturbation of the cross-polarization [19] and the power as well as the gain. Also, since scientists have suggested a lot of possible interaction models to explain the experimental results and the biological effects caused by RF-EMF as well as ELF interaction [20], we proposed a new model combining design of a customized microstrip antenna with special algorithm and the cellular assay of GJIC for assuring the biological effect being found. Even through in still, controversial outcome remains the conclusion in ambiguity.

2. Configuration of the Customized 2.4GHz RF-EMF Transmitter

The customized 2.4GHz transmitter (a microstrip antenna) mounted with a co-culture dish depicted in Fig.1. In the design, a V-shaped radiator provides RF-EMF at 2.4GHz. Cultured cell dish can be mounted on the slotted patch between the end point of V-shape radiator and the FR4 plate by two plastic clips to avoid the perturbation of the signals. A T-type patch ground was printed on 18.56mm×2.9mm×0.4mm FR4 plate and a small microstrip is linked to the SMA connector using as transmission line. The optimization length of the radiator is 20 mm.

3. Materials and methods

3.1 Cell culture:

The mouse osteoblastic MC3T3-E1 cell line was donated from Dr. C.C. Chang, Department of pediatrics, School of Medicine, Michigan State University, originally was obtained from D.T. Yamaguchi, Research Service and Geriatrics Research, Education, and Clinical Center, VAMC, West Los Angeles, California, USA and has been maintained in D-medium same as the cell line in Dr. C.C. Chang's Lab in Michigan State University, East Lansing, Michigan, USA. The cells were incubated at 37˚C in a humidified atmosphere containing 5% CO2

and 95% air and were fed or trypsinized every two to three days. Cells in culture for seven days can be used for experiments.

3.2 GJIC Assay:

The scrape load/dye transfer (SL/DT) technique was used to measure the GJIC within cells [21]. After the treatment, the cells were rinsed with phosphate buffered saline (PBS), and a PBS solution containing 4% concentration lucifer yellow fluorescence dye is injected into the cells by a scrape using a scalpel blade. Afterwards the cells were incubated for 3 minutes and extra cellular dye was rinsed off and fixed with 5% formalin. We then measured the area of the dye migrated from the scrape line using digital images taken by an epifluorescent microscope and quantitated with Nucleotech image analysis software for the GJIC images.

3.3 Measurements of the near filed fluctuation in exposure of RF-EMF and the ambient filed:

The probe is the accessory magnetometer of the instruement F.W. Bell 9550 provided by National Instruement, Austin Texas, USA. The scanning probe is fixed at 1mm above perpendicularly to keep the phase at 90 degree with the plan of the cell layer. The RF-EMF at 2.4GHz was transmitted by the antenna proposed as in Fig. 1. The experimental data was recorded and transferred to the 54621A oscilloscope, made by Agilent Compony, Santa Clara, California, USA and saving as the file of Microsoft

3.4 Math Analysis:

The signal s_{ij} (jth element in ith ensample) is used as input to a background n_{ij}, the output $\{x_{ij}\}$ can be transformed to electrical voltages shown on oscilloscope. By using HP Benchlink, we collected the output data and transformed it to Microsoft Excel as text files. Matlab and FORTRAN programs were performed to analyze the data and get power density spectrum. We proposed a simple one dimensional filter algorithm used to amplify the difference between the input signal amplitude and the output power to an observable level so that we can exam any biological responding signal embedded in noise by power density spectrum calculation [22]. Consider the data output sequence $\{x_{ij}\}= \{s_{ij}\}+\{n_{ij}\}$. Set six values from v_1 to v_6 by taking v_1 the maximum amplitude of ambient geomagnetic fluctuation and then take $v_2 = 0.95v_1$, $v_3 = 0.85v_1$, $v_4 = 0.75v_1$, $v_5 = 0.65v_1$, $v_6 = 0.55v_1$ for six levels, and therefore, $v_1>v_2>\ldots..>v_6$. If more values being selected, more calculation should be involved. And then, compute $\bar{x}_{ij}$ (the average value of x_{ij}), If $x_{ij} > \bar{x}_{ij}$, define m_h so that a high threshold value m_h is defined as $m_h = x_{ij}$. If $x_{ij} < \bar{x}_{ij}$, define a low threshold value m_1 so that $m_1 = \bar{x}_{ij}$. If $x_{ij} > m_h$, set $m_{hh} = x_{ij}$, then, a second high threshold m_{hh} should be defined. We first defined m level values. Select m so that m is more than $\bar{x}_{ij}$ but less than m_h and set m_{h1} being equal to $\bar{x}_{ij}$ and compare that If $m_1 < \bar{x}_{ij} < m$, $\bar{x}_{ij} = m_{1h}$, otherwise If $\bar{x}_{ij} < m_1$, set $\bar{x}_{ij} = m_{11}$, the $m_{hh} > m_h > m_{h1} > m > m_{1h} > m_1 > m_{11}$ should be kept. If $x_{ij} > m_{hh}$, set $\bar{x}_{ij} = v_1$, If $m_{1h} < x_{ij} < m_{hh}$, set $x_{ij} = v_2$, If $m_{h1} < x_{ij} < m_h$, set $\bar{x}_{ij} = v_3$, If $m < x_{ij} < m_{h1}$, set $x_{ij} = v_4$, If $m_{1h} < x_{ij} < m$, set $x_{ij} = v_5$, If $m_1 < x_{ij} < m_{1h}$, set $x_{ij} = v_6$. The noise is defined as all unpredictable signals in power density spectrum. We also must define ASNR = $\frac{A_s}{A_n}$ where A_s is the amplitude of the signal and A_n is the noise of the background. SNR = $\frac{P_s}{P_n}$ is defined where P_s is the power of the signal and P_n is the noise power of the background can be calculated, the plot of ASNR versus SNR produces a function curve showing the relation between the input signal amplitude and responding output power. Accordingly, even through noise may have its own characteristic; we can calibrate the function curve with the help of adjusting input signal's amplitude to amplify the power difference between the noise and the signal. The application of this function curve can be considered for the frequency component in power

density spectrum of the noise depends upon the characteristic of the signal. When the exposure RF-EMF source is absent, we can measure the signal dependent noise, which is the combination of the ambient field with the cell, induced signal fluctuations. Meanwhile, if the switch of the RF-EMF is open, we can measure the responding fluctuation from the cells under the reaction of RF-EMF if we can filter out the noise. Through the formula of the correlation,

$$R_q = \left(\frac{1}{N}\right)\sum_{p}^{N} V_p V_{p+q}, \quad S_k = \sum_{q=1}^{N} R_q e^{\frac{i2\pi Kq}{N}}$$

3.5 Algorithm to identify the intrinsic signal and it's SNR:

Let {1Hz, 2Hz, ...20Hz, 21Hz, 22Hz…58Hz,59 Hz} denote the given sequence of frequencies $\{\omega_i\}$, ω_1 =1Hz, ω_2 = 2Hz, ω_3 = 3Hz,.....ω_{50} = 50Hz,….ω_{59} = 90Hz, respectively.

1. Take the maximum Vmax from ambient geomagnetic fluctuation {V (t)}
2. Mathematically add sin(ωit) signal for a ωi with amplitude Vmax to { V(t) } and name the result as {Vg(t)}.
3. Perform autocorrelation and Fourier transform to get the power density spectrum (PDS) of {Vg (t)}
4. Calculate the SNR at maximum of {SK} and represented as S_{max} (ω_i) for checking every possible ω_i in PDS. Notably, (a) the power of the signal is defined as the area under the frequency at ω_i, and (b) the power of the noise is defined as the total power of the all possible ω_i in PDS, {S_k, noise(ω_i)} of the {Vg(t)}, and (c) the SNR is defined as the power of the source signal divided by the power of the noise of the system, therefore, SNR can be rewritten as $SNR = \frac{S_{max}(\omega_i)}{S_{k,\,noise}(\omega_i)}$.

5. Repeat step 2, step 3 and step 4 with the amplitudes 0.7Vmax at ω_i to calculate Smax (ω_i) at ASNR=0.7 by assuming $S_{max,0.7}(\omega_i) = X_{0.7}$.

0.4Vmax at ω_i to calculate Smax (ω_i) at ASNR = 0.4, by assuming $S_{max,0.4}(\omega_i) = X_{0.4}$.

0.03Vmax at ωi to calculate Smax (ω_i) at ASNR = 0.03 by assuming $S_{max,0.03}(\omega_i) = X_{0.03}$

0.003Vmax at ωi to calculate Smax (ω_i) at ASNR = 0.003 by assuming $S_{max,\,0.003}(\omega_i) = X_{0.003}$ and so on.

6. Thus, if $pX2 + qX + r_{ASNR}(\omega_i) = 0$, using square curve fitting, we can easily get the corresponding p,q and r_{ASNR} (ω_i) values at each ω_i .

$$pX_{0.7}^2 + qX_{0.7}^2 + r_{0.7}(\omega_i) = 0$$
$$pX_{0.4}^2 + qX_{0.4}^2 + r_{0.4}(\omega_i) = 0$$
$$pX_{0.03}^2 + qX_{0.03}^2 + r_{0.03}(\omega_i) = 0$$
$$pX_{0.003}^2 + qX_{0.003}^2 + r_{0.003}(\omega_i) = 0$$

Consequently, p, q and r_{ASNR} can be calculated. The most interesting result is that by extrapolation method, r_0 (ω_i) value is not equal to zero. Notably, the $r_0(\omega_i)$ spectrum is characterized by the possible given intrinsic frequency ω_i buried in {V(t)} [16]. By analyzing the measured {V(t)} of osteoblast cells in the exposure of RF-EMF and {Vg (t)} of ambient geomagnetic field, we found $r_{=0}(\omega_i)$=0 at 14Hz for osteoblast cells is about 50 times more than that in the ambient geomagnetic field. The filter algorithm that we previously proposed in reference [12] can improve the amplification of the extremely low frequency to 10^4 times more than the noise. The comparison of calculation results is listed in table I which shows that we can recognize easily if the ELF signal being kept 104 times lower than the ambient noise. Measurements of return loss (RL) means a measure of power reflected from imperfections in an electrical link being defined as the ratio PR / PT, representing the power of the wave reflected from the imperfection (PR) to that of the transmitted, wave (PT) [23]. For best performance, the reflected signal should be as small as possible, meaning the ratio PR / PT should be as small as possible. Return loss is expressed in decibels. The return loss value describes the reduction in the amplitude of the reflected energy, as compared to the forward energy. It will always be a loss and therefore

a negative dB. However, we can write, for instance, -3 dB as simply 3 dB of loss, dropping the negative sign and adding loss, which means the reflected energy from the device, PR, is always 3dB lower than the transmitted energy PT. When expressed in dB, larger (in magnitude) negative numbers represent larger return losses and thus smaller reflected power PR.

Measurements of Antenna Gain: It is defined as the ratio of the radiation intensity of an antenna in a given direction to the intensity of the same antenna as it radiates in all directions (isotropically). Since the radiation intensity of an isotropically radiated power is equal to the power into the antenna divided by 360 degrees, we can express the following equation: Gain = $4\pi\times\frac{\text{Radiation Intensity}}{\text{Input Power}}$ The near field magnetic fluctuation is defined for the electromagnetic induction and electric charge effects on the EMF which effects decreasingly with increasing distance from the antenna. Typically, near field magnetic fluctuation would not be important farther away than a few wavelengths of the operation frequency of the antenna [24]. These near field effects involve energy transfer coupling directly to receivers near the antenna and affecting the power output of the transmitter. In a sense, the near field offers the information of energy transfer which is available to a receiver but sensed by the transmitter. The source of 2.4GHz RF-EMF was provided by HP/AGILENT 8722A/C (50MHz to 40GHz) Microwave Vector Network Analyzer (MVNA) [25]. The MVNA can be used for various kinds of applications, both for the classical type microwave engineering circuit characterization and many novel ones in research. Because of its unique capabilities, we used MVNA to transmit the RF-EMF to the cells with the power density of 0.3mWatt/cm2 at 2.4GHz. It becomes a useful tool in our research to explore cell responding signal in RF-EMF exposure. The 1-1000 GHz frequency domain covered by the MVNA bridges the interval between ordinary microwaves and infrared techniques. In particular, in energy units, the Microwave Vector Network Analyzer covers the range 0.03~4 meV for each drifting electron. This range contains characteristic energies of many elementary excitations.

4. Results and Discussion

In Fig. 2, it depicts the measurements of the return loss and the antenna gain of the proposed antenna. The operation frequency is at 2.4 GHz. Both with cells and without cells in the mounted culture dish have no effect to the measurements of the return loss, antenna gain as well as the operation frequency. There is also no influence of all antenna measurements to the proposed antenna mounted culture dish in comparison to the antenna only. However, the GJIC of the osteoblast cells reveals the biological effect for the exposure of RF electromagnetic wave at 2.4GHz. Meanwhile, the new method we previously developed for the calculation of signal to noise ratio verified the experimental result which shows the absorption frequency at 14 Hz. The measure magnetic fluctuation and mathematical calculation results are shown in Fig. 3. Meanwhile, we found the GJIC modulation within osteoblast cells under 2.4 GHz exposure of electromagnetic wave is observed at 20% which is shown in Fig. 4. Basically, all cancers have been generally viewed as the result of a disruption of the homeostatic regulation of a cell's ability to respond appropriately to extra cellular signals of the body which trigger intracellular or intercellular signal transducting mechanisms by modulating gap junctional intercellular communication between the cells within a tissue. In short, carcinogenesis means mutation of the genetic material of normal cells to interrupt the normal balance between proliferation and cell death. From Fig. 4., we can see the modulation of the GJIC within the mouse osteoblast cells by RF-EMF. The consequence of the GJIC modulation by RF-EMF may cause the cell being possibly in mutant, quickly aging, stop

proliferation and even in instantaneous death [26]. The mechanism of releasing of 14Hz signal may through the models referred to calcium oscillation, cyclotron resonance, stochastic resonance and cell growth oscillation. However, due to the consideration of potential health impact, RF-EMF may be an odd factor to human health we should be careful to deal with. Additionally, not only RF-EMF can be characterized by the amplitudes of electric and magnetic field which oscillate in phase perpendicular to each other and to the direction of energy propagation, but also can be classified into types of energy and power mathematically according to the values of multiplication of frequency and amplitude [27]. Thus, the total absorbed power by the mouse osteoblast cell system exposed into RF-EMF is about 3×10-16 Watt which is very small and supposedly has no hurt to the cell for our design. However, experimental result has shown significant modulation of the GJIC . In this report, we only proposed a new process algorithm to show the existence of 14Hz signal by measuring near field fluctuation and reveal this signal is a power signal that may caused the modulation of GJIC within mouse osteoblast cells. No mechanism model we would suggest due to the complexity of the signal transduction on the surface of the cell membrane and the lack of molecular biology experimental evidence.

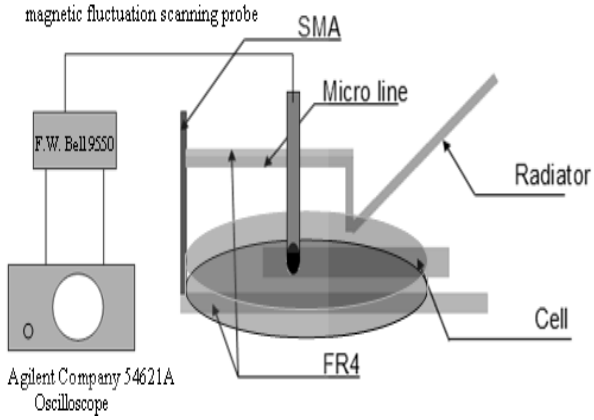

Fig 1: Schematic drawing of the cellular exposure

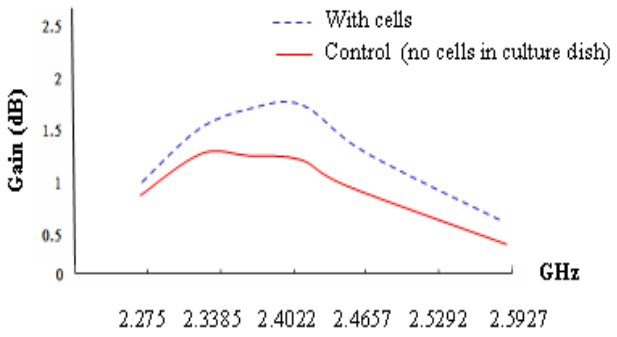

Fig 2: The measured (a) Return Loss
(b) antenna gain

(a)

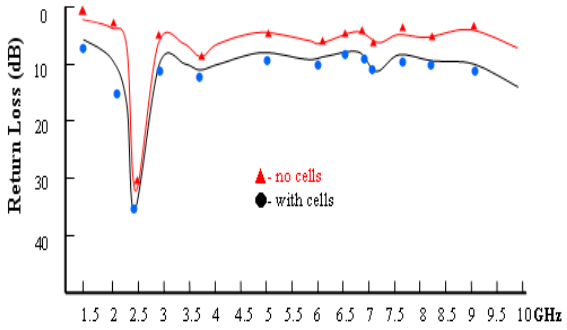

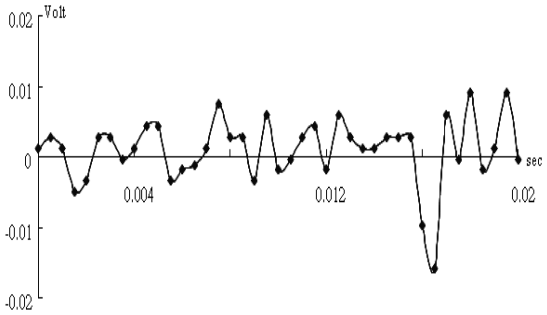

(a)

(b)

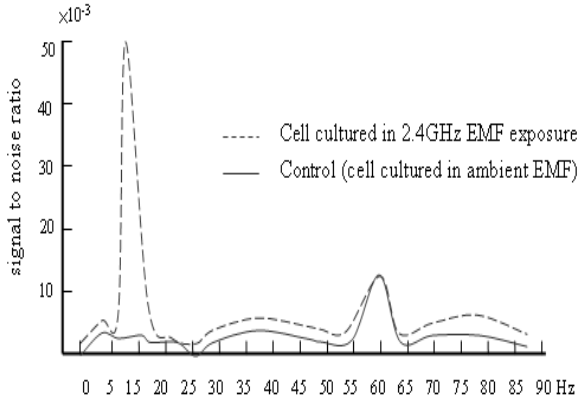

(b)

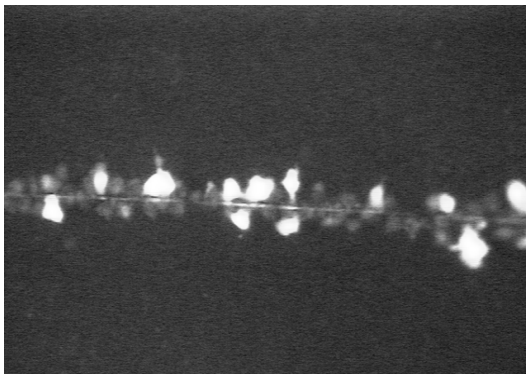

(a)

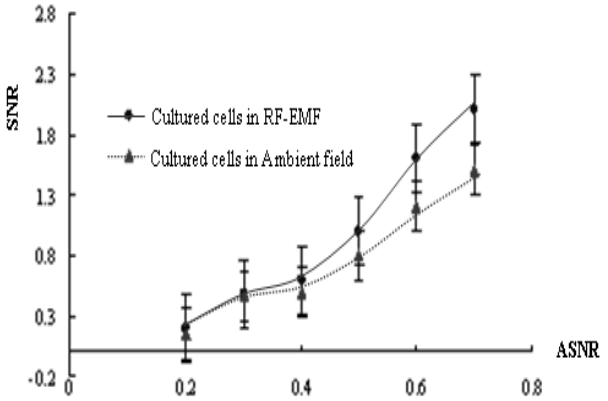

(c)

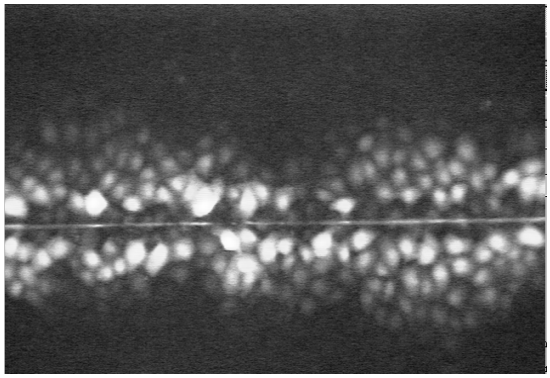

(b)

Fig 3. (a)Measurement of near field magnetic fluctuation of the mouse osteoblast cells by the exposure of RF-EMF at 2.4GHz (b) $r_0(\omega_i)$ spectrum of the frequency range from 0 to 90 Hz (c) SNR vs. ASNR fitting curve of exposure mouse osteoblast cells, which respond signal frequency at 14 Hz, in 2.4GHz RF-EMF Exposure.

Fig 4: (a) GJIC modulation within mouse osteoblast cells by RF-EMF at 2.4GHz (b) original GJIC within mouse osteoblast cells in ambient geomagnetic field

Table1.
Comparison of the power density spectrum calculation
-: not able to identify ELF at 15Hz embedded in ambient field
+: able to identify ELF at 15Hz embedded in ambient field

Input ASNR	PDS	PDS with adding filter algorithm	Output S/N Ratio
1.0	+	+	1.5
0.5	+	+	0.37
0.1	-	+	0.015
0.05	-	+	0.004
0.01	-	+	0.0001

5. Conclusion

According to the measurements, the proposed antenna mounted culture dish can provide an exposure of RF-EMF at 2.4GHz which can significantly affect GJIC within the mouse osteoblast cells cultured *in vitro*. The RF -EMF may stimulate the cultured mouse osteoblast cells to respond an extremely low frequency at 14Hz. Mathematical calculation can reveal the existence of 14 Hz signal in the power density spectrum of the probed near field magnetic fluctuation when the GJIC modulation being initiated significantly within the cells.

References

[1] Tang CL, Chou JY, Wong KL. Broadband dual-frequency v-shape patch antenna. Microwave and Optical Technology Letters. 2000;25:121-123.

[2] Maci S, Gentili GB. Dual-frquency patch antennas. IEEE Antennas Propagat Mag. 1999;39:13-20.

[3] Dawson, TW, Caputa K., and Stuchly, MA Influence of human model resolution on computed currentys induced in organs by 60Hz Magnetic field, Bioelectromagnetics 18:478-490 (1997)

[4] Trosko, JE, Chang, CC. Role of stem cells and jap junctional intercellular communication in human carcinogenwsis. Radiation Research 155, 175-190, (2001)

[5] Trosko, JE, Ruch, RJ. Cell-cell communication in carcinogenesis. Front. Biosci., 3, 208-238 (1998)

[6] Mongia, RK. Reduced size metalized dielectric resonator antennas, in IEEE Antennas Propagat.-S/URSI Symp. Digest, Montreal, Canada. 1997:2202–2205.

[7] Maeda T, Morooka T. Radiation efficiency measurement of electrically small antennas using radio waves scatterers. IEEE Antennas Propagat Int. Symp. Dig. 1988:324–327.

[8] Cain, CD, Thomas, DL, Adey, WR., Focus Formation of C3H/10T1/2 Cellsw and exposure to a 836.55MHz Modulateed Radiofrequency field. Bioelectromagnetics 18:237-243

[9] Formica, D, Silvestri, S. Biological effects of exposure to magnetic resonance imaging: an overview. http://www.biomedical-engineering-online.com/content/3/1/11, Biomed Eng Online, 2004

[10] Stephen A. Sebo and Eva A. Sebo Societal reaction to the power frequency electric and magnetic field effects of electric utility systems.International Journal of Technology Management Volume 19, Numbers 3-5 p439-452 2000

[11] Vance M. M. ; Wiley L. M. Gap junction intercellular communication mediates the competitive cell proliferation disadvantage of irradiated mouse preimplantation embryos in aggregation chimeras. Radiation research 1999, vol. 152, p544-551

[12] Teng, HC. A Puzzle of the Effect of Magnetic Field on Biological Cells. Life Science Journal , 2(1) , 16-21 2005

[13] Susan C. McKarns and David J. Doolittle Cell Biology and Toxicology Volume 8, Number 1 / March 1992 pp 89-103

[14] Chen, G., Shen Cherng, Hsien-Chiao Teng: The biological response of cell monolayer thin film under the patch antenna at operation frequency 2.4GHz. ROC Biomedical Annual Conference (Dec. 17~18, 2004) D-II-4 2004

[15] Yu-Min Li, Chia-Ching Chu, Yuan-Tung Cheng, Hsien-Chiao Teng, Shen Cherng: The Study of a Novel Microstrip Antenna Being Used for the Estimation of Sample Material Dielectric Coefficient under Electromagnetic Wave at 2.4 GHz. Nature and Science. 4(3):41-44; 2006

[16] Hsien-Chiao Teng, Shen Cherng: Recovering Extremely Low Frequency Signal from the Signal-Dependent Noise Background. Nature and Science, 2(4), Supplement, 95-97; 2004

[17] Hsien-Chiao Teng, Shen Cherng: The Non-Stationary Analysis of Osteoblast Cellular Response to the reaction of ELF magnetic Field. Nature and Science, 2(4), Supplement, 98-101;2004

[18] Hsien-Chiao Teng, Shen Cherng: Recovering Extremely Low Frequency Signal from the Signal-Dependent Noise Background. Nature and Science, 2(4), Supplement, 95-97; 2004

[19] Hsien-Chiao Teng, Chih-Sen Hsieh, Shen Cherng, Yuan-Tung Cheng: A 3D Crotched Double-band Dipole Antenna with Wide Impedance Bandwidth Novel Design for WLAN System. Nature and Science, 3(2), 47-50; 2005

[20] Hsien-Chiao Teng, Shen Cherng: The Characteristic Frequencies in Cell Induced Magnetic Fluctuation. Nature and Science, 2(4), Supplement, 102-107; 2004

[21] Upham, B., Deocampo, N.D., Wurl, B., Trosko, J.E. (1998)：Inhibitation of Gap Junctional

[22] Cellular Communication by Perfluorinated Fatty Acids is dependent on the chain length of the Fluorinated Trail. Int. J. Cancer 78: 491-485

[23] HC Teng, Y Tung, S Cherng: The intracellular communication study of the mouse osteoblast cells in 25Hz AC magnetic field. Proceedings electrical and information engineering symposium. CIEE. May 30, 2003, pp 86~pp 92, 2003

[24] Beyer, J.; Drung, D.; Kirste, A.; Engert, J.; Netsch, A.; Fleischmann, A.; Enss, C. (2007) A Magnetic-Field-Fluctuation Thermometer for the mK Range Based on SQUID-Magnetometry Applied Superconductivity, IEEE Transactions on Volume 17, Issue 2, June 2007 Page(s):760 - 763…

[25] P. Goy, "Antenna vector characterization in the mm- and submm-wave regions", Microwave Journal, June 1994, p.98.…

[26] Paolo Vecchia, Rüdiger Matthes, Gunde Ziegelberger James Lin, Richard Saunders, Anthony Swerdlow (2009) Exposure to high frequency electromagnetic fields, biological effects and health consequences (100 kHz-300 GHz), International Commission on Non-Ionizing Radiation Protection

[27] M. Hietanen, T. Alanko (2005-10). "Occupational Exposure Related to Radiofrequency Fields from Wireless Communication Systems" (PDF). XXVIIIth General Assembly of URSI - Proceedings. Union Radio-Scientifique Internationale. Retrieved on 2007-04-19

Tai chi exercise affects the isokinetic torque but not changes hamstrings: quadriceps ratios

Yen Ke Tien[1] and Chang Kuan Yu[2]

1. Cheng Shiu University, Kaohsiung, Taiwan, ROC

2. Mackay Memorial Hospital Taitung Branch, Taitung, Taiwan, ROC

Received March 10, 2009

Abstract: Tai chi, which originated in China, is a form of exercise that focuses on controlled movements. The aim of our study is to examine the differences in the eccentric/concentric functional ratio for the knee in the aged after 12 weeks Tai Chi training. Materials and methods include 20 aged subjects were recruited. To match their physical activity level following the physical performance testing procedures and then 12 week Tai Chi training program (practiced Tai Chi for a minimum of 4 $h \cdot wk^{-1}$). Physical characteristics, functional physical performance and isokinetic performance were measured. Concentric and eccentric isokinetic tests of the subjects' dominant knee extensors and flexors were conducted at an angular velocity of 30 $deg \cdot s^{-1}$. After 12 weeks Tai Chi training, functional physical activity were improving significant ($p < 0.05$). Subjects had higher total work in concentric and eccentric isokinetic contractions of their knee extensors and flexors but not Hamstring/Quadriceps ratio (H/Q) ($p > 0.05$). Conclusively, Tai Chi training enhance knee muscular performance but may not change H/Q. [Life Science Journal. 2009; 6(4): 50 – 55] (ISSN: 1097 – 8135).

Keywords: Micro drilling, Bones, Natural properties

1. Introduction

Conventionally, the quadriceps/hamstring ratio is calculated by dividing the torque of knee extensors and flexors at identical angular velocity and contraction mode. However, previous authors have suggested that to evaluate muscular balance of the knee eccentric (ECC)/concentric (CON) actions of the knee flexors (KF) and knee extensors (KE) should be examined (ECC_{KF}/CON_{KE} or CON_{KF}/ECC_{KE} ratio) and referred to as functional ratio rather than the established ratios often used (ECC_{KF}/CON_{KF} or ECC_{KE}/CON_{KE} ratio) [1]. Analyzing correlative muscle group ratios provides messages on knee function, injury risk ,and knee joint stability [2]. One previous study that used demonstrated that an ECC/CON ratio of less than 60% at 60 $deg \cdot s^{-1}$ represents a 77.5% probability of knee injury in elite soccer players [3]. There seems to be unavailable data on associative risk of injury from functional ratios.

Tai chi, which originated in China, is a form of exercise that adjusts to control movements coherent deep diaphragmatic breathing [4]. There are 5 major styles, Chen, Yang, Wu, Zheng, and Sun, each with its own different characteristics but all based on the same cardinal principles [5]. Sun and Zheng styles have recently become widely used to improve balance and reduce the risk of falls among the elderly population [6], and a specific Sun-style form of Tai Chi is currently endorsed by The Arthritis Foundation in the US as a methods for executive OA pain. In view of the raised popularity of this exercise in both North America and Australia, a growing body of research aimed at exploring the health benefits of Tai Chi has originated. Many of the individual experiments have reported Tai Chi to have positive effects on quality of life, pain, and physical function in populations with chronic situations[7], However, none of these papers have provided a quantitative evaluate of the influence on the prossession of Tai Chi for chronic musculoskeletal conditions. The purpose of this study was to examine the differences between the Functional physical performance and eccentric/concentric functional ratio for the knee in the aged after 12 weeks Tai Chi training.

2. Materials and Methods

2.1 Subject

*Corresponding Author: ktyen@csu.edu.tw

31 middle-aged subjects were recruited from several community older adult centers. They had no previous experience in practicing Tai Chi, though some took morning walks or did stretching exercises. To match their physical activity level following the general functional testing procedures and 12 week Zheng style Tai Chi training program (TC) (practiced Tai Chi for a minimum of 4 $h \cdot wk^{-1}$). Subjects visited the laboratory before testing to habituate themselves with the laboratory environment and realize the experimental procedures, including familiarization of concentric/eccentric isokinetic tests. The study received ethical approval from the Institutional Research Ethics Committee.

2.2 Functional physical performance

The functional physical performance [8] was performed the following ssessments for all the subjects before and after the Tai Chi exercise program.

(1) 2-min step marking. Walking endurance was assessed using a 2-min step marking. Each subject stepped marking for 2 minutes as soon as possible and raising knee higher than 1/2 thigh length. The total time of stepping by each subject was recorded.

(2). Chair rise. Subjects were asked to stand up consecutively from a chair with a seat level of 43.2 cm from the floor with their arms folded, and sit down as fast as possible. The time taken to complete the task from sit-to-stand was recorded in 30 seconds.

(3) Bicep curl. Subjects were asked to hold the dumbbells (2.27 kg) in dominate hand, consecutively rised with their arms from straight arm to curl, and as fast as possible. The time taken to complete the task was recorded in 30 seconds.

(4) Sit and reach. Subjects were asked to sit on a 43.2 cm chair and bent the dominate leg in 90 degrees. Then Subjects stretched undominate leg and two arms, and bend down the back as closer fingers to toes as possible. The closest distance taken to complete the task from fingers to toes was recorded.

(5) Timed up and go test. The subjects were asked to rise from a chair (0.42 m in height), walk 2.44 m, turn and return to the chair and sit down, as quickly as possible. The time required to perform the entire procedure was recorded.

2.3 Isokinetic test

Isokinetic concentric/eccentric knee extension and flexion were measured using a calibrated Biodex system 3 (Shirley, NY, USA). A specially designed chair was used which allowed for the various thigh lengths of the subjects. At all testing sessions, a standardized procedure included a warm-up of 2-min cycling on a Monark cycle ergometer 814E (Monark, Varberg, Sweden) at a moderate intensity and 2 minutes of stretching the hamstring and quadriceps muscles before the knee test. The dominant limb, determined from kicking preference, was used for assessment. Subjects were prepared for a seated position and the axis of rotation of the dynamometer lever arm was aligned with the lateral epicondyle of the knee. The force pad was placed approximately 3 cm superior to the medial malleolus with the foot in a plantar flexed position. The subject was asked to relax their leg so that passive determination of the effects of gravity on the limb and lever arm could be measured. Range of motion (ROM) for the knee test during concentric actions were 90 degrees and 15degrees for eccentric actions, due to the need for an applied preload torque of the eccentric limits. This reduction in ROM for eccentric actions was made necessary by the need for the preload activation torque that could not be performed at the terminal of the ROM, especially in the aged subjects. To ensure full extension, anatomical 0° was determined as maximal voluntary knee extension for each subject. Testing occurred at 30 $deg \cdot s^{-1}$. Subjects were guided to push the lever up, and pull it down, as hard and as fast as possible with extension/flexion undertaken first for concentric actions. For eccentric actions, subjects were instructed to opposing the lever arm with extension as the first movement. The subjects performed three maximal efforts to determine maximal peak torque during CON/CON and ECC/ECC cycles. A 2-min rest period was given between cycles with CON actions tested before ECC actions. All subjects were encouraged to give a maximal effort for each action by using both visual feedback and strong verbal encouragement.

2.4 Statistical analyses

Maximal CON and ECC isokinetic peak extension torque (PET) , peak flexion torque(PFT) and time to peak torque identified from the efforts were gravity corrected, filtered and windowed to only include constant velocity periods. At 30 deg·s^{-1} and 180 deg·s^{-1}, for CON and ECC actions respectively, Data were analysed using Statistical Package for Social Sciences (SPSS) (V10.0, SPSS, Inc., Chicago, IL, USA). Functional physical performance, ECC_{KF}/CON_{KE} and CON_{KF}/ECC_{KE} ratio for the knee joint were examined using before/after by paired *t*-test. Significance was accepted at the $p < 0.05$ level.

3.Results

3.1 Physical characteristics

Twenty participants completed the program and were later reassessed. Eleven participants failed to complete the exercise program assessment or intervention, primarily because of changes in address and worsening personal or family health. The mean age of the participants in the study group was 65.3(4.6) years. Additionally, 80.0% were housewives and 76.0% were retired. Among the participants, 92.0% were married, and 8.0% were single. The highest level of education attained among the participants was: 8% completed the elementary school level, 32% completed middle and high school, and 76% completed university. Furthermore, 28% lived alone. Of the participants, 4% had a history of geriatric falls. During the exercise period no falls by any of the participants were observed. Also, no analysis or record of the frequency of falling was done.

There is no physical characteristics difference after 12 weeks Tai Chi training (TABLE 1).

TABLE 1. Comparision of age ,height, weight, blood pressure and bone density after 12 weeks Tai Chi training (N=20)

ITEM	UNIT	Pre-training	Post-training
age	year	65.3(4.6)	65.5(4.8)
height	cm	159(7.2)	160(6.9)
weight	kg	67.5(10.2)	64.7(8.2)
fat	%	30.2(5.9)	29.5(4.3)
WHR	Ratio	0.9(0.12)	0.89(0.08)
systolic	mmHg	128(3.2)	122(2.5)
diostolic	mmHg	81(5.1)	82(4.9)
Bone density	T score	-2.0(1.5)	-1.8(1.6)

Ps.Value are mean(SD) . WHR, waist and hip ratio

3.2 Functional physical performance

Statistically significant improvement($p < 0.05$) was observed on all the Functional physical performance tests for the subjects after 12 weeks Tai Chi training,. It means that 12 weeks Tai Chi training can strengthen Functional physical performance and functional fitness for the aged [8]. **(** TABLE 2**)**

TABLE 2. Comparision of functional physical performance after 12 weeks Tai Chi training[8]. (N=20)

ITEM	UNIT	Pre-training	Post-training
Sit and reach	cm	-6(8.6)	0.5(4.4)*
	%	0.7(11)	35(5)*
30 sec Chair rise	time	16.2(5.8)	18.7(8.1)
	%	66(8)	83.5(8.3)*
30 sec bicep curl	time	17.1(6.2)	20.5(5.2)
	%	60(4.1)	82.5(2.1)*
Timed up and go	sec	6.0(6.1)	5.0(4.6)
	%	25(23.1)	55(21.5)*
2 min step marking	time	94.6(7.8)	112(6.2)
	%	56(2.2)	80(2.1)*

Ps.Value are mean(SD) .*: vs. Pre-training group, $p < 0.05$.

3.3 Knee isokinetic performance.

The isokinetic tests of the knee strength results indicated overall statistically significant effects including time to peak torque (*P=.043*), total work (*P=.038*), and fatique index (*P=.047*) after 12 weeks Tai Chi training. But Hamstring/Quadriceps ratio (H/Q) was in significant. It showed that there were statistically significant differences in the muscular endurance, and neuromuscular controlling. strength of concentric knee extensors Tai Chi practitioners achieved significantly higher peak torque-to-body weight ratios with both their

knee extensors and flexors in both concentric and eccentric isokinetic testing at 30 deg·s^{-1}. An examination of the concentric H/Q strength ratios for Pre/Post Tai Chi training subjects yielded 0.562 and 0.591, respectively (P=0.795 in the paired t-test). Our findings thus show that Tai Chi practitioners had similar agonist/antagonist strength ratios in concentric muscle contractions after training as before **(**TABLE 3**)**

TABLE 3. Comparision of isokinetic performance (30 deg·s^{-1}×6 repetitions) after 12 weeks Tai Chi training. (N=20)

ITEM	UNIT	Pre-training		Post-training	
		KE	KF	KE	KF
Peak torque	N-M	146 (12)	84 (11)	161 (13)	95 (12)
Time to peak torque	msec	451 (53.1)	516 (177.8)	399.6* (67.1)	485 (123.1)
Total work	J	483.1 (178.2)	323 (186.2)	531.1* (272.3)	352.3 (134.3)
Work fatique	%	13.6 (9.7)	12.1 (8.6)	7.1* (3.5)	6.8* (7.3)
H/Q	%	56.2(8.6)		59.1(7.9)	

Ps.Value are mean(SD). *: vs. Pre-training group, $p < 0.05$.

The low values for CON_{KF}/ECC_{KE} (0.33–0.51) **(**TABLE 4**)** are also consistent with previous literature [1] and suggest that either the hamstring muscles have reduced capacity for knee joint stabilization during dynamic knee flexion movements or that the quadriceps have a high eccentric capacity during concentric knee flexion.

TABLE 4. Comparision of isokinetic performance (30 deg·s^{-1}×6 repetition) after 12 weeks Tai Chi training (N=20)

ITEM	UNIT	Pre-training	Post-training
CON_{KF}/ECC_{KE}	%	42.2(11.9)	47.2(9.6)
ECC_{KF}/CON_{KE}	%	70.4(11.8) †	77.3(13.7) †

Ps.Value are mean (SD). *: vs. Pre-training group, $p < 0.05$.
† :vs. CON_{KF}/ECC_{KE} in the same group, $p < 0.05$.

4. Discussions

4.1 Tai Chi training

In our study, TC was effective for enhancing quadriceps strength in older men and women. After 12 weeks of TC, subjects showed strength increases ranging from 66% to 83.5% in chair sit. Other functional physical performances including flexibility, agility, cardiovascular/muscular endurance were raising too. In addition, increasing ranging from 483.1J to 531.1 J in total works during concentric contractions at 30 degrees angular velocities were also noted. Although TC practice requires no instrument and uses only body weight as the training workload, it appears that a significant demand is placed on lower extremities during the performance of TC. A similar result has been presented by Heislein and colleagues[9] reported an increase of 21% in knee extensor isometric strength after an 8-week low-to-moderate resistance program. Heislein's program consisted of exercises performed in a progressive weight-bearing sequence and placed significant demands on the quadriceps throughout the exercise. Previous studies have shown that exercise including concentric and eccentric contractions is more effective for enhancing muscular strength[10]. TC is achieved in a semi-squat posture at a slow speed. During the programming, various degrees of concentric and eccentric contraction are require playing lower terminals. The greater parts of TC actions are performed in a closed kinetic chain. The slow motion and low posture integrate a higher training load on the lower limbs for extensors/flexor. The overload stress to joints may be prevented during TC. The risk of musculoskeletal injury during TC practice was low, and TC is safe even for patients with rheumatoid arthritis [11].

TC is an exercise with fine gymnastic movements and can be practiced easily; it is possible for a large group of the aged. TC can support keeping strength gains achieved by more intensive high-tech training in gym. In the present study, our data indicated that TC can increase muscular strength of quadriceps concentrically and eccentrically. The results suggest that TC is as good as high-tech training for strength enhancement. TC is an exercise with low velocity and low impact, and the

orthopedic complication is minimal. Moreover, TC is a easy way to conditioning performance for the aged and with very low cost.

4.2 Isokinetic performance

Current literature suggests that the manifestation of the fact that hamstrings are used to a much greater extent than the quadriceps for limb deceleration during knee extension movements [8]. However, data from the present study indicate that if concentric hamstring torque that contributes to knee stability with simultaneous eccentric quadriceps actions, then the extent of this contribution remains constant across movement velocities. The ECC_{KF}/CON_{KE} ratio was significantly higher. Others have suggested that this increase in the ratio at higher velocities is due to the significant anterior tibial translation or shear at high quadriceps forces, and extend internal rotation of the tibia in relation to the femur. Irrespective of age, the increases in co-activation of the hamstrings during high velocity movements appear to significantly contribute to equilibrate this tibial sheer or rotation [9]. Although isolated isokinetic movements used in the present study do not measure the simultaneous activity of agonist and antagonist muscles, the functional ECC/CON ratio appears to be a more reative measurement of the capacity for muscular knee joint stability than accustomed ratios [1].

4.3 Tai Chi training specificity

Loss of muscular endurance also occurs with aging. Nevertheless, muscular endurance is maintained better throughout aging than muscular strength[12]. Exercise training may improve muscular endurance, and the effect may be ascribed to the increase of oxidative capacity of muscle fibers. In this study, muscular endurance in the TC raised from 66% to 83.5% after 12 weeks TC. It seems that a TC can promote muscular endurance as well as muscular strength. Most strength training studies have used instrument in the gym/laboratory[13]. Although a machine-dependent training program can improve systematized muscle strength, it is difficult for persons to keep such training permanently. Therefore, gymnastic exercises easily implemented daily should be worth more attention. In fact, gymnastic exercises using postural change or cheap instruments are efficient in increasing muscular performance in the aged.

4.4 Limitations

There were some limitations in our study, however. First of all, the results would be more conclusive had the study group been larger. Unfortunately, it was difficult to convince the would-be subjects to join the Tai Chi unit three times a week. Weather conditions, difficulty finding transportation and personal reasons were all factors, which played a role in limiting participation. Subjects who completed the study were all consistent with their involvement. Falling, an important potential health problem in this age group, was not included in the evaluation due to time limitations. Also, participants who were active and had a high physical capacity might also be thought as a restrictive factor. The study lacking controls weakens the internal validity of our major findings. In addition, isokinetic tests need to determine the baseline peak torque in the aged because the test-retest reliability is relatively low in this parts. Another source of error lies in the difficulties of measuring the workload during TC. Our results strongly suggest that TCC training may be beneficial to elderly individuals for muscular strength and endurance enhancement. Further controlled study is needed to validate this evidence.

5. Conclusion

Isokinetic performance ratio between knee flexors (KF) and knee extensors (KE) have been widely used during muscular balance evaluations. Such evaluations can be predictive overload actions of knee, frequently caused by inadequate hamstrings recruitment, when they should be a joint stabilizer. TC, being a form of exercise that focuses on controlled movements have recently become widely used to improve lower limbs performance among the aged. In our investigations have demonstrated that the use of eccentric contractions provide a more functional index (ECC_{KF}/CON_{KE}). We find that TC can increase muscular strength of quadriceps concentrically and eccentrically. Therefore, TC is a potential alternative for strength training because of its efficacy and safety.

Acknowledgement

The financial support by the National Science Council, Republic of China, through Grant NSC 97-2622-H-230-002-CC3 is gratefully acknowledged.

References

1. Aagaard P, Simonsen EB, Magnusson, SP, Larsson B, Dyhre-Poulsen, PA. new concept for isokinetic hamstring:quadriceps muscle strength ratio. The American journal of Sports Medicine, 1998, 26: 231-237.
2. Dauty M, Potiron-Josse M, Rochcongar P. Identification of previous hamstring injury by isokinetic concentric and eccentric torque measurement in elite soccer players. Isokinetics and Exercise Science, 2003, 11: 134-140
3. Lan C, Chen SY, Lai JS. Relative exercise intensity of Tai Chi chuan is similar in different ages and gender. The American Journal of Chinese Medicine, 2004, 32(1): 151-160.
4. Lam P, editor. Teaching Tai Chi effectively. Narwee (New South Wales, Australia): Tai Chi Productions; 2006. p. 222-225
5. Wolfson L, Whipple R, Derby C, Judge J, King M, Amerman P, et al. Balance and strength training in older adults: intervention gains and Tai Chi maintenance. Journal of the American Geriatrics Society, 1996, 44(5):599-600.
6. Wu, G. Evaluation of the effectiveness of Tai Chi for improving balance and preventing falls in the older population: a review. Journal of the American Geriatrics Society, 2002, 50(4): 746-754.
7. Haff GA, Whitley L, Mccov H, O'bryant J, Kilgore E, Haff KP, & Stone M. Effects of different set configurations on barbell velocity and displacement during a clean pull. Journal of Strength and Conditioning Research, 2003, 17(1): 95-103.
8. Gerodimos V, Mandou V, Zafeiridis A, Ioakinidis P, Stavropoulos N, Kellis S. Isokinetic peak torque and hamstring/quadriceps ratio in young basketball players. Journal of Sports Medicine and Physical Fitness, 2003, 43(4): 444-452.
9. Heislein DM, Harris BA, Jette AM. A strength training program for postmenopausal women: a pilot study. Archives of physical medicine and rehabilitation, I994, 75: 198-204.
10. Hakkinen K, Komi PV. Effect of different combined concentric and eccentric muscle work regimes on maximal strength development. Journal of Human Movement Studies, 1981, 7: 33-44.
11. Lacerte M, deLateur BJ, Alquist AD, Questad KA. Concentric versus combined concentric-eccentric isokinetic training programs: effect on peak torque of human quadriceps femoris muscle. Archives of Physical Medicine and Rehabilitation, 1992, 73: 1059-1062.
12. Kersteins AE, Dietz F, Hwang SM. Evaluating potential use of a weight-bearing exercise, Tai Chi Chuan, for rheumatoid arthritis patients. American Journal of Physical Medicine & Rehabilitation, 1991, 70: 136-141.
13. Nakao M, Inoue Y, Murakami H. Aging process of leg muscle endurance in males and females.European Journal of Applied Physiology, 1989, 59: 209-214.

Machiavellianism and Related Behavioral Problems in Chinese Boys with Attention Deficit Hyperactivity Disorder

Yaoguo Geng[1], Dong Liu[2], Linyan Su[3] , Changhong Wang[4] , Yan Li[5]

[1]Department of Psychology, School of Education, Zhengzhou University, Zhengzhou, Henan, China [2]Department of Nephrology, the First Affiliated Hospital, Zhengzhou University, Zhengzhou, Henan, China [3]Department of Psychiatry, the Second Xiangya Hospital, Central South University, Changsha, Hunan, China [4] Henan Mental Hospital, Xinxiang, Henan, China [5] College of Public Health, Zhengzhou University, Zhengzhou, Henan, China

Received November 20, 2009

Abstract The aim of this article is to examine the Machiavellian beliefs in boys with attention deficit hyperactivity disorder (ADHD) and related behavioral problems. A sample of 70 Chinese boys aged 8~12 years with ADHD (17 cases have co morbid oppositional defiant disorder, ADHD+ODD) and normal controls were evaluated with Kiddie-Mach scales and Child Behavior Checklist (CBCL). There were significant differences between patients and controls. Boys with ADHD showed significantly higher Machiavellian beliefs than controls. However, boys with ADHD+ODD did not differ from boys with ADHD alone in Machiavellian beliefs. Withdrawal subscales, social subscales, attention subscales, internalizing behavior subscales and total problems of CBCL were positively correlated with Mach ($p<0.05$~0.01); social relations, school performance and total competence were negatively correlated with Mach ($P<0.05$~0.01). Conclusively, boys with ADHD have more Machiavellian beliefs. No difference emerges between boys with ADHD+ODD and with ADHD alone in Machiavellian beliefs. There are moderate correlations between Machiavellianism and behavioral problems and social impairment, especially internalizing behavioral problems and interpersonal communication embarrassment. [Life Science Journal. 2009; 6(4):56 - 61] (ISSN: 1097 – 8135)

Keywords: Machiavellianism, attention deficit hyperactivity disorder, behavioral problems

1 Introduction

Attention deficit hyperactivity disorder (ADHD) is a serious and relatively common psychiatric condition affecting 3% to 5% of all school age children and affecting a larger proportion of male than female subjects [1] Some studies suggest that children with ADHD are more likely to subsequently develop oppositional defiant disorder (ODD) and/or conduct disorder (CD). Children with ODD or CD frequently also have coexisting ADHD. The combination of ADHD and CD (or ODD) is associated with more severe physical aggression and antisocial behavior than is CD alone [2, 3] .

Correspondence author: childpsy6@hotmail.com
Yaoguo Geng, PhD

In recent years, numerous studies have examined aggressive children and possible mechanisms responsible for aggressive and antisocial behavior. Social information processing models[4] have demonstrated that compared with normal controls, aggressive boys pay less attention to neutral cues and direct their attention selectively toward hostile cues[5]. This pattern of hyper-vigilance to hostile cues enhances the likelihood that they will interpret stimuli in hostile ways[6]. Similar tendency has been found in children with disruptive behavior disorder (DBD). Stephanie[7] compared the preference for aggressive stimuli between children with DBD and normal controls. They found that DBD children had a lower preference for nonaggressive stimuli. Aggressive

DBD children distinguished themselves in selecting aggressive stimuli earlier. Social information processing models propose that such cognitive operations are affected by latent mental structures.

As part of our latent mental structures, beliefs are of fundamental importance in interpersonal relationships. We quickly form impressions and make judgment or attributions concerning people we meet, and this process can guide our behavior towards them. Some may view people in general as untrustworthy and manipulable in interpersonal situations, whereas others may have a high degree of faith in human nature, feeling people as fundamentally kind and to be treated with honesty and respect. This variation in attitudes has been described as our degree of "Machiavellianism"[8].

In clinical practice, children with ADHD, ODD or CD were frequently found to involve in interpersonal conflicts due to impulsive and/or aggressive behaviors. So it is very important and interesting to clarify whether or not Machiavellian beliefs is component of latent mental structures of ADHD and DBD children that can guide their processing of social cues and impulsive, aggressive behaviors. To our knowledge, Machiavellian beliefs of children with ADHD or DBD have not been reported yet. The current study first compared the Machiavellian beliefs with boys who with ADHD plus ODD, ADHD alone and normal controls, and explored the association between Machiavellianism and behavioral problems. We predicted, first, patients would show higher Machiavellian beliefs than normal controls, boys with or without ODD could be distinguished from each other in Machiavellianism. Second, we predicted that there would be significant correlations between Machiavellian beliefs and behavioral problems.

1. Methods

1.1 Participants

Subjects were recruited by investigators from The Second Xiang-ya hospital. 70 cases of boys aged 8~12 years with ADHD (who met the DSM-□ criteria)[9] and 48 cases of healthy boys aged 8~12 years were included in this study. Diagnoses of the patients based on extensive psychiatric assessment and interviews with children and their parents. In ADHD group, 17 cases (mean age: 9.72±1.39) had co-morbid oppositional defiant disorder, 53 cases (mean age: 10.09±1.51) were ADHD alone. Volunteers in control group took place in two classes from Yu-hua primary school of Changsha and had no mental disorder or neurologic disorder, with age ranging from 8~12 (mean age: 10.18±0.53). All children and their parents completed the measures carefully according to the order. All the 118 boys and their parents were told that participation was on a purely voluntary basis and they could withdraw at any time.

1.2 Measures

1.2.1 The 20-item self-report Kiddie Mach Scale was used to assess attitudes towards human nature and trust in interpersonal relationships. Items include "Most people are good and kind" and "Sometimes you have to hurt other people to get what you want". Agreement with the statements was indicated on the following scale: agree very much (5), agree a little (4), disagree a little (2), and disagree very much (1). Non-Machiavellian items were scored reversely for consistency with the Machiavellianism construct, so that high scores on these items indicated disagreement and therefore Machiavellianism. The possible range of scores was 20-100. Christie and Geis[10] provide evidence of good reliability and validity for their Machiavellianism scales. Xiao-dong Fan provided evidence of good reliability and validity for Chinese version[11].

1.2.2 The Child Behavior Checklist[12] obtains reports from parents regarding children's competencies and behavioral/emotional problems. Parents provide information for competence items covering their child's activities, social relations, and school performance. The CBCL has 113 items that describe specific behavioral and emotional problems, include withdrawal, somatic complaints, anxious /depressed, social problems, thought problems, attention problems, delinquent behavior, aggressive behavior, internalizing behavior, externalizing behavior and total problems. Parents rate their child for how true each item is now or within the past 6 months using the following scale: 0 = not true (as far as you know); 1 = somewhat or sometimes true; 2 = very true or

often true. There are good reliability and validity for Chinese version [13].

1.3 Data analysis

All statistical analysis were performed by using SPSS for windows 11.5, methods contains ANOVA and Pearson correlation analysis.

2. Results

2.1 Comparison of the Age and Machiavellianism

No differences were found between boys with ADHD+ODD, with ADHD alone and normal controls in age and standard of education. Whereas, *F* test showed a statistically significant difference between three groups in Machiavellian beliefs（F（3.267）=P<0.05）. Meanwhile, test showed that patients were higher in Machiavellianism than normal controls, suggesting that ADHD boys and ADHD+ODD boys may view people in general as untrustworthy and dishonest. However, no differences were found between ADHD boys with or without ODD. (See Table 1)

Table 1. Comparisons of the Age and Machiavellianism

Items	ADHD (n=53)	ADHD+ODD (n=17)	Controls（n=48）	*F*Value
Mach	72.58±8.15	73.73±10.68	68.41±8.10	3.267*
Age	10.09±1.51	9.72±1.39	10.18±0.53	2.08

* *P*<0.05 level; ** *P*<0.01 level (all two-tailed)

Table 2. Association between Machiavellianism and CBCL

Items	Mach
activities	-0.159
social relations	-0.262 *
school performance	-0.299 **
total competence	-0.241 *
withdrawal	0.317 **
somatic complaints	0.196
anxious/depressed	0.138
social problems	0.244 *
thought problems	0.181
attention problems	0.321 **
delinquent behavior	0.180
aggressive behavior	0.173
internalizing behavior	0.287 *
externalizing behavior	0.168
total problems	0.250 *

* *P*<0.05 level； ** *P*<0.01 level (all two-tailed)

2.2 Association between Machiavellianism and behavioral problems

Results showed that Mach was positively associated with attention problems(r=0.321, P<0.01), withdrawal(r=0.317, P<0.01), social problems(r=0.244, P<0.05), internalizing behavior(r=0.287, P<0.01) and total problems(r=0.250, P<0.01) of CBCL. Meanwhile, there were significant negative correlations between Mach and social relations(r=-0.262, P<0.05), school performance(r=-0.299, P<0.01) and total competence

(r=-0.241, P<0.05) of CBCL. These findings reveal that an increase in dishonesty and distrust to others would associate with a corresponding rise in behavioral problems and a corresponding decrease in social competence. However, no statistically significant correlations were found between Mach and other subscales (activities, somatic complaints, anxious/depressed, thought problems, delinquent behavior, aggressive behavior and externalizing behavior) of CBCL. (See Table 2) .

3. Discussions

The data presented in this study indicated that there were significant differences in Machiavellian beliefs between patients and controls, our prediction that boys with or without ODD could be distinguished from each other in Machiavellianism was not supported by the data. But we can observe a disparity that boys with ADHD+ODD scored higher than boys with ADHD alone.

Braginsky[14] found that high Mach children used manipulative strategies more frequently and more effectively than low Machs and had greater control over the impressions they made on other people. Barnett and Thompson[15] found that children who scored highly on an affective-perspective taking task also showed lack of empathy and was claimed to be especially Machiavellian in their interactions with others. Graham [16] gave a summary of the high Machiavellian personality: lack of emotional involvement in interpersonal relationships, being cool and distant, treating people as objects to be manipulated, lack of concern for traditional morality, deceit is considered to be utilitarian rather than reprehensible, low ideological commitment, focus on maintaining oneself in power rather than on inflexible ideals. In accordance with Barkley[24], we think that boys with ADHD may lack of concern for regulation, and lack of empathy in other people.

Children with ADHD and ODD usually get themselves into troubles because of symptoms. Their interpersonal relations are full of rejection, denial, conflict and negative regards [25]. Therefore they are more likely than controls to respond to disadvantage by associating with delinquent peers and adopting a maladjusted attitudes and lifestyle. We speculate that Machiavellian beliefs may be one of variables that can partly explain the cause of co-morbid behavioral problems of boys with ADHD or ADHD+ODD. Following this reasoning, corresponding cognitive therapy and social skill training should be employed.

Our results indicated that it is social intercourse problems and internalizing behavior (such as withdrawal) of boys, not externalizing behavior (such as delinquent behavior and stimulation, as is similar to psychopaths aggressive behavior) is the main manifestation of Machiavellian beliefs. Perhaps, Machiavellianism may only be an interpersonal irritant [17] due to low agreeableness and not inevitably lead to delinquent behavior and aggressive behavior. In other words, nonsocial behaviors, rather than antisocial behaviors, is of close relationship to Machiavellianism. Our findings confirmed the viewpoint of Wilson, Paulhus and Williams, Williams and Paulhus[18-20], but were inconsistent with McHoskey, who found that Mach scores were positively associated with the Personality Diagnostic Questionnaire-4+ (PDQ-4+) total score and most of the specific PDQ-4+ personality disorder measures, including the antisocial, antisocial behavior, impulsivity, borderline, and passive-aggressive scales[21].

In addition, McHoskey[22] also found that Psychopathy and Machiavellianism were strongly correlated with each other. Smith [23] pointed out in his review that high Mach scores predicted a high need for

To summarize, we think that Machiavellian beliefs may be part of our latent mental structure which can result in behavioral problems and social impairment, especially internalizing behavioral problems and interpersonal communication embarrassment.

The rsults that we demonstrated may not be the final words on this issue. Further research should include longitudinal study to understand how and when such attitudes and behaviors develop for ADHD children, also cross-sectional comparison between ADHD children and children with other disruptive behavior disorder.

Acknowledgements

Thanks to the schools and children who took part in the study. This work was supported by grants from National Natural Science Foundation of China (30370521).

References

1. American Psychiatric Association. Diagnostic and statistical manual of mental disorders (4thed) (DSM-IV). Washington, DC: APA. 1994.
2. Walker JL, Lahey BB, Hynd GW, *et al*. Comparison of the specific patterns of antisocial behavior in children with conduct disorder with or without coexisting hyperactivity. J Consult Clin Psychol, 1987, 55, 910-913.
3. Biederman J, Newcorn J, Sprich S. Comorbitidity of attention deficit hyperactivity disorder with conduct, depressive, anxiety, and other disorders. Am J Psychiatry, 1991, 148: 564-577
4. Crick NR, Dodge KA. A review and reformulation of social information-processing mechanisms in children's social adjustment. Psychological Bulletin, 1994, 115, 74-101.
5. Gouze K. Attention and social problem solving as correlates of aggression in preschool males. Journal of Abnormal Child Psychology, 1987, 15, 181-197.
6. Dodge KA, Frame C. Social cognitive biases and deficits in aggressive boys. Child development, 1982, 53, 620-635.
7. Stephanie, H.M, Van Goozen, Peggy T, *et al*. Preference for aggressive and sexual stimuli in children with disruptive behavior disorder and normal controls. Archives of Sexual Behavior, 2002, 31(3), 247-253.
8. Jon Sutton, Edmund Keogh. Components of Machiavellian beliefs in children: relationships with personality. Personality and Individual Differences, 2001, 30,137-148.
9. American Psychiatric Association. Diagnostic and statistical manual of mental disorders (4thed.) (DSM-IV). Washington, DC: APA. 1994
10. Christie R, Geis FL. Studies in Machiavellianism. New York: Academic Press. 1970.
11. Wang XD, Wang XL, Ma H *et al*. Kiddie Mach Scale. Chinese Mental Health journal, 1999, 13,169-175.
12. Achenbach TM. Manual for the Child Behavior Checklist and 1991 profile. Burlington, VT: Department of Psychiatry, University of Vermont. 1991.
13. Su LY, Li XR, Luo XR. The newly revised norms of Child Behavior Checklist in Hunan Province. Chinese Mental Health Journal, 1998, 12, 67– 69.
14. Braginsky DD. Machiavellianism and manipulative interpersonal behaviour in children. Journal of Experimental Social Psychology, 1970, 6, 77-99.
15. Barnett MA, Thompson S. The role of perspective taking and empathy in children's Machiavellianism, pro-social behavior, and motive for helping. Journal of Genetic Psychology, 1985; 146,295-305.
16. Graham JH. Mchiavellian project managers: do they perform better? International Journal of Project Management, 1996, 14(2), 67-74.
17. Paulhus DL. Interpersonal and intrapsychic adaptiveness of trait self-enhancement: A mixed blessing? Journal of Personality and Social Psychology, 1998, 74, 1197–1208.
18. Wilson DS, Near DC, Miller RR. Individual differences in Machiavellianism as a mix of cooperative and exploitative strategies. Evolution and Human Behavior, 1998,19,203-212.
19. Paulhus DL, Williams K. The Dark Triad of personality: Narcissism, Machiavellianism, and Psychopaty. Journal of Research in Personality, 2002; 36,556-563.
20. Williams K, Paulhus DL. The hierarchical factor structure of the Self-Report Psychopathy scale. Presented at the meeting of the Canadian Psychological Association, Vancouver, Canada. 2002.
21. McHoskey JW. Machiavellianism and personality dysfunction. Personality and Individual Differences, 2001, 31,791-798.
22. McHoskey JW, Worzel W, Szyarto C. Machiavellianism and Psychopathy. Journal of Personality and Social Psychology, 1998,

74,192-210.

23. Smith RJ. Psychopathic behavior and issues of treatment. New Ideas in Psychology, 1999, 17,165-176.
24. Barkley RA. ADHD and the nature of self-control. The Guilford Press, 1997, 48,52 ,195.
25. Geng YG, Wang H, Su LY. Impulsive behavior of attention deficit hyperactivity disorder in child. International Journal of Pediatrics, 2008,35(6), 555-558.

Synchronous TBI and ABI measurement Scheme for Diabetes Patients Synchronous Sphygmomanometer of Four Limbs

Sung-Tsun Shih[1], Kuan-Yu Chang[2]

Department of Electronic Engineering, Cheng Shiu University, Kaohsiung , Taiwan.[2] Mackay Memorial Hospital Taitung Branch, Taitung, Taiwan

Received November 18, 2009

Abstract: Measurement of ankle blood pressure is a simple method of assessing lower limb arterial blood supply. It has been found through a large amount of experimental measurements that the differences of blood pressure among the four limbs and great toe are highly correlated with hyperlipemia, thrombosis blood vessel hardening and high density of blood on supine position. In this study, a synchronous TBI and ABI measurement scheme is built with six electronic sphygmomanometers work concurrently. We utilize six general electronic sphygmomanometers adding with transmission interface and an embedded microprocessor to build the brachial and great toe blood pressure synchronous measurement equipment. Then, the ABI and TBI reports are automatic calculated and displayed to guide clinicians make decision. Also we adopt the RFID system in the measurement scheme to identify user identity and as a user login mechanism. [Life Science Journal. 2009;6(4):62- 68] (ISSN: 1097 – 8135)

Keywords: Toe brachial index (TBI), Ankle brachial index (ABI), Diabetes, Blood pressure, RFID

1. Introduction

Macrovascular disease is common in diabetes and is the major cause of morbidity and mortality in this condition. The increase in vascular disease is not restricted to the coronary circulation but also occurs to the cerebrovascular and peripheral vascular systems. It has been estimated that > 30% of patients with diabetes have evidence of peripheral vascular disease (PVD). Assessment of the circulation in the lower limbs is not only important for patients with symptoms of ischemia, but also helpful in classifying foot ulcers and predicting the chance of healing. Clinical examination is the first step in this process but in many patients non-invasive vascular tests are required to confirm clinical judgment and to assess more quantitatively the degree abnormalities. Measurement of the ankle brachial index (ABI) by Doppler ultrasound is a simple and commonly used method for this purpose. However, the applicability of this technique to patients with diabetes is in some doubt because diabetic patients often develop calcifications of the lower limb arteries. The presence of calcification may invalidate the ABI as the arterial wall becomes stiffer and resists compression, giving a falsely high ankle systolic pressure. As a result, measurement of great toe artery pressure for calculation of toe brachial index (TBI) is commonly advocated in diabetic patients. However, before accepting this approach it should be borne in mind that toe arteries might also be calcified. Moreover, measurement of toe pressure is technically more demanding and requires expensive equipment beyond the scope of most clinicians. It would be worthwhile to have some clinical data to guide clinicians as to when pressure measurements should be taken at the toe rather than at the ankle.

Measurement of ankle blood pressure is a simple method of assessing lower limb arterial blood supply. However, its use in diabetes has been questioned due to the presence of medial artery calcification. Measurement of toe blood pressure has been advocated as an alternative but it is technically more difficult.

*Corresponding Author: Sung-Tsun Shih, PhD

E-mail: stshih@csu.edu.tw

In this study, we try to build a concurrent TBI and ABI measurement scheme with six electronic sphygmomanometers. We utilize six general electronic sphygmomanometers adding with transmission interface to build the brachial and great toe blood pressure concurrent measurement equipment. Then, the ABI and TBI reports are automatic calculated and displayed by the embedded microprocessor. Also we adopt the RFID system to identify user identity and as a user login mechanism.

A remotely physiological reporting system in accordance with the present utility model senses and identifies a unique entity, collects measured data, transmits and stores parametric data sensed by measurement apparatus, can be used in medical monitoring. The automatic matching and recording system comprises a Radio Frequency Identification (RFID) reader, a measurement apparatus, a local recording device and a remote monitoring device.

2. Methodology

The ankle-arm pressure index (also known as the Ankle / Brachial Index or ABI) compares the systolic blood pressure of the ankle to that of the arm (brachial). These measurements are useful in the assessment, follow-up and treatment of patients with peripheral vascular disease (PVD). ABI's provide an objective baseline to follow the progression of the disease process and evaluate the effectiveness of the treatment plan.

The ABI results are usually combined with Doppler or pulse volume waveform analysis (PVR). Significant changes in arterial systolic pressure between sites indicate reduced blood flow caused by obstruction of blood vessels. The effects of obstructions can be emphasized by increasing blood flow, either by exercise testing or by inducing reactive hyperemia with an occlusive cuff.

Patients, such as diabetics, with calcified vessels may show falsely elevated ankle pressures. In this case, pressure measurements can be made on the foot or toes by Photo Plethysmography (PPG) for more accurate results. Diagnostic information is obtained both from the waveform of the arterial flow when displayed on a chart recorder and from using the PPG sensor to determine the blood pressure in the digit.

ABI Interpretation Levels:

>1.3 Non-compressible

1.00 – 1.29 Normal

0.91 – 0.99 Borderline (equivocal)

0.41 – 0.90 Mild-to-moderate P.A.D.

0.00 – 0.40 Severe P.A.D.

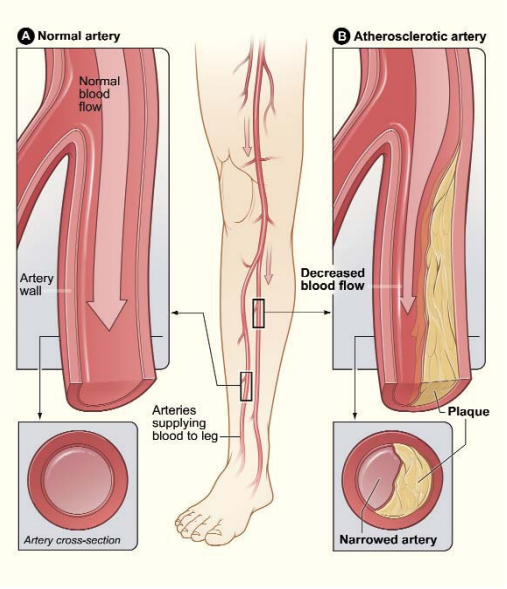

Figure 1. Normal artery and atherosclerotic artery

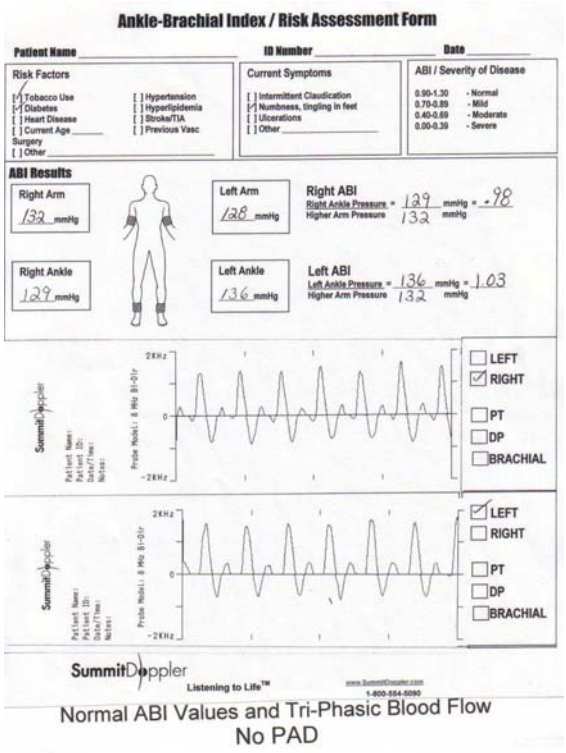

Figure 2. Normal ABI measurement result with manually recording

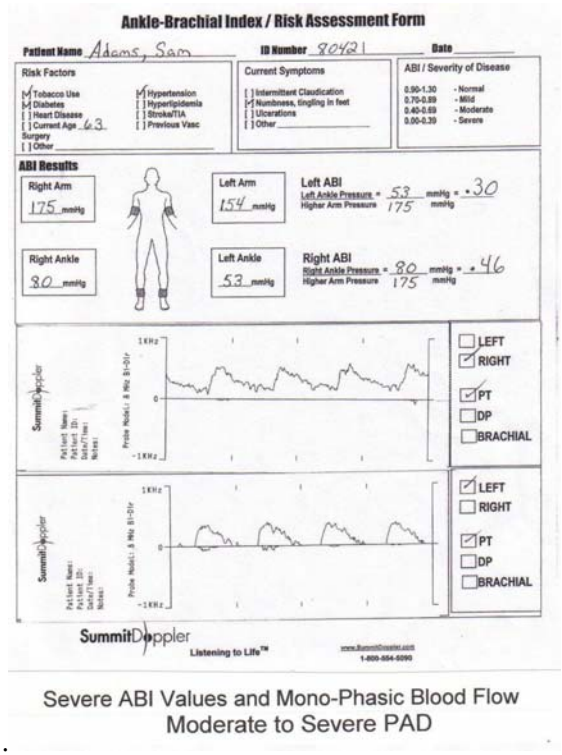

.

Figure 3. Severe ABI measurement result with manually recording

3. Experiment Scheme

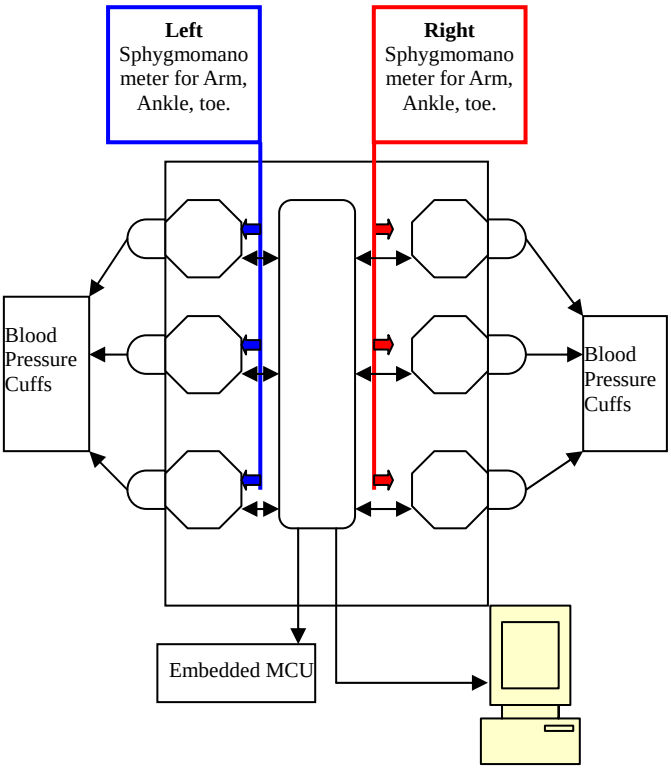

Figure 4. Synchronous TBI and ABI measurement scheme

The proposed system consists of signal acquisition, radio frequency (RF) transmission; signal processing, internet communication and database modules. The signal is amplified and filtered in the signal acquisition module. The bio-signal is digitized by the built-in analog-to-digital converter (ADC) in the micro-controller and organized into a data package. As soon as the package is established, it is sent by the transceiver using the high-frequency band. On the receiver side, it utilizes the same communication protocol to extract signals from the received package. Data is then passed to the personal computer (PC) through the RS232 interface, on the receiving side, for signal processing, analysis and storage. In addition to waveforms display, the PC processes the acquired signals and obtains biological parameters such as heart rate for evaluating user's physical condition. At the same time, the

application program on the PC can establish internet connection with the remote server in the hospital. After processing, data is saved in the Access database for long-term physical condition monitoring.

The embedded microprocessor is used to stimulate the six sphygmomanometers concurrently, and collect the systolic blood pressure, diastolic blood pressure and beat pulse from each cuff. Only the bigger value of each systolic blood pressure in arm, ankle, and toe are used to calculate the ABI (Ankle Brachial Index) and TBI(Toe Brachial Index) index.

Right ABI = (**Right Ankle** systolic pressure) / (bigger one of right and left **Brachial** systolic pressure) (1)

Left ABI=(**Left Ankle** systolic pressure)/(bigger one of right and left **Brachial** systolic pressure) (2)

Right TBI = (**Right great Toe** systolic pressure) / (bigger one of right and left **Brachial** systolic pressure) (3)

Left TBI = (**Left great Toe** systolic pressure) / (bigger one of right and left **Brachial** systolic pressure) (4)

4. Measurement of arterial pressures

The patient was asked to rest supine for 10 min and a 10-cm cuff was wrapped around the upper arm. The brachial pulse was then palpated and the Doppler probe placed at a 45^{o} angle to the skin surface with the probe directed towards the patient's head. Once the best signal was obtained the cuff was inflated until the signal disappeared. The cuff was then slowly deflated, and the point at which the signal returned was taken as the systolic blood pressure. This process was then repeated for the other arm and the higher of the two pressures taken as the brachial artery pressure.

The same cuff was placed around the ankle immediately above the malleoli. The dorsalis pedis pulse was palpated and the pressure reading obtained as described for the brachial pressure. The process was repeated for the posterior tibial artery. The pressure of the artery with the higher reading was taken as the ankle pressure and the ABI was calculated from the ratio of the ankle systolic pressure to brachial systolic pressure. The cuff was not inflated beyond the pressure of 250 mmHg, even if the Doppler signal was not obliterated. In this situation, the ankle systolic pressure was arbitrarily taken as 250 mmHg. To measure toe pressure a 25-mm digital cuff was placed around the proximal phalanx of the hallux and the Doppler signal was recorded from the distal pad of the great toe. The cuff was inflated to a maximum of 200 mmHg and then slowly deflated. The point at which the arterial waveform reappeared was taken as the toe systolic blood pressure. If an adequate Doppler signal could not be obtained for technical reasons, the pressure was measured using a photoplethysmograph (PPG). This method detects light reflected from blood flow in superficial tissues. It requires specialized equipment and a darkened room. Our controlled studies showed that the Doppler and PPG methods yielded the same toe pressure result.

Commonly used in patients with diabetes and peripheral arterial disease, a toe brachial pressure index (TBI) is a noninvasive way of determining arterial perfusion in feet and toes. You determine the TBI by using a sphygmomanometer to measure systolic pressure in the arm and the great toe. The TBI is a ratio of these two readings. (See Calculating Toe Brachial Pressure Index.)

What are the pros and cons of TBI compared with traditional techniques?

A disadvantage of TBI is that it may not reveal an arterial occlusion in the tip of the toe because the sphygmomanometer cuff is placed at the base of the toe. And because TBI is an indirect assessment of perfusion, it can't pinpoint the location of arterial occlusion.

How to measure TBI?

First, ensure the patient has avoided tobacco and caffeine for 30 minutes before the procedure; both can increase blood pressure. Next, gather the equipment: a handheld embedded system (PDA, ARM), a sphygmomanometer with an arm cuff 5 inches (12.5 cm) wide and 9 inches (22.5 cm) long, and a toe cuff 1 inch (2.5 cm) wide and 5 inches (12.5 cm) long.

Place the patient supine with her toes level with her heart. Cover her with a blanket if the room is cool. Have her rest there for 10 minutes. While she's resting, explain the procedure to her. Then, follow the steps shown in these photographs.

Fig. 5. Arm cuff, ankle cuff and toe cuff for sphygmomanometer

Peripheral arterial disease, or P.A.D., develops when your arteries become clogged with plaque—fatty deposits that limit blood flow to your legs. Just like clogged arteries in the heart, clogged arteries in the legs mean you are at risk for having a heart attack or stroke. Plaque buildup in the legs does not always cause symptoms, so many people can have P.A.D. and not know it. People who do experience symptoms, such as pain or cramping in the legs, often do not report them, believing they are a natural part of aging or due to another cause. In all, P.A.D. affects 8 to 12 million people in the United States, especially those over 50.

5. Conclusions

The ABI was calculated as the highest ankle systolic pressure divided by the highest brachial systolic pressure. For the purpose of this study, an ABI < 0.9 was taken as denoting the presence of PVD, those ≥ 0.9 and < 1.3 as normal, and ≥ 1.3 as evidence of medial wall calcification. The TBI was calculated as the toe systolic pressure divided by the brachial pressure. Synchronous TBI and ABI measurement scheme from both legs, great toes and arms are developed in this paper.

Measurement of ankle blood pressure is a simple method of assessing lower limb arterial blood supply. Measurement of toe blood pressure has been advocated as an alternative but it is technically more difficult. In this study, we try to build a synchronous TBI and ABI measurement scheme with six electronic sphygmomanometers. We utilize six general electronic sphygmomanometers adding with transmission interface to build the brachial and great toe blood pressure concurrent measurement equipment. Then, the ABI and TBI reports are automatic calculated and displayed by the embedded microprocessor. Also we adopt the RFID system to

identify user identity and as a user login mechanism.

Acknowledgement

The clinical suggested measurement method by the Mackay Memorial Hospital Taitung Branch is gratefully acknowledged.

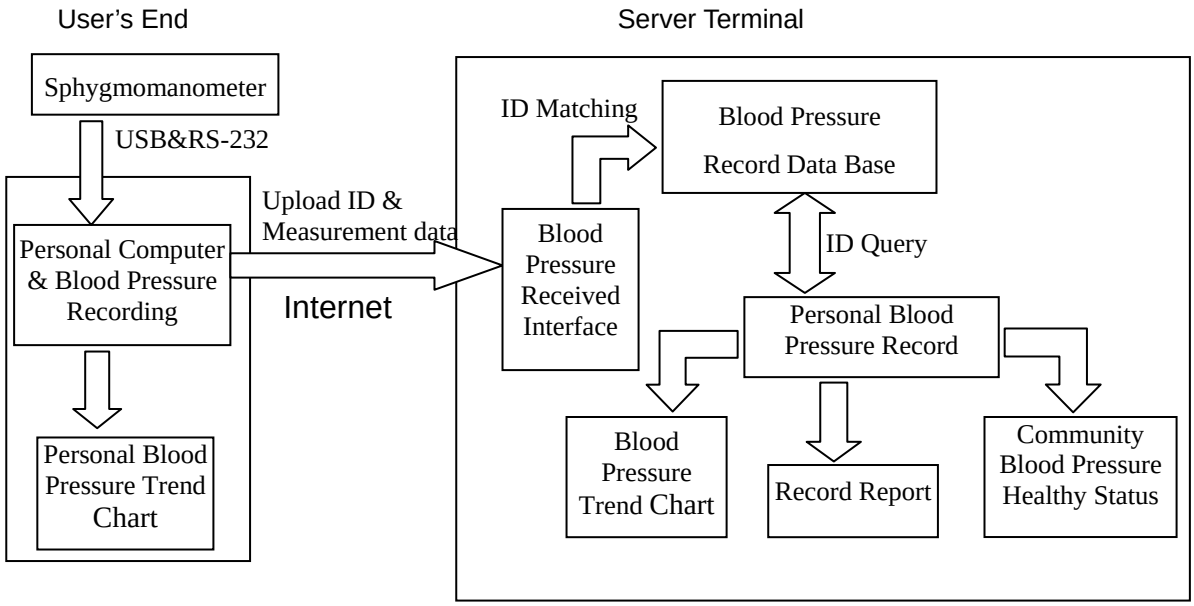

Figure 6. The Sphygmomanometer measurement and transmission block diagram

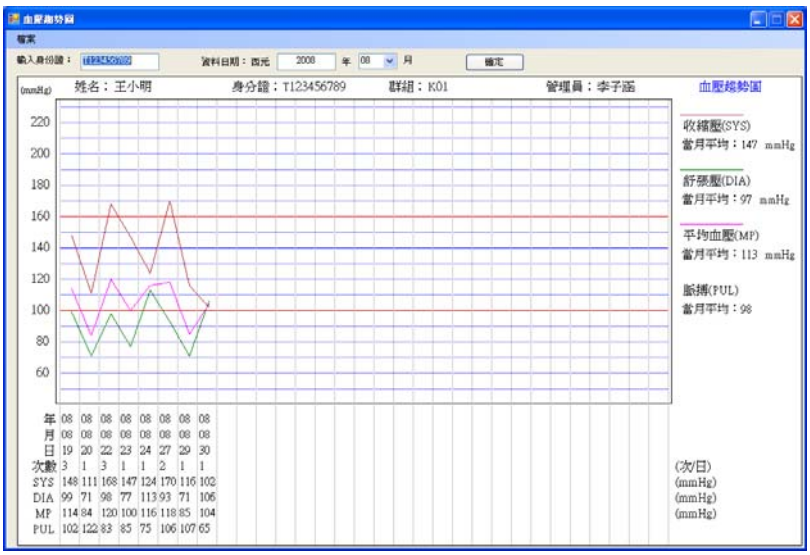

Figure 7. The blood pressure measurement trend graph

References

1. Vale PR, McGrath MA. Peripheral vascular disease: a GP's guide to current management. Mod Med Australia 1996; August: 92-103.
2. Vowden KR, Goulding V, Vowden P. Hand-held Doppler assessment for peripheral arterial disease. J Wound Care 1996; 5: 125-128.
3. Mayfield JA, Reiber GF, Sanders LJ, Janisse D, Pogach LM. Preventive foot care in people with diabetes. Diabetes Care 1998;21: 2161-2179.
4. Young MJ, Adams JE, Anderson GF, Boulton AJM, Cavanagh PR. Medial arterial calcification in the feet of diabetic patients and matched non-diabetic control subjects. Diabetologia 1993; 36: 615-621.
5. Bland JM, Altman DG. Statistical methods for assessing agreement between two methods of clinical measurement. Lancet 1986; 8: 307-310.
6. Bostrom K, Watson KE, Horn S, Wortham C, Herman IM, Demer LL. Bone morphogenetic protein expression in human atherosclerotic lesions. J Clinical Invest 1993; 91: 1800-1809.
7. Goebel FD, Fuessel HS. Monckeberg's sclerosis after sympathetic denervation in diabetic and non-diabetic subjects. Diabetologia 1983; 24: 347-350.
8. Brooks, B., et al.: "TBI or Not TBI: That Is the Question. Is It Better to Measure Toe Pressure than Ankle Pressure in Diabetic Patients?" Diabetic Medicine. 18(7):528-532, July 2001.
9. Leskinen, Y., et al.: "The Prevalence of Peripheral Arterial Disease and Medial Arterial Calcification in Patients with Chronic Renal Failure: Requirement for Diagnostics," American Journal of Kidney Diseases. 40(3):472-479, September 2002.

Study on the association of platelet membrane glycoprotein IaC807T gene polymorphism with the susceptibitity to ischemic cerebrovascular disease in Han population of Henan province.

Liu Wei[1], Lu Guangxiu[1#], Xu Yuming[2], Zheng Hong[3]

[1]Department of Neurology in HuaiHe Clinical Hospital Affiliated to Henan University, Kaifeng 475000 [2]Department of Neurology in the First Affiliated Hospital, Zhengzhou University, Zhengzhou 450052 [3]Department of Cell Biology and Medical Genetics, College of Basic Medical Science, Zhengzhou University , Zhengzhou 450001

Absract

Objective：To investigate the association of the platelet membrane glycoptein IaC807T gene polymorphism and the genetic susceptibility to ischemic cerebrovascular disease and its mechanism in Han poplulation of Henan province. **Methods**: Platelet membrane glycoprotein Ia gene C807T polymorphism in 317 samples of cerebral infarction and 311 samples of healthy control from Henan Han population was detected using PCR-restriction fragment length polymorphism (RFLP) technique. **Results**: There were two alleles (C and T)and 3 genotypes (C/C C/T T/T). The frequencies of GpIa T allele were significantly higher in cerebral infarction group among individuals yonger than the mean age of 55 years (x^2= 10.01 $p<0.05$) and individuals with high-risk factors (x^2=4.183 $p<0.05$) than those in the control group. **Conclusion**: The platelet collagen receptor GpIa-IIaT807 allele might be an independent risk factor for the development of cerebral infarction in younger patients and high-risk patients of Henan province. Life Science Journal. 2009; 6(4): 69 – 73] (ISSN: 1097 – 8135)

Key words：Platelet membrane glycoprotein Ia; genetic polymorphsim; ischemic cerebrovascular disease; Henan province ; Han population.

According to the medicine research in the latest years, the dysfunction of platelet aggregation and adhesion plays an important role in the process of occurrence and development in the ischemic cerebrovascular disease. platelet membrane glycoprotein Ia-IIa is an important collagen receptor of platelet , which belongs to integrin -family. it is made up of α and β subunit , also called α2β1 integrin, GpIa-IIa plays a critical role in the process of platelet activation and thrombosis through the GpIa-IIa platelet adheres to the exposed endothelial collagen [1,2], then was activated. In recent years,two types of polymorphism had been found in the GpIa gene transcription district 807 (C or T) and 873 (G or A).

Both 807T and 873A were completely chained [3]. It was reported that the polymorphism was significantly related to the level of GpIa-IIa on the surface of platelet [4] .So GpIa gene polymorphism may be a genetic risk factor of thrombotic disease.

In this study, the GpIaC807T genotypes of cerebral infarction and the normal controls from Han population in Henan province were detected and analysed the allele frquency in order to explore the relationship and mechanism between the gene polymorphism and ischemic cerebrovascular disease.

1. Materials and Methods

1.1 Clinical materials According to the diagnosis criteria of cerebrovascular disease made on the Fourth National Symposium on cerebrovascular disease, a total of 317 patients with IVCD from unrelated kindred of Chinese Han ethnicity in Henan area were inpatients or outpatients admitted to the top two hospitals of Henan

Corresponding lugx820@yahoo.com.cn
Lu Guangxiu

province from March 2008 to February 2009.In the IVCD group, there were 171 males and 146 females aging from 38 to 75 years old, with an average age of 58.3±17.6 years old.They were diagnosed as IVCD by clinical symptoms and CT or MRI scan. 311 healthy outpatients admitted to the top two hospitals in Henan province as controls, including 311 healthy individuals (165 males and 146 femals) aging from 39 to 74 years old, with an average age of 58.2±16.8 years old. All subjects in the research were of the Chinese Han ethnicity, severe systemic diseases such as cerebral infarction(CI) 、myocardial Infarction (MI) 、liver or renal diseases were excluded . There was no significant difference($p>0.05$) in the composition of gende、age、lipid level、blood glucoses and smoking history between the two groups ,so they can be comparable .

1.2 Methods

1.2.1 Samples collection and gene group DNA abstraction

Venous blood samples were drawn from the patients and controls in the fasting states in the morning . 5ml and 3ml blood were respectively collected with common biochemistry tube and EDTA-2Na anticoagulation tube. Biochemical indictator such as TG、BS were tested in the biochemical specimen. Gene group DNA was extracted with phenol/chloroform extraction proledure from peripheral blood leckocytes.

1.2.2 Measurement of GPIaC807T gene polymorphism

PCR-RFLP is used ,the amplification of aim fragment refers to a pair of primer designed by Reiner, method: the forward primer 5'-GTGTTTAACTTGAACACATAT-3',reverse primer 5'-ACCTTGCATATTGAATTGCTT-3', aim fragment is about 184bp. PCR reaction volume 25ul: 2xTaq Master Mix(contained 0.1U Taq DNA polymerase, 20mM Tris-HCl,100mM KCl,3mM MgCl2, 500uM each dNTP)8ul、upstream primer and downstream primer were respectively 2ul (10mmol / L) 、DNA template 2ul、ddH2O added to 25ul. PCR amplification condition: PCR was carried out with 35 cycles at 95℃for 5 min, 94℃ for 30 s, 55℃for 30S, 72℃ for 1 min and finally 72℃ for 5min. PCR product 10ul was detected in 20g/L agarose gel electrophoresis under ultraviolet rays lamp with reference of Marker I. the digestion reaction system 20ul, including PCR product 10ul, TaqI restriction enzyme 5^{u}, ddH2O 8ul was immersed in 65℃ water for 90 min, the digestion was detected in 20g/L agarose gel electrophoresis under ultraviolet rays gel imaging system with reference of Marker I took photograph, judging the length of PCR digestion by PCR brand.

1.3 Statistical analysis was performed by the spss 11.0 for windows Stastical package. Genotype frequencies were compared between the cases and conrtols by using chi-square test .The relative risk of genotypes and alleles was described by odds rations (OR) and 95%confidence intervals(95% CI). Logistic regression was used to analyse independent risk factors. Hardy-weinbery equilibrium was conformed with chi-square test. Pvalues were two-tailed and statistical significance was accepted as $p<0.05$.

2 Results

2.1 PCR amplification fragment is 184bp.According to the digestion results , there were 3 types of genotypes, The product 115bp in length was genotype TT, and 92bp in length was genotype CC, if there were two bands in the length of 115bp and 92bp,known as CT type.

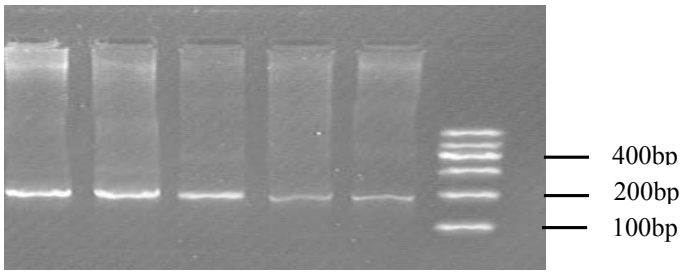

Figure 1. PCR amplification result

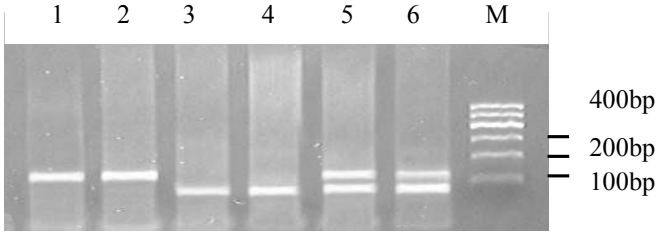

Figure 2. Result of PCR-RFLP

(1,2 were genotype TT; 3,4 were genotype CC; 5,6 were genotype CT;M was 100bp DNA ladder)

2.2 Hardy-weinberg test of gene GPIaC807T

Patients and controls' genotype distribution ratio was in accordance with Hardy-Weinberg equilibrium (P>0.05), With the representation of population. Two group genotypes and frequencies of alleles（Table 1）.

2.3 Distribution of GpIa genotype and ratio of allomorph of patients and controls. (See table 2),The difference of gene GpIa allele T ratio between patients and controls is not significant （$\chi 2=2.615$, $p>0.05$）

2.4 The distribution of GpIa genotype and ratio of allele of stroke patients aged below 55 and controls ,the difference gene GpIa allele T ratio between stroke patients aged below 55 and controls was significant（$\chi 2=10.01$, $p<0.05$）.(Table 3) allele T was significantly correlated with stroke patient aged below 55 [OR= 1.611, 95% CI is（1.198-2.167）].

2.5 The stroke patients were divided into high risk group and low risk group by whether with hypertension、diabetes mellitus、BMI≥26kg/㎡、hyperlipidemia .The difference ratio of gene GpIa allomorph T between high risk stroke patients and controls was significant（$\chi 2=4.183$，$p<0.05$）.(see table 4), allomorph T was significant correlation to the high risk stroke patients [OR=1.271,95% CI was （1.010-1.600）].

3 Discussion

Now, the effect of GpIa-IIa compound on platelet membrane is being payed more and more attention .GpIa-IIa, as the important collagen receptor on platelet membrane, belongs to a member of terminal antigen subfamily of the cell adhesion molecules integrin, it can mediate platelet to adhere to Ⅰ-Ⅷ type collagen. Kunicki [5, 6] ,et found the density of GpIa-IIa on platelet membrane differs among healthy persons about 4 times. Also some research found that gene polymorphism of GpIa is related to the expression rate of GpIa-IIa [7], so the variation of density of GPIa on platelet maybe the risk factor of thrombus disease. persons with T807 allelomorph express high level of GpIa-IIa, otherwise , persons with C807 allelomorph express low level of GpIa-IIa. high level expression of GpIa-IIa only relies on the existence of T807 allelomorph. Comparing to homozygote TT, heterozygote CT expresses the similar amount of GpIa-IIa. Therefore, the clinical meaning of gene polymorphism of GpIa is being payed more and more attention.

We analyzed the polymorphism of platelet gene GpIa C807T in ischemic stroke patients in han population of henan province with the method of PCR-RFLP, research results were as follows:(1)the difference of ratio of allele T807 between cerebral infarction patient group and the control is not significant （P>0.05）.(2) T807 allele in cerebral infarction patients beneath 55 years old showed a significant higher ratio than the control, stroke risk adds 1.6 times.(3) high risk cerebral infarction patient have significant higher ratio of GpIa gene T807 allele than the control (P<0.05), stroke risk adds 1.27 times, results shows: in cerebral infarction patients aged beneath 55 and high risk stroke patients, allele T807 maybe the independent risk factor of cerebral infarction.

Reiner's[8] research found that, female stroke patients beneath 45 years are significant related to GpIa gene allele T807.In one case-control study, Carlsson[9, 10], et analyzed alleles T807 of 227 stroke patients confirmed by CT or MRI and the control group (patients with cerebra vascular disease history、acute myocardial infarction and deep vein thrombus are excluded). After matching other risk factors, we found that in the population beneath 50 years, allele T807 is the independent heredity risk factor. Allele T carriers likely to have stroke 3 times more than the allele C carriers. Our result is the same as the statement above-mentioned, which showed GpIa gene allele T807 might be the independent risk factor of cerebral infarction of han population in henan province,and palyed an important part in the arterial thrombus disease.

Research indicates that allele T807 may be the independent risk factor in young ischemic infarction patients[11]. Also because ischemic stroke is a kind of muti-gene disease influenced by heredity、environment and so on ,the effect of allomorph T807 and other risk factors may accumulate. We can presume that the conclusion that allele T807 is correlated with high risk ischemic stroke patients is reasonable.

Our research found that young ischemic stroke group and high risk ischemic stroke group carried more TT and CT genotypes and T allomorph than the control, indicating allomorph GPIa807T carrier of han population in henan province maybe a heredity risk factor of ischemic stroke. The concrete mechanism needs further

investigation, the probable mechanism is that GPIa in plasma affects the formation of arteriosclerotic thrombus[12],then results in ischemic cerebrovascular disease.our research provided the relationship between allele GpIaC807T of han population in henan province and ischemic stroke. Indicated that allele T807 may be the heredity risk factor in young ischemic infarction patients and high risk ischemic infarction. But among the whole population the frequency of T allele was not significant correlation（P>0.05）.This result cound be explained in this way:GPIa807T may be the genetic susceptibility marker, however, with the age growing, many environment risk factors gradually become prominent[13], which may hide the potential risk of GPIa807T. So the carrier of GPIa807T in the young people should be discovered as early as possible. Because the number of cases is still relatively small,conclusion still needs confirmation by large-sample prospective research. Our research is valuable in the early recognition and intervention of the people who have the heredity risk factor of ischemic stroke,Also it provided theoretical basis for whether patients should receive anti-platelet treatment.

Table 1 Heredity equilibrium test of distribution of patients and controls GPIaC807T genotype

genotypes	controls		Patients	
	Real subjects(%)	Expected subject*	Real subjects (%)	Expected subject *
T/T	79 (25.40)	74.29	83（26.18）	74.33
C/T	146（46.95）	155.42	141（44.48）	158.34
C/C	86（27.65）	81.29	93（29.34）	84.33
	$\chi2$＝1.143，P＞0.05		$\chi2$＝3.802，P＞0.05	

Notice: * was figured by each allele frequency according to Hardy-weinberg equilibrium law

Table2 Distribution of GpIa genotype and ratio of allele of patients and controls

groups	cases	frequencies of genotypes（n,%）			frequencies of alleles（n,%）	
		CC	CT	TT	C807	T807
stroke	317	93（29.34）	141（44.48）	83（26.18）	327（51.58）	307（48.42）
control	311	86(27.65)	146(46.95)	79(25.40)	318(51.13)	304（48.87）
					$\chi2$＝2.615 P＞0.05	

Table 3 GpIa genotype ratio of stroke patients aged below 55 and controls

Groups	cases	frequencies of alleles（n,%）	
		T807	C807
Stroke	131	166 (63.36)	96(36.64)
Control	311	304 (48.87)	318(51.13)
		$\chi2$＝3.859 P<0.05 OR=1.337	95%CI（1.001-1.787）

Table 4 Ratio of gene GpIa allomorph T of high risk stroke patients and controls

Groups	cases	frequencies of alleles（n,%）	
		T807	C807
Stroke	279	322 (57.71)	236(42.29)
Control	311	304 (48.87)	318(51.13)
		$\chi2$＝3.859 P<0.05 OR=1.298	95%CI（1.0321.633）

References

[1].Jiangyan, platelet membrane glycoprotein and its research of polymorphism [J]. China Diagnostic Test ,2003,7:281-283.

[2].Yeh PS,Lin HJ,Li YH,et al.Prognosis of young ischemic stroke in Taiwan: impact of prothrombotic gen etic polymorphisms[J]. Thromb Haemost, 2004; 92(3):583~589.

[3].Kunicki TJ,Kritzik M,Annis DS,et al.Hereditary variation in platelet integrin alph 2 beta 1 density is associated with two silent poly-morphisms in the alpha 2 gene coding sequence[J]. Blood, 1997; 89: 1939-1943.

[4].Kritzik BM, SavageB,Nugent DJ, etal. Nucleotide polymorphism in the a2 gene define multiple alleles that are associated with differences in platelet a2b1 density[J].Blood, 1998,92(7):2382-2388.

[5].Kunicki TJ,Orckekowski R,Annis D,et al.Viariability of integrin alpha2 beta 1a activity on human platelets[J].Blood, 1993,82(9):2693-2703.

[6].ikolopoulos GK,Tsantes AE,Bagos PG et al.Integrin,alpha 2 geneC807Tpolymorphism and risk of ischemic stroke:a meta-analysis[J].Thromb Res.2007 ; 119:501-510.

[7].Hsieh K,Funk M ,Schillinger M,et al.Vienna StrokeRegisty. Impact of the platelet glycoprotein Ib alpha Kozak，polymorphism on therisk of ischemic cerebrovascular events :a case-controlstudy[J]. Blood Coagul Fibrinolysis,2004;15(6)：469~473.

[8].Reiner AP,Kumar PN,Schwartz SM,et al.Genetic variants of platelet glycoprotein receptors and risk of srotke in young women. Stroke[J] .Blood, 2000, 31: 1628-1633.

[9].Carlsson LE,Santoso S,Spitzer C,et al.The α2 gene coding sequence T807/A873 of the platelet collagen receptor integrin α2β1 might be a genetic risk factor for the decelopment of stroke in younger patients[J]. Blood,1999,93:3583-3586.

[10].Gao XC,Huo Y,Liu XZ,et al.Gene Polymorphism of Platelet Glycoprotein I balpha in Chinese Patients with Large-and Small Artery Subtypes of Ischemic Sroke[J].Eur Neurol, 2005;54(2):73-77.

[11].Loncar R,Stold V ,Thomas V ,et al:The 807 C/T polymorphism in the a-subunit of integrin a2ß1 modulates platelet adhesion onto immobilized collagen under arteral flow conditions[J]. Transfus Med –Hemother, 2004 ;31(suppl 3):12

[12].Ringleb PA. Thrombolytics, anticoagulants, and antiplatelet agents.Stroke,2007;38:1113-1114.

[13].Luzak B, Golanski J,Rozalski M,et al.Effect of the 807 c/t polymorphism in glycoprotein is on blood Platelet reactivity .J Biomed Sci.2003,10(6 Pt 2):731-737.

Self-Care Ability Development of 45 C Mode Heart Failure Patients

Zhang Zhenxiang

The second affiliated hospital of Zhengzhou University, Zhengzhou, 450014

Received Nov 10, 2009

Abstract

Self-care ability development of 45 C mode heart failure patients treated during 2005-2008, has been proved to be of great significance. The experience has illustrated that patients have been able to recognize subtle changes of self-health, to prevent inducing factors and to participate in assessing symptoms and pathological signs manifesting in the early period, and to moderately take part in treatment and care and to behave in a healthy way, which are very significant to improve patient's life, reinforce the results of clinical treatment and care to reduce frequency of being hospitalized. [Life Science Journal. 2009; 6(4): 74 – 77] (ISSN: 1097 – 8135)

Key words: C mode heart failure, self-care, ability development

1. INTRODUCTION

Congestive heart failure, a very common cardiovascular syndrome in coinic (abbr. heart failure), is the end period of various organic heart diseases. China has 36 million of chronic heart failure patients, among whom death rate is 37% within two years and within 6 years this rate is up to 82% [1]. Based on clinical treatment requirements [2], heart failure is usually divided into four modes of A, B, C, L, C mode of which is most dangerous. Its clinical treatment is so bad that patients have to be hospitalized frequently and their life was influenced badly. Statistically, it is quite helpful to teach patients about health with a clear aim, to help then obtain accesses to related information and skills and to strengthen the ability of self-care, which can improve their future expectations, and reduce death rate and the frequency of being hospitalized [3]. However the difficult and key points of developing self-care ability for heart failure patients are to present them and /or their family member's effective instructions in time, and to help them take an active part in self-health management, to recognize subtle changes of their disease and lead a healthy life. Under such guidelines, 45 C mode heart failure patients treated from Jan.2005-Jan.2008, have developed self-care ability and have received expected care results.

Correspondence: Zhang Zhengxiang,
zhangzx6666@126.com

2. Materials and Methods

2.1 Objects

Clinical objects: 45 C mode heart failure patients, who were finally diagnosed as this disease in department and received treatment from Jan. 2005-Jan.2008. This group is made up of 29 males and 16 females, whose average age is 68±8, 38 cases with coronary heart disease, 3 cases with rheumatic valve diseases and 4 cases with dilation myocardiopathy.

2.2 Methods

2.2.1 Individual case collection: The designated nurse learns how patients and /or their family members think about the disease, masters their ability to participate in and coordinate treatment and care, and their compliance of leading a healthy life.

2.2.2 Questionnaire: In the questionnaire there are 18 questions covering five areas: the early symptoms and pathological signs of heart failure, inducing factors, drug reactions, responsive measures and further consultations on time with doctors. Questionnaires would be handed to patients or their family members by the nurse within a week when they were hospitalized and in the afternoon when they were to be out of hospital, then are required to be handed in for statistic after being filled in.

2.2.3 Training methods: Patients would be trained and instructed at proper moments based on conditions of their disease. Methods: (1) Individual training: The designated nurse would make an individual training plan for the patient at the beginning when he or she was hospitalized, including patient's self-examination contents, coordination in the process of treatment and result assessment. Training can be carried out in the form of oral instruction and explanation of instruction album, which is made by a fixed nurse to their patient individually. (2) Collective training The department of the hospital would prepare collective training plans personally for patient's self-care in various forms such as filmstrip, series lectures, handbooks, blackboard newspaper, etc. (3) Bedside instruction The sickbeds would be supplied with a list of nurses' instructions recording what self-cares should be done every day. During daily morning care, the nurse, patients and their family members would go over and summarize how self-care was carried out the day before, then assess and record it in the levels of "Excellent" "Better" and "Continuous improvement". Finally the nurse would tell patient and their family how treatment and self-care should be carried on this day, and reminds them of what should be specially paid attention to. As the nurses make rounds of the ward, they will immediately respond to all questions from patients and their family and learn how patients and their family think about self-cares according to patients' responses to their questions.

2.3 Training contents

2.3.1 Early symptoms and inducing factors of heart disease Patients and their family members will be instructed how to examine by themselves and how to recognize early symptoms and pathological signs of heart failure. Left heart failure shows itself as short breath, accelerated heart beat (faster 10 times/second than before) and being tried after activities, being stifled to wake during nights, coughing in the back, sleeping with high pillow (20-30 cm), bubbled-shaped sputum, etc; right heart failure shows itself as feeling sick, poor appetite, weight obtain, strong jugular vein pulse, compression edema in low-dropped parts, etc. Patients should be instructed to pay more attention to noticing changes of their pulse, urine volume and weight, and actively communicate with their doctors and nurses so that effective treatment measures can be taken in the early period to improve the cure rate. Patients and their family members should be also taught how to recognize the relationship between heart failure and inducing factors, and how to avoid these inducing factors. Heart failure is usually induced from infections, irregular heart beat, over taken-in sodium salt, being overtired or excited, or taking medicine without following up doctor's advices, etc.

2.3.2 Moderate participation in treatment and cares during the morning care, the nurse should learn how patients are getting along with self-care and their disease, such as emotion, sleep, diet, activities, treatment and cares, etc, and then tell patients and their family possible treatments and cares this day, and that what should be paid attention to. The nurse should also communicate with patients or their family to learn their practical difficulties, and then discuss with them to find out solutions to them, for instance, to teach to patients or their family self-test pulse, watch heart beat and pulse and find out irregular heart rate; in the process of injection, to remind patients or their family of drop speed, tell them not to change the speed without permission from the nurse and then teach them to feel if where there is liquid leakage. The nurse should watch drug function, poisonous after effects and ill reactions, such as low potassium blood symptoms resulting from diuretic and digitalis poison, which usually result from improperly taking medicine. The nurse should teach patients to recognize signs of digitalis poison. Once such things occur, patients or their family will contact with the doctors and the nurse so that they can take active and effective measures in the early period. The nurse should explain to patients and family the significance of long treatment, and tell them to take medicine according to doctors' advices, and not to stop or reduce medicine freely in order to help patients to comply with treatments.

2.4 **Training in self-comfort adjustment**

2.4.1Psychological comfort: Since they have shouldered heavy economic burden, and being hospitalized frequently because of bad disease, most of C mode heart failure patients have to suffer from so much psychological pressure that their reactive ability to occurrences in life and compliance have been on decrease.

Patients will be focused on self adjustment in psychological comfort then they receive trainings in self-care ability development; they are also taught to make use of psychological defense system, to recognize responsibilities and value of self existence, and to realize significance of self existence and life quality to their family and society so that they can adjust their emotion themselves; at the meantime, encouragements from family and supports from society can strengthen their confidence to comply with treatments[4].

2.4.2 Body comfort Patients should sit erect to reduce sufferings from being stifled; to wear loose clothing under the condition of edema; to protect their skin; often to cut their nails and change the body positions; to eat dark color of vegetables, red jujube and the mushrooms, which can supplement potassium; to control the take-in volume of sodium salt, to prevent cold and to strike the balance between work and rest, which can effectively avoid inducing factors; actively to prevent complications. Patients should be instructed to take moderate activities or be given moderate passive activities, and to soak upper limbs from time to time in order to reduce vein thrombosis. Since C mode heart failure patients have to be in bed for long time and have extravagated blood in their lung, which can easily cause complications in lung, the patients' room should be kept in proper temperature and well ventilated, and patients' family should help then turn over, pound their back and encourage then to discharge sputum.

2.4.3 Pay subsequent visits to doctors on time: It is an effective way for doctors to master their patients' disease, so they should pay subsequent visits to doctor on time in accordance with their doctors' advices after they got out of hospital for recuperation at home. When they are about to leave hospital, according to their specific conditions, patients would be offered individual "out-of-hospital instructions" containing the date when they should pay subsequent visits to doctors, their medicine usage and volume, side effects of the medicine, notices when the medicine is taken, the precautions against ill reactions, restricted foods, food exchange when different complications occur, and so on. Patients will also be instructed to form the habit of writing diary recording diet, activities and conditions of taking medicine, which are very important for doctors to find out changes of their patients' disease, so such information should be offered when patients pay subsequent visits to doctors or communicate with their doctors on line.

3. RESULTS

In comparison of patients' mastering related self-care information before and after being trained in is shown in Table 1. The results demonstrated that all the effective factors are relatively promoted in Master % after training.

Table 1. Conditions of 45 C mode heart failure patients before and after being trained in mastering related self-care information

Time	Cases	Symptoms and body signs		Inducing factors		Drug reactions		Self-comfort adjustment		Subsequent visits on time	
		Master (%)	Not (%)	Master (%)	Not (%)	Master (%)	Not (%)	Master (%)	Not (%)	Master (%)	Not (%)
Before training	45	19/45 (42.2%)	26/45 (57.8%)	12/45 (26.7%)	33/45 (73.3%)	17/45 (37.8%)	28/45 (62.2)	18/45 (40.0%)	27/45 (60.0%)	30/45 (66.7%)	15/45 (33.3%)
After training	45	43/45 (95.6%)*	2/45 (4.4%)	41/45 (91.1%)*	4/45 (8.9%)	40/45 (88.9%)*	5/45 (11.2%)	44/45 (97.8%)*	1/45 (2.2%)	45/45 (100%)*	0

Note: Compared with the pre-training, *P<0.001.

4. Conclusion

Self-care is conscious and continuous behaviors that can be obtained though learning when an individual of human beings is guaranteeing their life and existence, and keeping and strengthening their health [5, 6]. For patients, it enables them to get related information and self-care methods to prompt them to take an active part in cares and self-management which can infiltrate into

people around the instructed objects so that consciousness of people groups can be improved. When patients are active in participating in forming correct and healthy life habits and take effective self-cares, it can intensify treatment effect on C mode heart failure [7]. However as nurses are training C mode heart failure patients in developing self-care ability, their focuses should be put on how patients can recognize self-symptoms and body signs, how patients can manage to lead a healthy life, how patients can take medicine correctly and how patients can realize poisonous after-effect of medicines. The aim of training patients in developing self-care ability is to improve C mode heart failure patients' life quality, to decrease death rate and to reduce the frequency of being hospitalized.

Experiences have shown that there are noticeable differences ($p<0.05$) between being hospitalized and out of hospital in many aspects such as recognition of early symptoms and body signs, preventing from inducing factors, avoiding ill reactions of medicine as possible as patients can , self-comfort adjustment ability, paying subsequent visits to doctors on time, etc. through training plan with clear aim, which have improved patients and their family's initiative, displayed their self- function to the fullest, improved patients' life quality and reduced occurrence of complications. Patients and their family's moderate participation in treatment and cares can improve patients' emotion, reduce the gap between nurses and their patients, and improve the relationship between doctors and their patients.

References

1. Gu DF, Huang GY, He J, et al. Investigation on epidemiology of heart failure in China and the incidence rate. Chinese cardiovascular disease magazine. 2003; 31(1): 3-6.
2. Hu DY, Ma CS. Practices on heart disease 2005-new advances and clinical cases. People's hygiene press. 2005; 551-556.
3. Tian FY, He Z, Li GZ. Investigation on self-care of chronic heart failure patients. Nursing study. 2005; 2: 205-207.
4. Chen JY. Care interventions of obstinate heart failure patients. PLA nursing magazine. 2006; 41(12): 58-59.
5. Orem DE. Nursing: Concepts of practice. New York: Mc Grawhill, 1991w; 236.
6. Li XS. Nursing compendium. Beijing: People's hygiene press. 2008; 40.
7. Hu CL. Feasibility analysis of application of self-management theory in clinical care. PLA nursing magazine. 2007; 10(24): 31.

Study of the Expressions of level of sex hormones and their receptors for lung cancer patients

Xiufang Chen [1], Shuling Wang [2]

1 Modern medical research institute of Henan province, Zhengzhou, Henan, China; 2 College of Basic Medical Science, Zhengzhou University, Zhengzhou, Henan, China;

Received February 2, 2008

Abstract

Most of lung cancer patients are with disorder expressions of estrogenic and androgen as well as their receptors ER and AR. In this study, a mechanism is proposed by testing Testosterone (T) and Estradiol (E_2) levels and to look into the expressions of ER and AR for male non-small cell lung cancer patients to clarify the influence of sex hormones and their receptors. [Life Science Journal. 2009; 6(4): 78 – 86] (ISSN: 1097 – 8135).

Keywords: lung cancer; sex hormones; AR; ER

1. Introduction

Primary Bronchogenic Carcinoma can be referred as lung cancer, typically originated in bronchia mucosa. Lung cancer is constantly malignant and seriously threat to people's health and life. In the United States, lung cancer accounts for most of the cancer deaths [1]. It is expected that by the year 2020, cases of cancer all over the world will reach 15 million. Most of these cases are Lung cancer which shall be the highest morbidity and mortality of diseases [2].

Presently, pathogeny of lung cancer is not yet fully understood. The epidemiology survey shows that smoking is the most possible for lung cancer in etiology. About 85% of lung cancer patients have smoking history[3]. Air pollution, employment, nutrition, diet, ionizing radiation, chronic lung disease is by closely related to biological factors of lung cancer. In recent years, animal experiments and clinical data indicate that, in certain non-malignant tumor, the expression of sex hormones receptors' can be also found in target organs like liver cancer, colon cancer, throat cancer, lymphoma etc. [4-6]. The growth of lung cancer is affected by sex hormones and its receptor. Sex hormone regulates the differential of the lung and its development. The lung should be involved in the metabolism of estrogen and progesterone procedure; estrogen and progesterone have their own receptor-binding to play their role as well as estrogen and progesterone receptors. The high expression of estrogen causes the organ of lung cancer to change endocrinic micro environment. The cells of lung cancer originate the estrogen and progesterone receptor protein synthesis genes. The synthesis of lung cancer cell with binding activity of receptor protein basically tells the characteristics of the female and male hormone receptors as well as the origination of the lung cancer and its growth [7]. Especially in advanced stage, patients with lung cancer can be found the hormone disorder in the expression of ER and AR [8, 9]. In this report, we use immunohistopathologic assay to detect the expression of the estrogen receptor (ER) and androgen receptor (AR). Meanwhile, we also use radiant immunological assay to detect T and E_2 levels for checking the possible etiological mechanisms for male non-small cell lung cancer patients.

2. Materials and methods

2.1 Materials and Samples

All cases obtained since July 2007 through July 2008 were from Department of thoracic surgery in Zhengzhou University first affiliated Hospital. Patients, a total of 56 cases, with the histological classification of lung cancer WHO1999, 34 patients with squamous cell carcinoma, 22 cases of adencarcinoma were pathological

Correspondence: fang1518@126.com

Dr. Xiufang Chen

confirmed in diagnosis as male non-small cell lung cancer. 29 cases were classified as in stage I, 17 cases in phase II, 10 patients in stage III. The youngest is 34-year-old, by averagely with the eldest 75-year-old, is 59.2 years old. Non of them were been in chemotherapy or radiotherapy and have not been prescribed sexual hormone-disrupting medicine in one month before operation. The control group was 30 healthy male volunteers selected through carefully physical examination.

Serum preparation: Collecting blood 3ml from patients in the morning before surgery, put into 3,000r/min centrifugation, taking the serum saved at -20 .

Tissue specimen's preparation: Taking the fresh surgical resection with diseased tissue and adjacent tissues from patients fixed with 4% formaldehyde solution for more than 24h and then after ethanol gradient dehydration, using paraffin embedding at low melting point paraffin, cut in as 3 ~ 4μm slices. The experimental Testosterone (T) reagent was purchased from DPC Biotechnology Company; estradiol (E_2) reagent was purchased from Beijing North Biotechnology Institute products. And both AR monoclonal antibody and ER monoclonal antibody were produced by the United States Santa Cruz Inc. S-P immunohistochemical reagent was purchased in Beijing Jinqiao Bio Co., Ltd.

2.2 Methods

2.2.1 Method to determine serum testosterone (T) and estradiol (E_2): With radioimmunoassay (RIA) kit, testosterone can be determined by using coated tube method; meanwhile, E_2 can be determined by using pairs of anti-method.

2.2.2 AR, ER immunohistochemical staining: By using of Streptavidin-biotin-peroxidase immunohistochemical method (referred to http://www.kpl.com/catalog/), we checked from microscope by view of films to compare experimental group and the cancer adjacent tissue (from cancer tissue more than 5cm) group which was used the control group. Positive control including ER and AR photos was referred to the photos provided by Beijing Chungshan Company.

2.2.3 The assessment of immunohistochemistry assays: The assessment of the immunohistochemical staining was referred to the literature [10] to develop criteria for immunohistochemical. The ER, AR can be cataloged by the number of plasma brown granules appeared as positive in nuclei of tumor cells shown in high-powered microscope. Every slice selected needed five horizons, each horizon counting 100 cells. If the positive plasma brown granules appeared more than 25% was recorded as positive. High-powered microscope could take four different points for each view and each count has 200 cells. The percentage of cells, according to the degree of positive was marked as one (+) to three (+). In contrary, no positive cells, we marked it as negative (-). When the positive cells were around 30%, we gave it marked as +, if positive cells accounted for 30% to 50%, we gave it marked as + +, meanwhile, if positive cells were over 50% , we gave it marled as + + +. The percentage of positive cells referred to the reference [10] under (100 times) microscope view, we randomly selected four viewing fields to calculate the percentage of positive cells in tumor and defined that the percentage of positive cells between 0% -5% as 0 point, 5% -25% as 1 point, 26% -50% as 2 points, 51-75% as 3 points and more than 76 as 4 points. Comparatively, staining index points of 0-2 is defined as the negative; 3-7 is defined as positive expression.

2.2.4 Statistical Methods: The count information was based upon mean ± standard deviation. All statistical analysis was used by SPSS13.0 statistical software.

3. Results

3.1 The relationship between the clinical pathology and the serum sex hormone levels

In comparison of non-small cell lung cancer group to the normal control group, we found that the T level was significantly lower (P <0.01). However, the E_2 level was significantly higher (P <0.01). (Table 1) The E_2-T

ratio was significantly higher (P <0.01). The serum sex hormone level of 60-year-old and elder senior group patients were significantly higher than others (P <0.05). The T level was negatively correlated with age (P <0.05). As the age reduces, the level T and E_2 were positively correlated (P <0.05), namely, E_2 levels increased with age rising. The lung cancer patients with high, medium, poorly differentiated levels of serum E_2 level between the two groups was statistically significant difference (P <0.05), which differentiated the serum E_2 level was significantly lower than the poorly differentiated group, the differentiation of serum E_2 was significantly lower than the poorly differentiated group (P <0.05). (Table 2)

Table 1. The serum sex hormone levels of Lung cancer group and normal control group comparison ($\bar{x} \pm s$)

group	samples	serum sex hormone level		
		T (ng/mL)	E_2 (pg/mL)	E_2/T
Patient	56	3.87±1.45*	59.90±26.67*	3.48±2.01*
Control	30	6.72±1.43	87.00±23.54	1.48±1.00

Notice：*; P <0.01

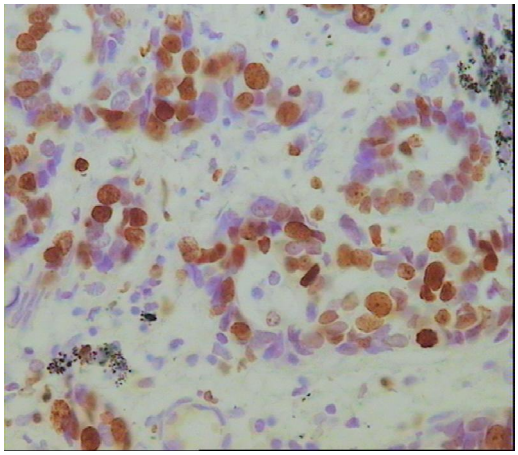

Fig. 1 AR expression in lung adenocarcinoma (IHC×400)

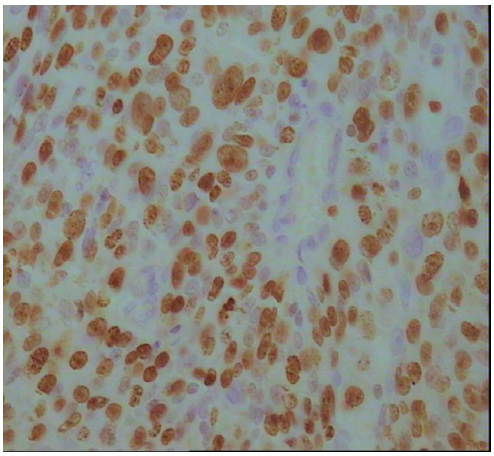

Fig. 2 AR expression in squamous cell carcinoma (IHC×400)

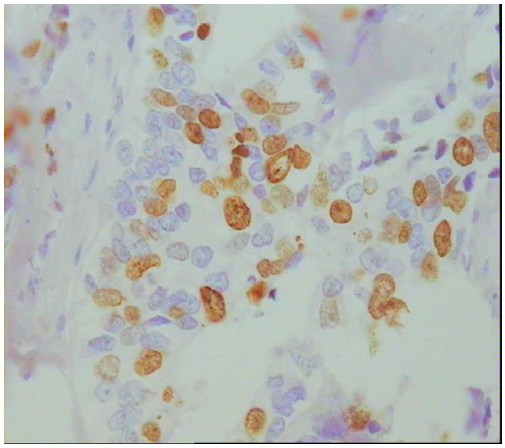

Fig. 3 ER expression in lung adenocarcinoma (IHC×400)

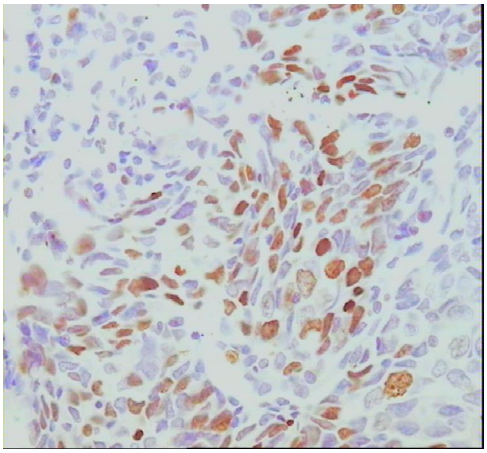

Fig. 4 ER expression in squamous cell arcinoma (IHC×400)

Table 2. Relationship between sex hormones levels and clinicopathological characteristics of lung cancer patients

Characteristic	samples	sex hormones levels	
		T (ng/mL)	E_2 (pg/mL)
Tatals	56	3.87±1.45**	59.90±26.67**
Age(y)			
≥60	27	3.38±1.14*	94.78±20.30*
<60	29	4.32±1.56	79.76±24.35
Histology			
Squamous cell	34	2.67±1.47	91.29±25.88
Adenocarcinoma	22	3.61±2.33	96.32±26.66
Grade			
I	29	4.36±1.5*	75.93±22.06**
II	17	3.49±1.06*	92.82±19.50**
III	10	3.08±1.18	109.20±13.76*
Metastasis (TNM) Stage			
I	33	3.27±1.80*	93.10±19.98
II	12	3.32±2.57	103.00±27.94
III	11	2.023±0.80	91.55±25.145
T Stage			
1-2	52	3.11±1.95	93.02±22.48
3-4	11	2.08±0.05	119.50±10.38
N Stage			
0	34	3.05±2.00	98.15±19.90
1	10	3.04±1.49	86.31±23.11
2	12	3.01±2.02	92.92±29.65

Notice：*: P <0.05； **: P <0.01

Table 3. Relationship between expression of AR, ER and clinicopathological characteristics of lung cancer patients

Characteristic	n	Expression of AR		*P* value	Expression of ER		*P* value
		Positive	Positive(Rate)		Positive	Positive(Rate)	
Tatals	56	13	23.21		12	21.43	
Age(y)				0.865			0.523
≥60	27	6	22.22		7	25.93	
<60	29	7	24.14		5	17.24	
Histology				0.240			0.111
Squamous cell	34	8	23.53		5	14.71	
Adenocarcinoma	22	5	22.72		7	31.82	
Grade				0.751			0.301
I	29	7	24.14		6	20.69	
II	17	4	23.53		4	23.53	
III	10	2	20.00		2	20.00	
TNM Stage				0.906			0. 231
I	33	7	21.21		4	18.18	
II	12	4	33.33		2	16.67	
III	11	2	18.18		6	36.36	
T Stage				0.227			0.401
1-2	52	11	21.15		9	21.15	
3-4	4	2	50.00		3	25.00	
N Stage				0.760			0.193
0	34	7	20.59		6	17.65	
1	10	4	25.00		4	25.00	
2	12	2	16.67		2	33.33	

3.2 The relationship of the clinical pathology for the ER and AR expression

ER and AR in lung cancer the overall positive were 23.21% (13/56) and 21.43% (12/56) (table 3). ER positive expression in lung cancer does not correlate with age, tumor histological type, histological grade, TNM stage. Meanwhile, AR positive expression in lung cancer does not correlate with age, tumor histological type, histological grade, TNM stage either. But TNM stag of lung cancer patients in Phase III were significantly higher than in phase I lung cancer. Lymph node metastasis, there are no difference (X^2 = 5.2032, P <0.05) between N2 group and N0 group.

4. Discussion and Conclusion

It is reported in the literature [11] that 40% to 60%

of human cancers are related with endogenous or exogenous sex hormone effects. In recent years, sex hormone disorders and the relationship between the occurrence and development of lung cancer are concerned by scientists specifically about the relationship between sex hormones and lung cancer which have a complex duality, being with carcinogenic and on the other hand role of tumor suppressor.

Hormonal environment of the body imbalance, sex hormone deficiency and excess could lead to cancer. Hormone itself is not carcinogenic substances, but it can through the proliferation of target cells, so that to play a role in promoting the carcinogenic process to start. The roles of sex hormones also have a mechanism of catalyst to promote the start-up phase in the proliferation of cancer cells. In addition, sex hormones can promote the rapid proliferation of the cells to the malignant cell transformation. As early in 1977, Fairlamb et al. [12] have found that men with breast development may associate with lung cancer with increasing the level of estradiol and drawing down the testosterone level [13-14].

David et al. [15] has studied 39 cases of male patients with lung cancer. They reported that blood testosterone level was lower (<12nmol / L) than the positive control. Low level of testosterone can be used as an indicator of lung cancer metastasis. The results of our study has show that serum T level of male patient with lung cancer in comparison to the normal control group was also significantly lower (P <0.01). Serum E_2 level compared with normal control group significantly increased (P <0.01). E_2 / T ratio increased may mean that comparing with lymph node metastasis group and no lymph node metastasis group revealed T at significantly lower that indicating the patients with lung cancer in serum sex hormone level presented in disorder. But there are also opposite findings from Chen Ming-wei [16]. The sex hormone levels were correlated with the pathological type of tumor, cell differentiation; clinical staging and tumor size with no significant relationship between the sizes of tumor. David [17] reported that leading to a lower level of serum T may be the effect caused by reducing and increasing consumption jointly; peripheral blood level of estrogen increase was mainly attributable to increase in estrogen or metabolic disorder. In normal male, 50% to 70% female hormone was produced by testosterone in fat, muscle and skin tissue transforming with aromatase from the secretion of cortex. The reason why the male obesity patient appears peripheral blood reduction of androgen and increasing estrogen is due to the aromatase in adipose tissue transforming the androgen into estrogen-induced [18]. Some studies suggested that [19] the androgen aromatase catalytic in lung tissues converted to estrogen and the release into the blood may result in male patients with lung cancer with elevation of estrogen but reducing testosterone. Estrogen, androgen and their receptors are correlated with the occurrence, development and prognosis of cancers not only in target organs such as the uterus, breast, and prostate cancer organs but also non-target organs. Chaudhuri et al reported on 1982 that the frequency of ER was 14.29% (15/105) that revealed the lung cancer may be estrogen-dependent [20]. Our study supported that the frequency of expression of ER-positive at 23.21%. However, some other studies have shown [21] ER in non-small cell lung cancer cases was in negative expression. Radzikowska et al [22] suggested the opposite outcomes might be the applications of the error in different technology and the effect of polyclonal antibodies, such as the operation of antigens hot fix, non-standardized operation of the process and monoclonal antibodies Clone. The morbidity and mortality for male lung cancer patients were much higher than females. The reason may be the occurrence of AR in the development of lung cancer. ER relatively to the AR of lung cancer is much less expressed varied (0-76%). such as Liang Peng et al [23] using immunohistochemical SP method detected 47 cases of

lung cancer tissues in AR expression, AR-positive rate was 61.7%, Yan-ming [8] using immunohistochemical staining of 105 cases of lung cancer tissue specimens AR expression, AR-positive rate of 20%. This study showed that AR was negative in normal lung tissue expression of AR in lung cancer tissues positive rate of 21.43%. For lung cancer patients, the expressions of AR and ER are highly related to the characteristic of Clinical and pathological features as well the degree of differentiation and clinical stages and the age of the patients. Due to these differences, it is believed that the expression of ER may be related with histological types of lung cancer, accordingly, the positive expression frequency of adenocarcinoma was publicized significantly higher than squamous cell carcinoma, and adenocarcinoma, and this is also possibly the reason that the observed incidence of female was higher than male [24-31]. However, in our study, we did not find the expressions of ER and AR being significant different between squamous cell carcinoma and adenocarcinoma. Our study has demonstrated that the experimental group of male with non-small cell lung cancer patients being observed serum sex hormone disorders and high expressions in cancer tissues of ER as well as AR, which suggested that the abnormal sex hormone disorders and its receptor expression may be the initiation factor in the development of lung cancer. Despite the ambiguities of the statistical results, study of sex hormone and its receptors ER, AR expressions in origination for lung cancer and metastasis should be further investigated in depth.

References

1. Jemal A, Siegel R, Ward E, *et al*. Cancer statistics, 2008[J]. CA Cancer J Clin, 2008, 58: 71–96.
2. Jemal A, Siegel R, Ward E *et al*. Cancer statistics, 2007[J]. CA Cancer J Clin, 2007, 57:43– 66.
3. Peto R, Darby S, Deo H *et al*. Smoking, smoking cessation, and lung cancer in the UK since 1950: Combination of national statistics with two casecontrol studies [J]. BMJ, 2000, 321:323–329.
4. Lindahl B, Alm P, Fetto M, *et al*. Prognostic value of steroid receptor concentration and flow cytometrical DNA measurement in stage I-II endometrial carcinoma [J]. Arta Oncol, 1989, 28(4):595.
5. Harrison JD, Watson S, *et al*. The effect of sex hormones and tamoxifen on the growth of human gastric and colorectal cancer cell lines [J]. Cancer (Philadelphia), 1989, 63: 2148-2151.
6. Schwartz MR, Randolph RL, *et al*. Steroid hormone binding macromolecules in meningiomas: failure to meet riteria of specific receptors [J]. Cancer (Philadelphia), 1984, 53:922-927.
7. Oliaycsl CW, Riordan GP, Rushin JM. Estrogen receptor detection in paraffin sections of adenocarcinoma of the colon, pancreas, and lung [J]. Arch Pathol LabMed, 1994, 118:630.
8. Yan M, Chen XB, Wang SL, *et al*. The expression of AR and ER in lung cancer [J]. Chinese Journal of Lung Cancer, 2008, 1 (11):126-129.
9. Li QS, Zhao XM, Jin XP, *et al*. Expression and significance of estrogen and progesterone receptor in lung cancner[J]. Chinese Journal of Lung Cancer, 2003, 8(3):192-194.
10. Fang N, Shao R, Chen DY. Expression of PTTG, c-myc and p53 Protein in Non-Small Cell Lung Carcinoma and Its Significance. Journal of Jiangsu University, 2008, 2(18):131-134.
11. Li JJ, Mueller GC, Sekely LI. Workshop report

from the Division of Cancer Etiology, National Cancer Institute, National Institutes of Health. Current perspectives and future trends in hormonal carcinogenesis[J]. Cancer Res, 1991, 51(13):3626-3629.

12. Fairlamb D, Boesen E. Gynaecomastia associated with gonadotrophin secreting carcinoma of lung cancer [J]. Postgrad Med J, 1977, 53 (619): 269-271.
13. Shu QJ, Chen JG, Wang YN, *et al*. On Sex Hormones in Male Patients with Lung Cancer. Military Medical Journal of South China, 2007, 21(6):13-14.
14. Wang NH, XU L. The study of serum sex hormone levels changes in male malignant tumors patients [J]. Journal of Modern Laboratory Medicine, 2007, 22(3):79-80.
15. David PT, Christina G, Kenneth Gd. Low serum testosterone as indicator of metastic bronchial carcinoma [J]. Thorax, 1987, 42:661.
16. Chen MW, Hu GY, Li ZM *et al*. Using Double antibody radioimmunoassay detected serum sex hormone levels change in lung cancer. Xi'an Med Univ, 1999, 20(2):202-204.
17. David PT, Christina G, Kenneth GD. Low serum testosterone as an indicator in metastatic bronchila [J]. Thorax, 1987, 42: 661.
18. Xu B, Zhou L, Zhang J. **Sex hormones and obesity**[M]. China Science &Technology Press, 1997, 189-198.
19. Zhou XD, Cao WQ, Cai HW. Study on the relationship between estrogen receptor expression and level of serum sexual hormones in male patients with lung cancer. Chinese Journal of Lung Cancer, 2002, 5(5):349-351.
20. Chaudhuri PK, Thoms PA, Walker MT, *et al*. steroid receptor in human lung cancer cyetoslos. Cancer Lett, 1982, 16(3):327-332.
21. Li JL, Zhu HY, Chen TX, *et al*. Expressions of BRCA2, ER, PR and c-erbB-2 in Non-small cell lung carcinoma [J]. Chinese J. of Histochemistry and Cytochemistry, 2008, 17(4):306-310.
22. Radzikowska E, Langfort R, Giedronowicz D. Estrogen and progesterone receptors in non small cell lung cancer patients [J]. Ann Thorac Cardiovasc Surg, 2002, 8(2):69-73.
23. Liang P, Liu ZH, Wang Q, *et al*. The significance of detect sex hormone receptors in Primary lung cancer [J]. Chinese Journal of Clinical Oncology and Rehabilitation, 1998, 5(2):16-17.
24. Mollerup S, Jorgensen K, Berge G, *et al*. Expression of estrogen receptors alpha and beta in human lung tissue and cell lines [J]. Lung Cancer, 2002, 37(2):153-159.
25. Li QS, Gao XH, Lv XY, *et al*. Expression and Clinical Significance of ER, PR in NSCLC. Clinical Focus, 2003, 18(24):1390-1392.
26. Mao WH, Xun JP, Mao JL. Expression and Clinical Significance of ER, PR in lung cancer tissue [J]. Zhejiang Practical Medicine, 2005, 10(4):225-245.
27. Chen DY, Hu YX, Bi JB, *et al.* Expression of estrogen and Progesterone Receptors in Non small cell Lung Cancer and its Clinical Significance [J] .China Medical Univ, 1998, 27(2):161-163.
28. Zhou JJ, Chen HJ, GaoY, *et al.* Expression of Estrogen and Progesterone Receptors in Non-Small Cell Lung Carcinoma [J]. Chin J Clin Oncol, 2004, 31(9):1108-1110.
29. **Lu ZH.** Expression of Estrogen and Progesterone Receptors in Pulmonary Carcinoma and Its Correlation of Clinical Significance and Prognosis [D]. Jiangxi Medical College, 2003
30. Peng AM, Yin SJ, Fu PF, *et al.* P53 Protein, Estrogen/Progesterone Receptor Expression and DNA Ploidyin Lung Cancer. Journal of Tongji University, 2005, 26(3):16-18.

31. Peng AM, Cang LQ, Liu DF, *et al*. A study on the expression of estrogen receptor and the effect of Tamoxifen treatment in lung cancer [J]. Journal of Shanghai Tiedao University, 2000, 21(1):59-62.

Expression changes of DSCAM in induction of MSCs to differentiate into neurons

Tao Peng, Yanjie Jia *, Junfang Teng, Boai Zhang, Guiyuan Fang

Department of Neurology, First Affiliated Hospital of Zhengzhou University, Zhengzhou, Henan, China. *Projects supported by National Natural Science Foundation(30770758)*

Received November 1, 2009

Abstract: Objective. To explore the role of Down syndrome cellular adhesion molecule (DSCAM) in the course of the rat marrow mesenchymal stem cells (MSCs) differentiated to neurons in vitro. **Methods.** MSCs from Sprague-Dawley rats were induced into neurons by baicalin. Immunocytochemistry, Western blot and other methods were performed to detect DSCAM in neurons. At the same time, RNA interfere technique was performed to observe the induction and differentiation after DSCAM-siRNA was transfected into MSCs. Results Before induction, the expression of DSCAM was not detectable in MSCs. After 24h pre-induction, DSCAM was slightly expressed in MSCs (1.71％±0.67％).After 6h induction by baicalin, the expression of DSCAM increased (15.79％±4.24％) and reached the peak (53.16％±5.94％) after 3d induction. After 6d induction, DSCAM expression obviously decreased (28.99％±6.72％). After DSCAM-siRNA was transfected into MSCs, DSCAM expression obviously decreased. However, MSCs did not express neuron-specific β-III-tubulin, expression of β-III-tubulin was (1.40％±0.79％) after 6h induction, （41.59%±3.17%） after 3d induction and (59.11％±4.76％) after 6d induction. But after DSCAM-siRNA was transfected into MSCs, expression of β-III-tubulin obviously decreased （28.57%±2.91%、43.90%±12.31%） after 3d and 6d induction. **Conclusions.** DSCAM might play an important role in MSCs differentiation into neurons. [Life Science Journal. 2009; 6(4): 87-91] (ISSN: 1097 – 8135)

Key Words: Down syndrome cellular adhesion molecule; marrow mesenchymal stem cells；neuron; RNA interfere

1. Introduction

Down syndrome cell adhesion molecule（DSCAM）, which Gene is located at 21q22, if over-expressed (such as the chromosome 21 trisomy), that is Down syndrome. It results in abnormality of nerve cell migration, proliferation, differentiation, leads to congenital intellectual maldevelopment [1]. Moreover, DSCAM is the imperative cell adhesion molecule in connections between nerve cells, and plays an important role in the formation and maintenance of the neural network [2]. In the process of inducing marrow mesenchymal stem cells (MSCs) to nerve cells in vitro, we firstly observed the changes of DSCAM expression and explored the function.

2 Materials and methods

2.1 The main reagents and animals

Correspondence: jiayanjie1971@yahoo.com.cn
Yanjie Jia.

DMEM liquid medium, B_{27}, fetal calf serum, Trizol purchased from Gibco Company; basic fibroblast growth factor (basic fibroblast growth factor, bFGF) purchased from Pepro Tech EC Inc.; mouse anti-polyclonal DSCAM, nerve cell marker protein β -III-tubulin antibody purchased from Abnova Corporation; goat anti-mouse-Cy3, goat anti-mouse-AP antibody purchased from Sigma company; Rat Rn-DSCAM-siRNA (FITC tags), transfection reagent HiPerFect, positive control Rn-MAPK1 Control siRNA, negative control AllStars Negative Control siRNA (FITC tags) purchased from Qiagen Inc.; RT-PCR kit purchased from Promega Corporation; The remaining biological and chemical reagents are imported or domestically analytical reagent. MSCs was extracted form femur of SPF-class Sprague-Dawley rats by the University Center, and passaged more than 10 generations, regular cryopreservation in liquid nitrogen.

2.2 Induction of MSCs to nerve cells in vitro

In the light of our approach [3], the culture and induction of MSCs differentiation was carried out. In accordance with the 2 × 10^4 cells / hole ratio, the 10th generation of MSCs was vaccinated in the 6-hole culture plate with plastic coverslip, cultured 3d, the induction experiment began when 80-90% was fused. After 3 washes with D-Hank's fluid, a pre-induction medium (DMEM medium, 10% fetal calf serum, 10 ng/ml bFGF) added, cultured 24h. After pre-induced, induced 6h by adding liquid (DMEM medium, 200-400 μM baicalin), then adding liquid (DMEM medium, 200-400 μM baicalin, 10 ng/ml bFGF, B27) to maintain 6d.

2.3 DSCAM-siRNA transfected MSCs

According to the Qiagen company's operating instructions for MSCs transfection as follows: 1250ng siRNA was dissolved in 100 μl DMEM medium (no serum) and then adding 12μl HiPerFect transfection reagents, and incubated 10m at room temperature after mixing; the complex was dropped on the surface of MSCs, and then added to the DMEM medium (containing 10% FBS), so that the final concentration of siRNA to achieve 24 nM, incubated 12-24 h. Positive control (Rn-MAPK-1 Control siRNA) and negative control (AllStars Negative Control siRNA) apply the same approach.

2.4 Immunocytochemistry method，image collection and analysis

After washed with PBS, the cells were fixed 20 min at 4°C in stationary liquid (4% paraformaldehyde), reacted 10 min in 0.2% Triton, blocked 1h with 10% Bovine Serum Albumin (BSA), then incubated 24 h at 4°C with Anti-DSCAM (1:200), Anti-CD90 (1:200) or Anti-β -III-tubulin (1:800).The cells were stained and observed at room temperature with second antibody after 3 washes.

The cells image were photoed 10x or 20× by microscope using 300 dpi resolution. Every independent experiment collected more than 30 region of cells. Furthermore, the image collected in bright field contains the same counts of cells. Double person and double mind random method were counted positive cells and computed positive cells percentage.

2.5 Western Blot method

Collected cells of each group were cracked, degenerated, centrifuged in the cell lysate (50 mM Tris-Cl, pH 6.8, 10 mM EDTA, 2% SDS, 5 mM DTT, 0.5 mM PMSF) 100 μl, collecting the supernatant protein samples and quantificating protein by Bradford method. Protein lysate was added in 4× gel upper sample buffer, and transferred to PVDF membrane after SDS-acrylamide gel electrophoresis, blocked with 5% defatted milk (1 h at room temperature) and incubated overnight at 4°C with TBST. The membrane was washed 3 times, and reacted 1h at room temperature with IgG tagged by horseradish peroxidase, then washed 3 times. ECL reaction was conducted, followed by exposure and development.The same experiment needs 3 repeats.

2.6 RT-PCR

Total cellular RNA was extracted with Trizol reagent and quantitated conventionally. RT-PCR amplification reaction was performed on the light of Promega kit manual, the reaction system was 50μl, reverse transcription and PCR were accomplished in one step (35-40 cycles), 10μl of amplification product were added to 1.5% agarose gel, ultraviolet transilluminator was used to observe and photograph after electrophoresis. Primer was from Shanghai Public Health Synthesis Ltd. (Table 1).

2.7 statistical treatments

ImagePro Express software was used to collect and process all images. The data was expressed by $\bar{x} \pm s$. GraphPad Prism 5.01 was used to make picture. Analysis of variance was used to evaluate the data, the P value less than 0.05 was considered to be significantly different.

3. The results

3.1 Induction of bone marrow mesenchymal stem cells to differentiate into nerve cells in vitro of rats cultured 10 generations are mainly spindle, squamous cells and expressed MSCs marker (Figure 1A). After 6h induction with Baicalin, some cells changed to a triangle, cell microfilament contracted, pseudopodium formed slender

processes and interlaced locally , similar to nerve cells; After 6d the majority of cells changed to be cone-shaped, interlaced into a network, and formated typical nerve cell structure (Figure 1B). This study chose β-III-tubulin as a marker of mature nerve cells, MSCs were not found to express β-III-tubulin before the induction and after 6h induction (1.40% ± 0.79%). With the cells differentiation, β-III-tubulin expression increased rapidly to (41.59% ± 3.17%) with 3d induction and (59.11% ± 4.76%, Figure 1C) with 6d induction. Western Blot also had similar results (Figure 2).

Table 1. Primer sequence

Gene name	*Primer sequence*	*product*
SCAM	Forward: 5'-AGAAGTGCCCACCAATTGAG-3'	135 bp
	Reverse: 5'-CACCCAGGTTCCTTCTGATC-3'	
β-III-tubulin	Forward: 5'-TGCGTGTGTACAGGTGAATGC-3'	240bp
	Reverse: 5'-GGCTGCATAGTCATTTCCAAG-3'	
GADPH	Forward:5'-CCCACGGCAAGTTCAACGGCA-3'	430bp
	Reverse: 5'-TGGCAGGTTTCTCCAGGCGGC-3'	

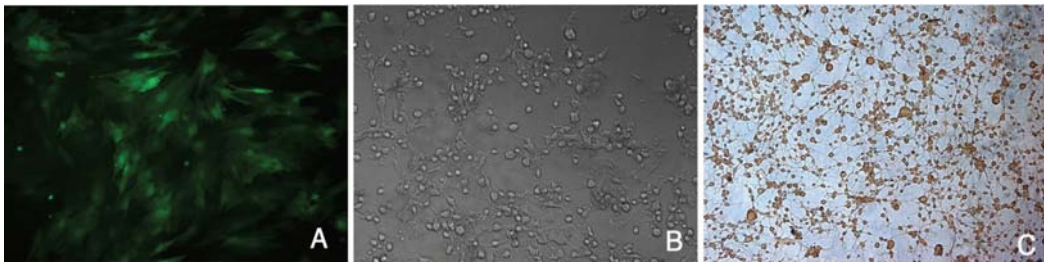

Figure 1. Induction of MSCs to neuron. A: pre-induction**,** the 10th generation of MSCs (CD90 staining, FITC,×200); **B:** 6d after induction, change of cell morphology (×200), the cells were cone shaped, similar to neuron; **C:** 6d after induction, expression of β-III-tubulin in differentiated cells (DAB coloration, ×100), most cells were cone shaped, interlaced to net, β-III-tubulin was hyperexpressed.

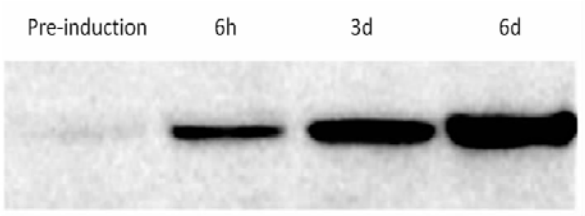

Figure 2. Changes of β-III-tubulin expression before and after induction (Western blot). β-III-tubulin expression increased rapidly with the time.

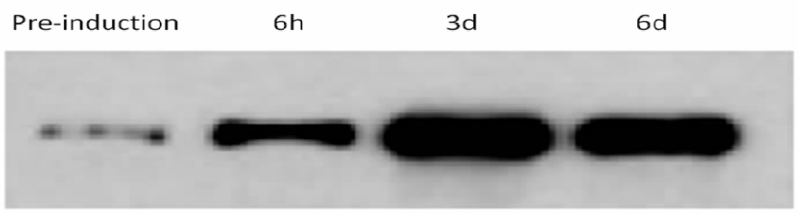

Figure 3. Changes of DSCAM expression before and after induction (Western blot). DSCAM expressed partially at 6h after induction. The expression increased gradually to the peak at 3d and decreased at 6d.

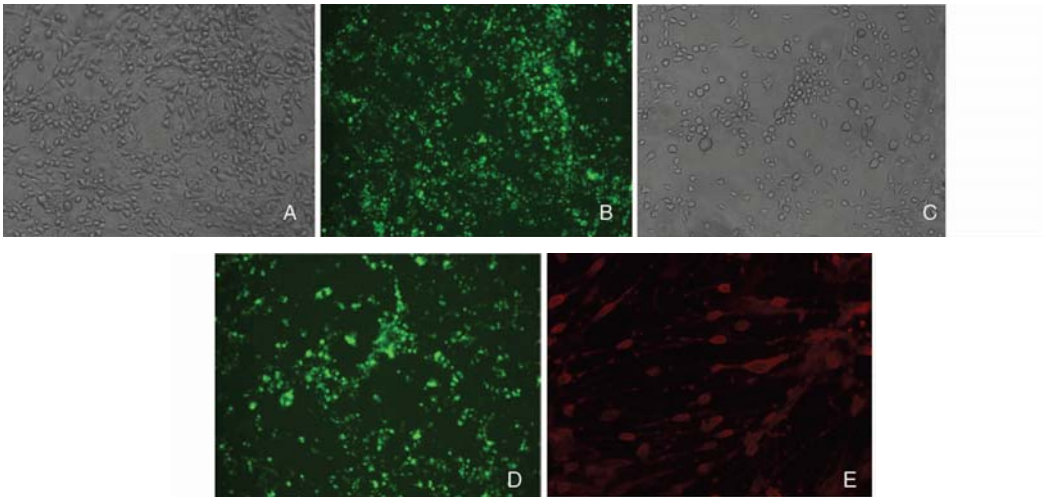

Picture 4. DSCAM-siRNA transfected MSCs A: Cell morphology of MSCS did not chang obviously after DSCAM-siRNA transfected MSCs (×100); **B:** Green fluorescent granules in cells can be observed in same visual field (×100); **C:** 6d after DSCAM-siRNA transfection and induction ,the differentiation of transfected cells were poor, the neural networks were sparse (×100); **D:** Green fluorescent granules can be observed in differentiated cells in same visual field (× 100); **E:** 6d after siRNA transfection and induction, the change of DSCAM expression (immunofluorescence，Cy3 staining,×200) .

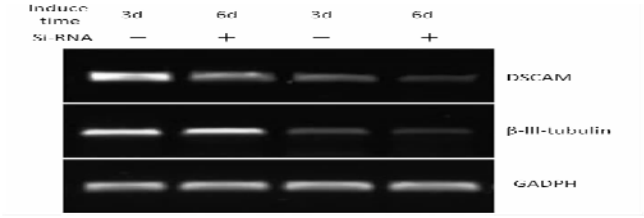

Picture 5. Changes of DSCAM mRNA expression before and after induction (RT-PCR). DSCAM β-III-tubulin expression decreased significantly than untransfected group after siRNA transfection (p<0.01, p<0.05).

3.2 Changes of DSCAM expression

The rats MSCs did not express DSCAM before induction., MSCs began to express a small amount of DSCAM (1.71% ± 0.67%) after 24h pre-induction and express partially on cell membrane and processes after 6h induction (15.79% ± 4.24%); With the extension of time the expression continued increasing, and to the peak after 3d induction (53.16% ± 5.94%). But DSCAM expression decreased significantly (28.99% ± 6.72%) after 6d induction , and it was significantly different from 3d induction (t = 8.516, P<0.01). Western Blot method had similar results (Figure 3).

3.3 DSCAM-siRNA transfected MSCs

MSCs had no obvious morphological changes after DSCAM-siRNA transfection, Green fluorescent granules can be observed in cells by fluorescence microscope after 24h transfection and can express more than 1 week (Figure 4A, 4B). The efficiency is (78±12.9)%. However, after baicalin induction, cell differentiation was poor, processes was short, straight .Branches and neural network formation were sparse (Figure 4C, 4D). Immunocytochemical stain (Figure 4E) and RT-PCR (Figure 5) prompted that DSCAM expression decreased significantly after DSCAM-siRNA transfection. But after DSCAM-siRNA transfection, with 3d or 6d induction, β-III-tubulin expression decreased significantly (28.57% ± 2.91%, 43.90% ± 12.31%), the difference was significant compared to untransfected cells (P<0.01, P<0.05).

4. Discussions

DSCAM belongs to immunoglobulin super family. In 1998, Yamakawa isolated DSCAM gene and found

that most of these genes expressed in the development phase of the nervous system [4]. Sequence analysis shows that, DSCAM consists of the N-end signal peptide, 10 immunoglobulin domain, 6 3-type fibronectin domains, a transmembrane domain and an intracellular domain. DSCAM can be cuted to 38,000 kinds of isomers through RNA, the protein may help nerve cells link exactly in the process of nerve network formation. Over-expression of DSCAM have the direct result of nerve cell migration, proliferation and abnormality of differentiation, this is the molecular genetics basis of Down's syndrome [1].

Nearly 10 years, the study found that MSCs can be directed to differentiate into nerve cells and glial cells.As a class of ideal "seed cells", MSCs have the advantages of proliferation, security, autologous transplantation without immunological rejection. It can be applied to the clinical therapy of cell transplantation in the nervous system injury and degenerative diseases [5]. But the mechanism of MSCs differentiating to neural cells is not clear, it involves a number of signal transduction accesses. This study found that for the first time, the development of the nervous system as an important functional proteins, before the induction rat MSCs did not express DSCAM, with the induction time extending, expression of DSCAM gradually increased to the peak after 3d induction, and then began to decline. At the same time, the expression of nerve cell marker protein β-III-tubulin increased in the differentiated cells. The results suggested that, the cells induced and differentiated from MSCs had a certain degree of nerve cell function, but the process may also be the recurrence of nerve cell development, and furthermore, DSCAM express mainly in the nervous system development phase, including the spinal cord, cerebral cortex, cerebellum and so on, it plays a vital role to ensure the accurate and close connections of nerve cells in growth and directed extension of its axon branches [6,7]. The expression of DSCAM increase gradually in the course of MSCs differentiation, it may be associated with growth of induced cell axon branches and establishment of cell junctions. nduced cells have the network structure and function of nerve cell. Interference of DSCAM siRNA affected DSCAM expression and led to the decline of effect of induction and differentiation and reduce of nerve cell junction.

A recent study found that, DSCAM play a role in the formation of particular retinal layer. The other two adhesion molecules, that is, the Sidekick-1 and Sidekick-2, play a role in a similar manner. These elements are widely distributed in the nervous system, may be the components of adherence code in formation of brain nerve connection [8]. Therefore, whether the mechanism of MSCs induced to differentiate into neural cells is similar will be involved in an in-depth study.

References

1. Zinn K. Dscam and neuronal uniqueness[J]. Cell 2007, 129(3): 455-456.
2. Schmucker D. Molecular diversity of Dscam: recognition of molecular identity in neuronal wiring[J]. Nat Rev Neurosci 2007, 8(12): 915-920.
3. 贾延劼, 杨于嘉, 周燕, 等.黄芩甙诱导骨髓基质细胞向神经细胞分化的研究[J]. 中华医学杂志 2002, 82(19): 1335-1339.
4. Yamakawa K, Huot YK, Haendelt MA, et al. DSCAM: a novel member of the immunoglobulin superfamily maps in a Down syndrome region and is involved in the development of the nervous system[J]. Hum Molecular Genetics 1998, 7(2): 227–237.
5. Dezawa M, Hoshino M, Ide C. Treatment of neurodegenerative diseases using adult bone marrow stromal cell-derived neurons[J]. Expert Opin Biol Ther 2005, 5(3): 427-435.
6. Hughes ME, Bortnick R, Tsubouchi A, et al. Homophilic Dscam interactions control complex dendrite morphogenesis[J]. Neuron 2007, 54(3): 417-427.
7. Ly A, Nikolaev A, Suresh G, et al. DSCAM is a netrin receptor that collaborates with DCC in mediating turning responses to netrin-1[J]. Cell 2008, 133(7): 1241-1254.
8. Yamagata M, Sanes JR. Dscam and Sidekick proteins direct lamina-specific synaptic connections in vertebrate retina[J]. Nature 2008, 451(7177): 465-469.

1V Square-Root Domain Low-Pass Filter using Translinear Loop Technology in Biomedical Engineering

Gwo-Jeng Yu[*1] Yu-Jen Tsao[2] Yu-Shian Lin[2]

[1]*Department of Computer Science and information Engineering, Cheng Shiu University. University, Niaosong, Taiwan.,*

[2]*Department of Electronic Engineering, Cheng Shiu University, Niaosong, Taiwan*

Received November 1, 2009

Abstract A low voltage square root domain filter based on the MOSFET square law is proposed in this report. Through the verification of HSPICE simulation, the extendibility and the reliability of the design procedure are proved. Furthermore, the voltage supply is successfully leveled down to 1V by the level shifter low-voltage technique without regarding the performance of the filters. The proposed filter structure has the merits of low-power voltage supply operation, high frequency operation, and the wide range of pole frequency tuning ability. The proposed circuit has been fabricated with TSMC 0.35 μm CMOS technology. The experimental results have verified the center frequency f3dB of the low-pass filter can be electronically tunable in the range of 0.4 MHz to 2.9 MHz. The total harmonic distortion (THD) is less than 0.7% for signal amplitude of 100 mV, and the power dissipation is less than 1.05 mW. [Life Science Journal. 2009; 6(4): 92–96] (ISSN: 1097 – 8135)

Key Words square-root domain , translinear Loop, low-Pass Filter, square-root domain filter, flipped-voltage follower

1 Introduction

Recently, there is a growing interest in the field of translinear filters. Main advantages of these various filters are regarding to large dynamic range and low-voltage/low power operation capability. Since the voltage swings of the internal capacitors are compressed, the dc power supply voltage will be less restrictive to the maximum input signal. Initially, a subclass of translinear filters is log-domain filters introduced by Adams [1]. On the other hand, a subclass of translinear filters, named "square-root domain filter" was introduced. Toumazou [2] proposed the state-space synthesis of the second filter which is the first filter structure using the MOSFET square law. Although an alternative biasing of MOS translinear loops based on the application of the Flipped-Voltage Follower (FVF) is proposed [3-5], it allows to significantly reduce the voltage supply requirements. In order to improve the problem of Germanovix'a [6] method, Psychalinos [7], Yu [8] and Lopez-Martin [9-10] also adopted MOSFETs operated in saturation region to implement the square-root domain filters. In this paper, a square-root domain filter with voltage supply down to 1V has been proposed. The paper is organized as follows: In Section II, the principle and architecture of the square-root domain filter using state-space approach is derived and explained. Then in Section III, the most supply-voltage critical block, i.e. the square-root circuit, which performs the geometric-mean function, is proposed to operate at a supply as low as 1V. By using the proposed circuit implementation as well as the state-space approach, several filter prototypes are designed for the verification of the proposed idea in Section IV. Finally, a brief conclusion is given at the end of this paper.

Correspondence: gjyu@csu.edu.tw

Gwo-Jeng Yu, Ph.D.

. 2. Principle And Architecture

Consider the transfer function of the first-order low-pass filter (LPF):

$$H(S)=\frac{\omega_0}{s+\omega_0}=\frac{Y(S)}{U(S)} \quad (1)$$

where $Y(s)$ and $U(s)$ are output and input respectively, and the relationship between them is obtained by

$$Y(S)=\frac{\omega_0}{S+\omega_0} \tag{2}$$

Apply the inverse Laplace transform to (2), and then set the initial value to zero.

$$\dot{y}=-\omega_0 y+\omega_0 u \tag{3}$$

Let $y=x$ and take the derivative of both side.

$$\dot{y}=\dot{x} \tag{4}$$

According to the state-space approach, we could map the original transfer function into the stat-space equation.

$$\begin{cases}\dot{x}=-\omega_0 x+\omega_0 u\\ y=x\end{cases} \tag{5}$$

Assume the state variables are the node voltage, then $x=V_1$ and, $u=U$ and substitute them into (5).

$$\begin{cases}\dot{V}_1=-\omega_0 V_1+\omega_0 U\\ y=V_1\end{cases} \tag{6}$$

Multiply a constant C on both sides in (6).

$$\begin{cases}C\dot{V}_1=-C\omega_0 V_1+C\omega_0 U\\ y=V_1\end{cases} \tag{7}$$

The drain current of a MOSFET transistor operated in saturation can be expressed as

$$I_D=\frac{\mu_0 C_{OX} W}{2L}(V_{GS}-V_T)^2\equiv\beta(V_{GS}-V_T)^2 \tag{8}$$

where β, V_{GS} and V_T are the transconductance parameter, the gate-to-source voltage and the threshold voltage, respectively. Next, we define two new current variables I_1 and I_U to be

$$\begin{cases}I_1=\beta(V_1-V_T)^2\Rightarrow V_1=\sqrt{\frac{I_1}{\beta}}+V_T\\ I_U=\beta(U-V_T)^2\Rightarrow U=\sqrt{\frac{I_U}{\beta}}+V_T\end{cases} \tag{9}$$

And substitute the (9) into (7)

$$\begin{cases}C\dot{V}_1=C\omega_0\left(\sqrt{\frac{I_U}{\beta}}-\sqrt{\frac{I_1}{\beta}}\right)\\ y=V_1\end{cases} \tag{10}$$

Induce a new current variable here, and we know that the pole frequency ω_0 can be tuned by changing the DC current bias current source I_0.

$$I_0=\frac{C^2{\omega_0}^2}{\beta} \tag{11}$$

or

$$\omega_0=\frac{\sqrt{I_0\beta}}{C} \tag{12}$$

Thus, the state- space equation become

$$\begin{cases}C\dot{V}_1=\sqrt{I_0 I_U}-\sqrt{I_0 I_1}\\ y=V_1\end{cases} \tag{13}$$

The transfer function of a second-order low-pass filter can be expressed as

$$H(s)=\frac{\omega_0^2}{s^2+\left(\frac{\omega_0}{Q}\right)s+\omega_0^2} \tag{14}$$

This transfer function of a low-pass filter can be expressed as

$$\begin{cases}\dot{x}_1=-\omega_0 x_2+\omega_0 u\\ \dot{x}_2=\omega_0 x_1-\left(\frac{\omega_0}{Q}\right)x_2\\ y=x_2\end{cases} \tag{15}$$

Where x_1, x_2, y, and u are state variables, output and input signals, respectively. If the node voltages V_1 and V_2 are assumed to be the state variables, x_1 and x_2, and a voltage signal U denotes the input u, the Eq.(15) can be rewritten as

$$\begin{cases}C\dot{V}_1=-C\omega_0 V_2+C\omega_0 U\\ C\dot{V}_2=C\omega_0 V_1-\left(\frac{C\omega_0}{Q}\right)V_2\\ y=V_2\end{cases} \tag{16}$$

Where C is a multiply factors. $C\dot{V}_1$ and $C\dot{V}_2$ in Eq.(16) can be regarded as the time-dependent current through

the two capacitors C connected from V_1 to ground and from V_2 to ground, respectively.

The drain current of a MOSFET transistor operated in saturation can be expressed as

$$I_D = \frac{\mu_0 C_{ox} W}{2L}\left(V_{GS} - V_{th}\right)^2 = \beta\left(V_{GS} - V_{th}\right)^2 \quad (17)$$

Where β, V_{GS} and V_{th} are the device trans-conductance parameter, the gate-to-source voltage and the threshold voltage, respectively. thus, the state-space equation becomes

$$\begin{cases} C\dot{V}_1 = \sqrt{I_0 I_U} - \sqrt{I_0 I_2} \\ C\dot{V}_2 = \sqrt{I_0 I_1} - \dfrac{\sqrt{I_0 I_2}}{Q} \end{cases} \quad (18)$$

According to Eq. (17), and supposing Q=1, the state equations in Eq. (16) can be written as

$$\begin{cases} C\dot{V}_1 = \sqrt{I_0 I_U} - \sqrt{I_0 I_2} \\ C\dot{V}_2 = \sqrt{I_0 I_1} - \sqrt{I_0 I_2} \end{cases} \quad (19)$$

where

$$I_1 = \beta(V_1 - V_T)^2 \quad (20)$$

$$I_2 = \beta(V_2 - V_T)^2 \quad (21)$$

$$I_U = \beta(U - V_T)^2 \quad (22)$$

and

$$\omega_0 = \frac{\sqrt{\beta I_0}}{C} \quad (23)$$

$$I_0 = \frac{C^2 {\omega_0}^2}{\beta} \quad (24)$$

Note that ω_0 is inversely proportional to the capacitance C and is proportional to the square root of I_0; hence the cutoff frequency ω_0 is dominated by the capacitance C and I_0 is used to tune the cutoff frequency.

3. Circuit Implementation

3.1 Current-mode Flipped-Voltage Follower circuit

Fig. 1 [3-5] shows a flipped voltage follower (*FVF*), which consists of a current source and two transistors. One transistor is cascaded another. The current source supplies the drain current of M_1, and the drain of M_1 connects to the gate of M_2 can be expressed as

$$V_{io} \equiv V_x + V_{th}$$
$$V_x = \sqrt{\frac{I_B}{\beta}} \quad (25)$$

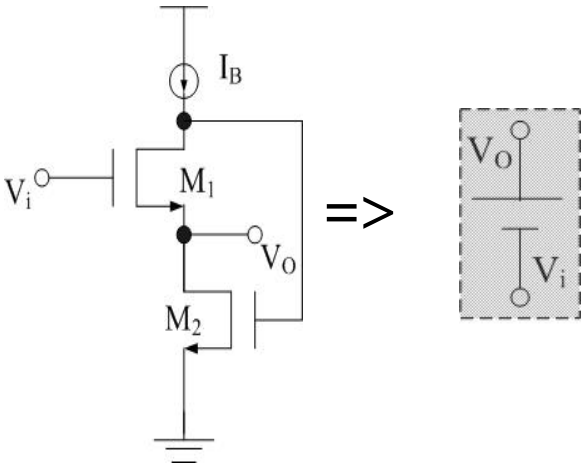

Fig 1. Current-mode Flipped-Voltage Follower (*FVF*) circuit

3.2 Current-mode square-root circuit

The proposed current-mode square-root circuit is shown in Fig. 2 operating as follows: Ix and Iy are input currents, and these currents generate the corresponding voltage, VX and VY through the current to voltage conversion of diode-connected MOS. The matched transistors M1-M4 which is forced to operate in subthreshold region and the dc current sources, depicted as Ib altogether construct a voltage-averaging circuit.

The voltage averaging circuit produces a gate voltage VXY , which is forced to be equal to the average of the gate voltage of MX and MY as VXY = (VX+VY)/2. The detailed circuit operation of averaging function is explained as follows: As we know, the I-V relationship between the drain current and gate-source voltage for a MOS operated in subthreshold region can formulated as the following equation:

$$I_D = I_{D0} \exp\left(\frac{V_{GS}}{\xi V_{th}}\right) \quad (26)$$

where ξ and VT stand for non-ideal factors and thermal voltage respectively. We can easily find the following equation holds since ID1+ID2=ID2+ID3= Ib

$$I_{D3} = I_{D1} \quad (27)$$

Substitute Eq.(26) into Eq.(27) , the equation can be rewritten as

$$I_{D0}\exp\left(\frac{V_{S2}-V_X}{\xi V_{th}}\right)=I_{D0}\exp\left(\frac{V_{S3}-V_{XY}}{\xi V_{th}}\right) \tag{28}$$

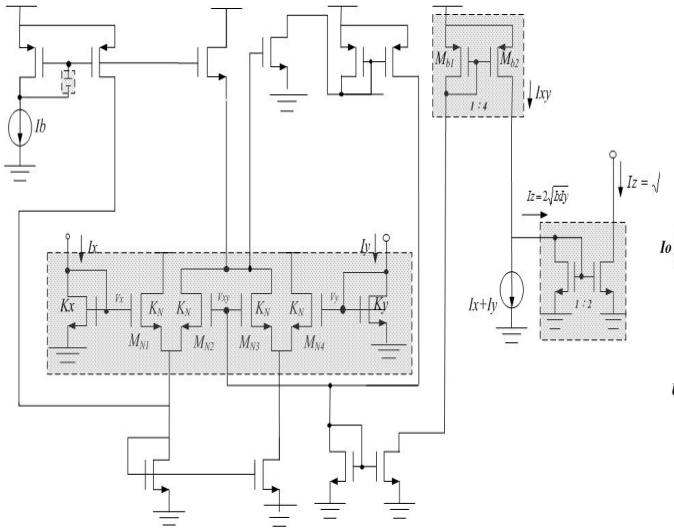

Fig. 2. Current-mode square-root circuit (a) Circuit diagram, (b) Equivalent block diagram

From Eq.(27) we can derive the result :

$$V_{XY}=V_{S3}-V_{S1}+V_X \tag{29}$$

In the similar way, we can get the following result by the same analysis procedure.

$$V_{XY}=V_{S1}-V_{S3}+V_Y \tag{30}$$

According to Eq.(29) and Eq.(30), we can prove the following Eq.(31).

$$V_{XY}=\frac{V_X+V_Y}{2} \tag{31}$$

According to the translinear loop formed by transistors MX, MY, and MXY, realized under the assumption that βb12 = 4β and βx = βy = β where β is the aspect ratio, the following equation can be derived.

$$I_{xy}=I_x+I_y+2\sqrt{I_xI_y} \tag{32}$$

Again writing the KCL equation at output node of this circuit, the equation can be inducted as follows:

$$I_z=2\sqrt{I_xI_y} \tag{33}$$

Hence if the ratio of the output stage current mirror in Fig. 2 is set to be 2:1, the output current Iout can be derived as:

$$I_{out}=\sqrt{I_xI_y} \tag{34}$$

The circuit diagram of second-order low-pass filter is shown in Fig. 3.

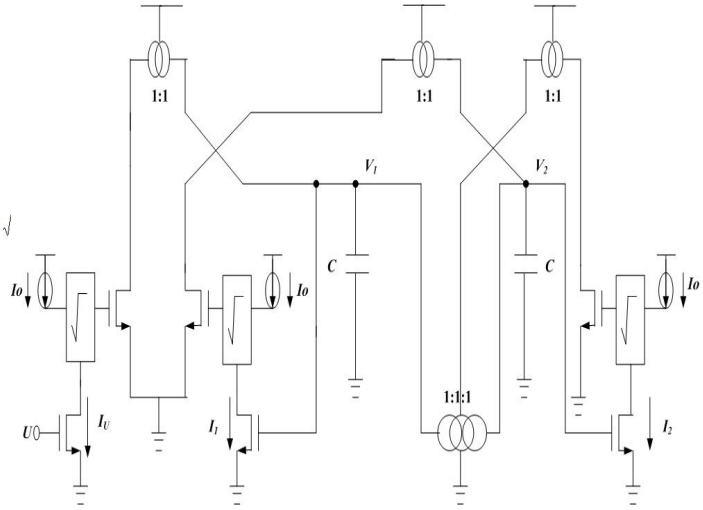

Fig. 3. Circuit diagram of the second-order low-pass filter

4. Simulation Results

Fig. 4 is the simulated result of the current-mode square-root circuit while VDD = 1V, Ix and Iy are a 40 μA DC current and a triangle wave current with values between 0 and 45 μA, respectively. Fig. 5 is the frequency f3dB tuning range of second-order low-pass filter shown in Fig. 3 which is from 0.420MHz, 0.779MHz and 1.12 MHz by changing the current I0 from 20uA, 30uA and 40uA. The total harmonic distortion (THD) with a 1KHZ 100mV peak-to-peak sinusoid is 0.681%. The specifications of second-order low-pass filter are shown in Table 1.

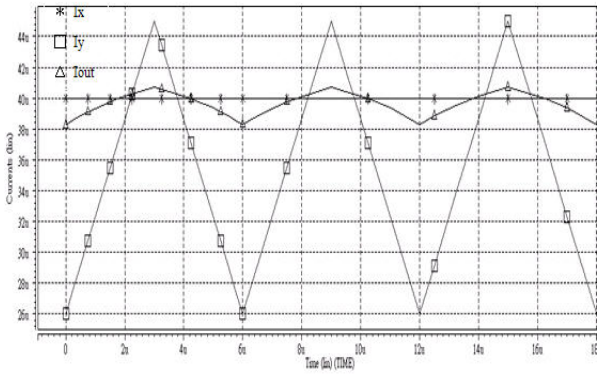

Fig. 4 Simulated result of the square-root circuit

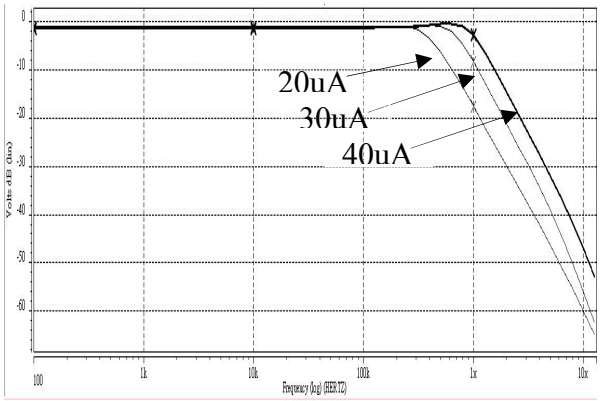

Fig 5 Frequency response of the second-order low-pass filter.

5. Conclusion

In this paper, based on the MOSFET square law, on square-root domain low-pass filters with low voltage and low power operation is proposed. Operated in 1V power supply voltage, low-pass filter has been fabricated in 0.35μm CMOS technology; shown that the center frequency f0 is not only attainable at megahertz frequencies but also tunable electronically. The proposed circuit, thus, has the advantages of high frequency operation, low supply voltage operation and low power consumption. Furthermore, implementation via standard digital CMOS technology for the proposed filter is quite suitable for system-on-a-chip (SOC) application.

Table 1. Specifications of the second-order low-pass filter

Parameters	Simulation results
Filter order	2
Technology	TSMC 0.35 μm
Supply voltage	1V
I_0	20uA, 30uA, 40uA
f_{3db} tuning range	0.420 MHz, 0.779 MHz, 1.12 MHz
power dissipation	0.599mW, 0.864mW, 1.035mW
THD (V_{PP}=0.1V)	0.872%, 0.696%, 0.681%

References

[1] R. W. Adams, "Filtering in the log-domain," in Proc. AES Conj, 1979, preprint 1470.

[2] M. H. Eskiyerli, A.J. Payne, and C. Toumazou, "State-space synthesis of biquads based on the MOSFET square law." In Proc. IEEE Int. Symp. Circuits and Syst., 1996, vol. 1, pp. 321–324.

[3] Ramirez-Angulo, I., Carvajal, R.G., Torralba, A., Galan, A., Vega-Leal, A.P., and Tombs, J., ”The flipped voltage follower: a useful cell for low-voltage low-power circuit design,” in Proc. lSCAS2002, Phoenix, AZ, pp. 111 615.618,

[4] C. A. De La Cruz-Blas, A. J. Lopex-Martin, and A. Carlosena, “1.5V tunable square-root Domain filter”, Electron. Lett, vol. 40, Feb. 2004.

[5] J. Ramirez-Angulo, S. Gupta, R. G. Carvajal, and A. Lopez-Martin, “New improved CMOS class AB buffers based on differential flipped voltage followers,” in Proc. IEEE Int. Symp. Circuits Syst., Kos, Greece, May 21–24, 2006, pp. V3914–V3917.

[6] W. Germanovix, G. O’Neill, C. Toumazou, E. M. Drakakis, R. I. Kitney, and T. S. Lande, “Analogue micropowered log-domain tone controller for auditory prostheses,” Electron. Lett., vol. 34, pp. 1051-1052, May 1998.

[7] C. Psychalinos, and S. Blassis, "A systematic design procedure for square-root-domain circuits based on the signal flow graph approach," IEEE Trans. Circuits Syst. I, vol. 49, pp. 1702-1712, Dec. 2002.

[8] G. J. Yu, B. D. Liu, Y. C. Hsu, and C.Y. Huang, "Design of log domain low-pass filters by MOSFET square law." In Proc. The Second IEEE Asia Pacific Conf. on ASICs, 2000, pp. 9–12.

[9] A. J. Lopez-Martin and A. Carlosena, "A 1.5 V CMOS companding filter." Electron Lett, vol. 38, pp. 1346–1347, Oct. 2002.

[10] A. J. Lopez-Martin and A. Carlosena, "A 3.3V tunable current-mode square-root domain biquad." In Proc. IEEE Int. Symp. Circuits and Syst.,vol. 5, May. 2000, pp. 375–378.